Ecology and Development Series No. 36, 2006

Halidou Compaoré

The impact of savannah vegetation on the spatial and temporal variation of the actual evapotranspiration in the Volta Basin, Navrongo, Upper East Ghana

Cuvillier Verlag Göttingen

For everything you have done, I dedicate this work to you, dear mother, Mariam CONGO

ABSTRACT

The savannah landscape in West Africa and in the Volta Basin is characterized by a rapid land-use and land-cover change due to climatic variability and a high human pressure on the natural resources. This rapid change in the vegetation layer has important implications for the interrelations of the soil-vegetation-atmosphere interface in general and the hydrological role of savannahs in the Volta Basin in particular.

To study the impact of savannah vegetation on the spatial and temporal distribution of the actual evapotranspiration, the landscape was first characterized into biophysical and hydrological units using remote sensing and field data. A Landsat image from the 30 October, 2002, was used to derive 10 major land-use and land-cover ($LULC$) types applying a hybrid classification method. Further, an ASTER image from the early dry season was enhanced through a principal component analysis and used to map the spatial distribution of fire traces in the Navrongo area.

To map tree density from the study area, spectral vegetation indices of the Landsat image were related to field data acquired during a field survey. In total, six tree density classes were found varying from 0-3 to >160 trees ha^{-1}. In addition, the Vegetation Index Temperature Trapezoid ($VITT$) approach was used to describe the spatio-temporal variation of 11 hydrological units at the beginning and end of the dry season.

The Surface Energy Balance Algorithm for Land ($SEBAL$) model was used to compute the actual evapotranspiration (ET_a) distribution on a pixel basis. The temporal change in ET_a in the savannah was defined using two Landsat7 ETM+ datasets acquired at two time periods during the dry season. The temporal integration of the ET_a was realized through the implementation of an adjusted crop coefficient (K_c) calculated at the satellite overpasses.

The relationships between the biophysical and hydrological characteristics and the spatial distribution of the ET_a were determined using a GIS-based analysis. The analyses enabled evaluating the spatial distribution of the ET_a according to $LULC$ types, tree density classes and hydrological units during the dry season. Specifically, the sap flow technique was used to estimate individual tree water use, and an up-scaling method was applied to estimate the transpiration for the whole fallow vegetation which is dominated by *Vitellaria paradoxa* tree species.

The ET_a was related to $LULC$ types, hydrological units and TD classes, but the relationships vary seasonally. The results of the study show that the agricultural land and the natural savannah were the dominant $LULC$ types, each covering about 40% of the study area. At the beginning of the dry season, woodland and farmland classes show an ET_a of 2.8 and 2.0 mm day^{-1}, respectively; at the end of the dry season, the ET_a was 1.22 and 0.2 mm day^{-1} for the woodland and farmland, respectively. Tree density varies from dense to scarce, while the hydrological units were qualitatively classified from very wet to dry. Early dry season ET_a values of 1.3 mm and 3.8 mm day^{-1} occurred in TD0-3 and TD 71-160, respectively. Later in the dry season, the ET_a decreased to 0.0 mm and 1.1 mm day^{-1} for TD0-3 and TD 71-160, respectively. Similarly, ET_a for hydrological units located in gallery forest varied from 3.2 mm to only 0.9 mm day^{-1}

from the beginning to the end of the dry season, respectively. Drier hydrological units, generally related to bare land, farmland and park savannah (units 3, 4, 5, 6 and 7) showed a low ET_a of about 2.2 mm day^{-1} and close to 0.0 mm day^{-1} at the beginning and at the end of the dry season, respectively.

Sap flow measurements on individual tree species to assess their water use show differences among the principal trees species of the experimental site. During the dry season, *Acacia albida* consumed the largest amount of water with about 120 l day^{-1} and 90 l day^{-1} at the beginning and the end of the dry season, respectively. On the other hand, water use by *Vitellaria paradoxa*, the most common tree species at the experimental site, was estimated at about 79 l day^{-1} and 32 l day^{-1} at the beginning and the end of the dry season, respectively. Mean water transpiration over the fallow vegetation was estimated at about 0.14 and 0.05 mm day^{-1} at the beginning and the end of the dry season, respectively.

Einfluss der Savannen-Vegetation auf räumliche und zeitliche Variationen der aktuellen Evapotranspiration im Volta-Becken (Navrongo, Upper East Ghana)

KURZFASSUNG

Die Savannenlandschaft in Westafrika und im Voltabecken ist durch eine rapide Veränderung der Landoberfläche und der Landnutzung charakterisiert, bedingt durch Klimaschwankungen und hohen anthropogenen Druck auf die natürlichen Ressourcen. Diese schnelle Veränderung der Vegetationsdecke hat wichtige Auswirkungen auf die Beziehungen von Boden, Vegetation und Atmosphäre im Allgemeinen, und auf die hydrologische Rolle von Savannen im Voltabecken im Speziellen.

Um die Auswirkung der Savannenvegetation auf die räumliche und zeitliche Verteilung der aktuellen Evapotranspiration zu studieren, wurde die Landschaft mittels Fernerkundung und Felddaten zuerst in ihre biophysikalischen und hydrologischen Untereinheiten untergliedert. Anhand eines Landsat-Bildes vom 30. Oktober 2002 wurden mittels Hybridklassifizierungsmethode zehn größere Landnutzungs- und Landbedeckung- (*LULC* s) Klassen unterschieden. Zusätzlich wurde ein ASTER Image in einer Hauptkomponentenanalyse ausgewertet und dazu benutzt, Buschbrände in der Navrongo-Gegend zu kartieren.

Die Baumdichte der Untersuchungsregion wurde ermittelt, indem die spektralen Vegetationsindices des Landsat-Bildes mit Daten einer Felderhebung abgeglichen wurden. Insgesamt konnten sechs Baumdichteklassen unterschieden werden, beginnend bei 0-3 Bäumen bis hin zu >160 Bäumen pro Hektar. Zusätzlich wurde der so genannte Vegetationsindex-Temperatur-Trapezoid-Ansatz (*VITT*) angewendet, um die räumlich-zeitliche Variabilität von elf hydrologischen Untereinheiten am Beginn sowie am Ende der Vegetationszeit zu bestimmen.

Das Landoberflächen-Energiebilanz-Algorithmus-Modell (*SEBAL*) wurde benutzt, um die Verteilung der aktuellen Evapotranspiration (ET_a) auf Pixelebene zu berechnen. Die zeitliche Veränderung von ET_a der Savanne wurde mit zwei Landsat7 ETM+ Datensätzen aus zwei unterschiedlichen Zeiträumen in der Trockenzeit definiert. Die zeitliche Integration von ET_a wurde über die Implementierung von angepassten 'Crop-coefficients' (K_c) realisiert, die für die Zeitpunkte berechnet wurden, an denen der Satellit das Gebiet überflog.

Die Beziehung zwischen biophysikalischen und hydrologischen Charakteristika und der räumlichen Verteilung von ET_a wurde GIS-gestützt analysiert. Diese Analysen ermöglichten die Evaluierung der räumlichen Verteilung von ET_a in der Trockenzeit gemäß der *LULC* Klassen, der Baumdichteklassen und der hydrologischen Untereinheiten. Im Besonderen wurden Saftflussmessungen dazu benutzt, die Wasseraufnahme von einzelnen Bäumen zu bestimmen. Diese wurden auf die gesamte Brachevegetation, die von *Vitellaria paradoxa* dominiert wurde, hochskaliert.

Die aktuelle Verdunstung stand in Beziehung zu den *LULC* Klassen, den hydrologischen Untereinheiten und den Baumdichteklassen, variierte jedoch jahreszeitlich. Die Ergebnisse der Studie zeigen, dass die *LULC* Klassen 'landwirtschaftliche Anbaufläche' und 'Savanne' vorherrschten und 40% der

Untersuchungsregion einnahmen. Zu Beginn der Trockenzeit zeigten die Klasse 'Waldland' ein Verdunstung von 2.8 mm d^{-1}, die Klasse 'Farmland' 2.0 mm d^{-1}; am Ende der Trockenzeit reduzierte sich die ET_a dieser beiden Klassen auf 1.2 bzw. 0.2 mm d^{-1}. Die Baumdichte variiert von dicht bis vereinzelt, während die hydrologischen Untereinheiten in die Klassen 'sehr feucht' bis 'trocken' eingeteilt wurden. Zu Beginn der Trockenzeit traten ET_a Werte von 1.3 bzw. 3.8 mm d^{-1} in den TD0-3 bzw. TD 71-160 auf. Im späteren Verlauf der Trockenzeit reduzierten sich diese Werte auf 0.0 bzw. 1.1 mm d^{-1}. In ähnlicher Weise variierte die Verdunstung jener hydrologischen Untereinheiten, die den Galeriewald umfassten. Sie reduzierten sich von 3.2 mm d^{-1} am Beginn auf 0.9 mm d^{-1} am Ende der Trockenzeit. Trockenere hydrologische Einheiten, die generell Bracheland, Farmland und Savannenpark umfassten, zeigten eine geringe ET_a von 2.2 mm d^{-1} am Beginn und nahe 0.0 mm d^{-1} am Ende der Trockenzeit.

Die Saftflussmessungen von einzelnen Bäumen ergaben Unterschiede zwischen den Baumarten der Untersuchungsfläche. In der Trockenzeit war *Acacia albida* ein großer Wasserkonsument mit rund 120 l d^{-1} am Beginn und 90 l d^{-1} am Ende der Trockenzeit. Auf der anderen Seite belief sich die Wassernutzung von *Vitellaria paradoxa*, der am weitest verbreiteten Baumart, auf 79 l d^{-1} am Anfang und 32 l d^{-1} am Ende der Trockenzeit. Die mittlere Verdunstung der Brachevegetation wurde auf 0.14 bzw. 0.05 mm d^{-1} am Beginn bzw. am Ende der Trockenzeit geschätzt.

TABLE OF CONTENTS

LIST OF ACRONYMS AND ABBREVIATIONS

ANOVA	Analysis of variance
ASTER	Advanced Spaceborne Thermal Emission and Reflection Radiometer
CA	Crown area
CSIR	Counsil for Scientific and Industrial Research
Cv	Coefficient of variation
CUT	Combining an unsupervised algorithm and training data
DBH	Diameter at breast height
DOY	Day of the year
ET	Evapotranspiration
ET_o	Reference crop evapotranspiration
ET_p	Potential evapotranspiration
ET_{24}	Daily actual evapotranspiration
ET_a	Actual evapotranspiration
ET_c	Crop evapotranspiration
7-day ET	Seven-day actual evapotranspiration
ETM+	Enhanced Thematic Mapper Plus
FAO	Food and Agricultural Organization
FCC	False color composite
GDP	Gross Domestic Product
GIS	Geographical Information System
GPS	Global Positioning System
Glowa-Volta	Global Change in the Hydrological Cycle of the Volta Basin
HD	Heat dissipation
HFD	Heat field deformation
HPV	Heat pulse velocity
IGBP	International Geosphere-Biosphere Program
ISODATA	Iterative self-organizing data analysis technique
K_c	Crop coefficient
K_{bc}	Transpiration coefficient
LAI	Leaf area index
LULC	Land use and land cover
L1B	Level 1B
MODIS	Moderate Resolution Imaging Spectro-radiometer
NDVI	Normalized difference vegetation index
NOAA/AVHRR	National Oceanic and Atmospheric Administration/A very high resolution radiometer
NPP	Net primary production
ORSTOM	Institut de Recherche pour le Développement
PCA	Principal Component Analysis
RMSE	Root mean square error
SAVI	Soil adjusted vegetation index
SE	Standard error of the estimate
SEBAL	Surface Energy Balance Algorithm for Land
SEBI	Surface Energy Balance Index
SEBS	Surface Energy Balance System

SFP	Sap flow experimental plot
SHB	Stem heat balance
SRID	Statistics, Research and Information Directorate-Ghana
Stdev	Standard deviation
SVATS	Soil Vegetation Atmosphere Transfer Schemes
S_{WIR}	Shortwave infrared
TD	Tree density
THB	Trunk segment heat balance
TIR	Thermal infrared
UNESCO	United Nations Educational, Scientific and Cultural Organization
UTM	Universal transverse Mercator projection
VITT	Vegetation Index Temperature Trapezoid
Vnir	Visible near infrared
VPD	Vapor pressure deficit
WGS 84	World geodetic System 1984
WRI	World Resources Institute

LIST OF SYMBOLS

Symbol	Representation	Dimension
e_a	Actual vapor pressure	kPa
e_s	Saturation vapor pressure	kPa
λE	Latent heat flux	W/m^2
J	Sap flow velocity	cm/h
$K^{\downarrow}$	Incoming broadband short-wave radiation	W/m^2
$K^{\uparrow}$	Reflected broadband short-wave radiation	W/m^2
$L^{\downarrow}$	Incoming broadband long-wave radiation	W/m^2
ε_o	Surface emissivity	-
σ	Stefan-Bolzman constant	$W/m^2/K^4$
T_o	Surface temperature	K
α	Surface albedo	-
ρ	Spectral reflectance	-
ρ_{air}	Atmospheric air density	Kg/m^3
C_p	Air-specific heat at constant pressure	J/Kg/K
ΔT_{air}	Near-surface air temperature difference	K
r_{ah}	Aerodynamic resistance to heat transport	s/m
Ψh	Psychometric buoyancy parameters for heat transport	-
Λ	Evaporative fraction	-
γ	Psychrometric constant	$kPa°C^{-1}$
G	Soil heat flux	(W/m^2)
R_n	Net radiation	(W/m^2)
R^2	R-squared	-
R_{n24}	Averaged daily net radiation	(W/m^2)
L	Monin-Obukov Length	-
H	Sensible heat flux	(W/m^2)
r_o	Average daytime surface reflectance	-
u	Wind speed	ms^{-1}
z	Arbitrary height level	m
z0m	Surface momentum roughness	m
T_{rad}	Radiometric surface temperature	K
T_{aero}	Aerodynamic surface temperature	K

1 INTRODUCTION

Savannahs are mainly located between the latitudes 5 to 15° north/south of the Equator. Savannah vegetation has also developed in the interiors of continents such as northern Australia, South America and most of Central Africa surrounding the Congo Basin. This wide distribution of savannah means that this biome is able to develop over a broad range of climatic conditions ranging from sparse grassland with scattered trees with an average annual precipitation of less than 100 mm to tall moist woodland savannah with an annual precipitation of more than 1500 mm (Scholes and Walker, 1993; Cole, 1982; Huntley, 1982).

Savannah vegetation accounts for more than 10% of the surface of the earth (Scholes and Hall, 1996) and about 50% of the area of Africa, South America and Australia (Scholes and Walker, 1993; Cowling et al., 1997). These landscapes are occupied by 20% of the human population and the majority of the world's livestock, including large mammals. This large number of inhabitants and herbivores results in a high pressure on the natural resources of those regions. Savannah ecosystems are therefore changing, and the dynamics of changes are currently poorly understood. Indeed, little attention has been paid to these areas in the past, particularly to the African savannah.

Characteristics of land cover have been widely recognized in the scientific community as a key element in the study of global change (e.g., IGBP, 1990; Henderson-Sellers and Pitman, 1992). Several climatic studies have indicated that atmospheric circulation and rainfall are significantly affected by the large-scale variation of soil moisture and evaporation (Savenije, 1996b; Enthekhabi et al., 1999). Furthermore, human or natural alterations of land cover also play a major role in the global-scale patterns of climate and biogeochemistry of the earth system (Nicholson et al., 1998; Mohr et al., 2002). While some of these changes in land cover are caused by natural processes, such as long-term changes of the climate due to astronomical causes, or shorter-term vegetation successions and geomorphological processes, human activity is increasingly modifying surface cover through direct actions, such as deforestation, farming activities, urbanization, or indirectly through human-induced climatic change (FAO, 1995, Turner, 1989).

The land surface has considerable control over the planet's energy balance, biogeochemical cycles, and hydrologic cycle, which in turn significantly influence the climate system (Turner et al., 1994; Bastiaanssen, 1995). Indeed, land cover is the biophysical state of the earth's surface and immediate subsurface (Turner et al., 1995). Changes in the land cover, including the savannahs, play a major role in global environmental change and could therefore lead to significant shifts in the earth-atmosphere interactions. The resultant global climate change may in turn force changes in land-use and land-cover, a cyclical process that may culminate in desertification and abandonment of land (Glowa-Volta Proposal, 1999).

Part of the energy reaching the ground is reflected directly, while another fraction, dependent on the vegetation cover, is utilized for photosynthesis and evaporation of free water or of water transpired by vegetation (Leroux, 2001). The remaining energy is absorbed by the soil, which reradiates at longer wavelengths and in its turn warms the overlying air. Therefore, variations in vegetation cover and physical characteristics of the land surface such as albedo, emissivity, roughness and plant transpiration could be the critical parameters to generate variations of weather and climate by altering the hydrologic cycle and land-atmosphere energy fluxes (Avissar et al., 1989).

In West Africa, hydrologic interactions between the atmospheric water content and vegetation layer enable specific hydrological processes to potentially have an impact on the evapotranspiration flux into the atmosphere (Marengo et al., 1997). The last droughts had severe impacts in the savannah environment of West Africa, and they occurred simultaneously with a rapid increase in the population of the area. The population of five Sahelian countries (Senegal, Niger, Mali, Sudan and Chad), for example, rose from 20 million in 1950 to 55 million in 1990, and is projected to rise to over 135 million by 2025 (WRI, 1994). This rise in population, as well as political constraints on nomadism (Middleton, 1999), could cause extensive land-cover conversion. In Sub-Saharian Africa, increased food production, food security, and poverty alleviation will require the intensification of agricultural production (Vlek, 1993). Overgrazing of the natural rangelands by livestock, natural vegetation conversion to agricultural land, agricultural intensification and an increased fuel-wood extraction, coupled with severe drought, are the most cited causes of land degradation in the Sahel

(Dregne and Chou, 1992; Middleton, 1999; Stephenne and Lambin, 2001). Previously uncultivated areas experience agricultural expansion as a result of migration into unsettled areas, aided by newly developed technologies (Goritz 1985; Goudie, 2000).

Some authors have challenged the view of large-scale land degradation (Nicholson et al., 1998; Nicholson, 2002) based primarily on satellite data from the late 1970s. Their investigations show that during the 1983 to 1988 period, the albedo change rate was remarkably small and in the range of 3% per year. This conclusion seems to be a major contradiction to previous studies by Charney (1975) or Entekhabi et al. (1992) supporting the hypothesis that a feedback between the atmosphere and surface hydrology has played a role in the droughts in the Sahel region.

Vegetation cover has been identified as one of the most important biophysical parameters of terrestrial surfaces due to its specific role in geosphere-biosphere-atmosphere interactions (Mennis, 2001). This parameter regulates the energy (including water) exchanges between the earth-atmosphere interfaces, and dominates the functioning of hydrological processes through modification of interception, infiltration, surface runoff, and its effects on surface albedo, roughness, evapotranspiration, and root system modification of soil properties (Middleton et al., 1997). Vegetation density is the parameter that controls the partitioning of incoming solar energy into sensible and latent heat fluxes, and changes in vegetation cover will result in long-term changes in local and global climates, which in turn will affect the vegetation growth (Dickinson and Henderson-Sellers, 1998; Lean and Warilow, 1989). Changes in the vegetation cover will have an impact on the water recycling function and therefore on the role of the vegetation in the hydrological cycle.

Evapotranspiration is a major component of the hydrological balance representing the water flux that returns to the atmosphere from land surfaces. On the global scale, it represents more than 60% of precipitation inputs (Vörösmarty et al., 1998) and, for example more than 70% of the annual precipitation of the United States (Brooks et al., 1997). In general, forest ecosystems have higher ET rates than non-irrigated agricultural or urban settings (Arnold and Gibbons, 1996). In the Volta Basin, West Africa, most evapotranspiration also consists of plant transpiration, and vegetation determines to a large extent the exchange of latent heat and momentum between the atmosphere and the earth surface (Glowa-Volta Proposal, 1999). A thorough knowledge of the vegetative cover in this basin is of great importance for studying the variability of evapotranspiration across different $LULC$ types. Estimation of evapotranspiration has been investigated since the operation of earth resource satellites in the 1970s, and many remote-sensing-based evapotranspiration estimation techniques have been developed (e.g., Jackson et al., 1977; Moran and Jackson, 1991). Models such as Soil Vegetation Atmosphere Transfer Schemes (SVATS), Surface Energy Balance Index (SEBI) and Surface Energy Balance System (SEBS) have been widely applied in estimating spatially distributed energy balance equation components. Satellite remote sensing is a powerful tool providing a viable source of data from which updated land-cover information can be extracted efficiently and cheaply in order to inventory and monitor these changes effectively (Mas, 1999; Skole and Tucker, 1994). Remotely sensed data combined with ground data could be used to estimate surface energy fluxes, the partitioning of net available energy from incoming short and long wave radiation in general, and the spatial and temporal variation of the actual evapotranspiration using the Surface Energy Balance Algorithm for Land ($SEBAL$) model based on the energy balance approach (Bastiaanssen et al., 1998a, 2000)

The present work is part of **the Glowa Volta sub-project L4 Vegetation characterization and modeling** (Glowa-Volta Project Proposal, 1999). Within the Glowa Volta Project, management of surface water and the extension of irrigated agriculture are of extreme interest. One main concern is how to mitigate water scarcity in the basin. The main object in this study is to assess water loss to the atmosphere during times of limited water availability. For this, direct field measurements with the sap flow technique and the energy balance method with hydrological modeling and integrated with remote sensing data were combined to assess the status of evapotranspiration for different landscape parameters in the Navrongo area of the Volta Basin. The Surface Energy Balance Algorithm for Land ($SEBAL$) model and meteorological data will be employed to assess the spatial and temporal variation of ET_a. Landsat images acquired at two major time periods will be used to study the spatial distribution of the ET_a at the beginning and the end of the dry season in the Navrongo area. Field and satellite data will be integrated to characterize the landscape in terms of different parameters such as $LULC$ types, hydrological units and tree density. Finally, the variability of evapotranspiration across these land units during the two dates will be evaluated.

1.1 Problem statement

Land use and land cover is increasingly recognized as being an important driver of global environmental change (Turner et al., 1994). To ensure a sustainable management of natural resources, it is necessary to understand and quantify the processes of landscape change. Patterns of landscape modification are the results of complex interactions between physical, biological and social forces (Turner, 1987). The changes in land cover, in particular tropical areas, have attracted attention because of the potential effects on erosion, increased run-off and flooding, increasing CO_2 concentration, climatological changes and biodiversity loss (Myers, 1998; Fontan, 1994). The amount, spatial distribution, and temporal pattern of vegetation are some of the most important physical properties of terrestrial surfaces, because they control the partitioning of the energy fluxes, hydrological fluxes through modification of the surface albedo, surface roughness, and soil moisture (Commeraat and Imeson, 1999). Large changes in vegetation distribution and composition will likely affect local climate, which in turn will modify the amount and distribution of vegetation. Monitoring the dynamics of vegetation and characterizing its spatial distribution will provide important indications about the changing environment and enable a better understanding of the physical processes across the geosphere-biosphere-atmosphere boundaries.

To understand and predict change processes, one needs to monitor and characterize spatial patterns of land-use and land-cover change. Field-based studies allow the observation and description of processes of land-cover change in a detailed and spatially disaggregated way. Such studies describe the interactions between human activities and their environment and thus highlight the driving forces of land-cover change (Lambin and Ehrlich, 1996). However, field studies are generally not sufficient to quantify and analyze all spatio-temporal patterns of land-use and land-cover changes at an aggregated level (Liverman et al., 1998).

Generally, land-use change in West Africa and especially in the the Volta Basin means intensification of the agricultural use of the land (Ademola, 2004; Duadze, 2004; Glowa-Volta project, 1999). Agriculture is intensified through reduction of the land under fallow and increased inputs in the form of labor, chemicals, and irrigation. Changes in the vegetation are, of course, the first and foremost result of land-use intensification. In turn, changes in vegetation may have desirable outcomes among others increased food security and rural income, but also negative ones such as diminishing soil nutrient status or intensified erosion (Ademola, 2004; Glowa-Volta, 1999). Land-use and land-cover change also plays a role in the capacity of the vegetation layer's water transpiration function in the hydrological cycle. As most evapotranspiration in the Volta Basin in fact consists of plant transpiration and as vegetation also determines to a large extent the exchange of latent heat and momentum between the atmosphere and the earth surface, it is of great importance to have a thorough knowledge of the vegetative cover if one is to know the relation between land use and climate. Therefore, it is necessary to analyze the role of $LULC$ types and their dynamics on the variability of ET_a. In the past, estimation of evapotranspiration on local to regional scales have for long time been based on thermodynamic and meteorological ground-based measurements (Penman-Monteith method, Blaney-Criddle method, Pan-evaporation method). Nowadays, new direct methods are based on Eddy covariance and scintillometric measurements. The computational methods (temperature based, radiation based) for calculating potential evapotranspiration (ET_p), however, vary in data demands from very simple (more empirically based), requiring only information on monthly average temperatures, to complex (more physically based), requiring daily to hourly meteorological data such as air temperature, solar radiation, relative humidity, soil moisture and wind speed, as well as characteristics of the vegetation indices.

The major advantage of using meteorological station data for evapotranspiration estimation is the availability of data, their simplicity and easy computation. However, the main disadvantage of this approach is that those meteorological methods are all based on point measurements and are therefore not representative of a large area. The reference output at the station is always an integration of the influence of a number of variables depending on land-cover type, wind speed and direction and soil moisture. The estimation of ET at a regional scale is usually obtained by scaling up measurements at the point, and that opt small watershed scales by statistical analysis (Lu et al., 2003). However, those methods are often based on different mathematical algorithms thus providing different results at local to regional scales. A solution such as by providing a sufficient number of measuring sites through a river basin could be costly and not affordable for developing countries of Africa such as Burkina Faso or Ghana that are located in the Volta Basin.

Solutions to these problems can be approached in three ways:

1) Application of remote sensing methods such as energy balance equation of the land surface,
2) Utilization of existing hydrological modeling (Savenije, 1997),
3) Utilization of appropriate up-scaling methods to spatially integrate point data.

Each of these methods has its limitations, and an optimal procedure probably would be a combination of the three approaches. To maximally profit from remote sensing and hydrological modeling, data assimilating is gaining popularity in hydrological studies (Walker et al., 2001; Jhorar et al., 2002; Schuurmans et al., 2003) as well as in climate studies (Dolman et al., 2001). Extensive reviews of remote sensing flux determination methods have been presented by Choudhury (1989), Moran and Jackson (1991) and Kustas and Norman (1996).

1.2 Research objectives

1.2.1 The Glowa-Volta Project

Because of the huge size of the Volta Basin, remote sensing data is useful to study the whole area. To cover the basin, one would need about 400.000 NOAA/AVHRR pixels or 400 million Landsat pixels. For all information to be manageable in the Glowa Project, it may be necessary to reduce the spatial resolution of the study. A standard pixel size of 3 km x 3 km has been proposed for modeling and for basin-wide information exchange between different vegetations and the atmosphere and underlying soil (Glowa-Volta Project Proposal, 1999). Therefore, there is a need to study representative biophysical and agro-climatic zones across the Volta Basin for detailed characterization in order to understand and to capture the soil-vegetation-atmosphere interaction and determine hydrological processes.

The present "Subproject L4 - Vegetation Characterization and Modeling" analyses the main vegetation covers under different land-use types in all different ecological zones. It will also develop a classification scheme to capture the significant fractions of land-cover within a 3 km x 3 km pixel that can be used in hydrological modeling. For this purpose representative agro-ecological experimental sites were selected and located at (1) Edjura in the humid tropical savannah; (2) Tamale in the transitional dry Guinea-Sudanese savannah; (3) Navrongo, Kompienga and Dano representative of Sudanese savannah; (4) the Boudtenga experimental site near Ouagadougou representative of the Sudanese-Sahelian zone. This study focuses on the Sudanese – Savannah in the Navrongo area.

1.2.2 Specific objectives

The main goal of the study is to estimate the spatial and temporal evolution of actual evapotranspiration (ET_a) in the Volta Basin in relation to the biophysical and hydrological characteristics of the savannah landscape. The specific objectives are to:

- classify the savannah environment into relatively homogeneous $LULC$ types, tree density classes and hydrological units;
- assess the spatial distribution of the ET_a over the study area using the $SEBAL$ model integrated with field and remote sensing data;
- measure the hydrological contribution of principal tree species to atmospheric water vapor applying the sap flow technique;
- evaluate the temporal variability of ET_a among the main landscape components, $LULC$ types, hydrological units and tree density during the dry season.

1.2.3 Structure of the thesis

The thesis is organized in five main Chapters. Chapter 1 introduces the problem and defines the major objectives of the study. In Chapter 2, special attention will be paid to the general description of the study area. The general framework used in the study is also presented along with the main components of savannah landscape suitable for explaining the ET_a variation. Chapter 3 deals with the land classification process of the biophysical and hydrological characterization of savannah landscape using remotely sensed data. The first part is based on *LULC* classification to derive different vegetation types found in the study area. It also looks at the spatial distribution of fallow vegetation related to fire traces. The second part deals with delineating homogeneous hydrological units of similar moisture conditions applying the vegetation index temperature trapezoid (*VITT*) approach. The last part is related to an approach to deriving tree density from remotely sensed spectral vegetation indices and field data. Chapter 4 examines approaches of ET_a assessment in the study area. Firstly, the *SEBAL* model based on the energy balance method is used to compute the ET_a distribution on a pixel basis. To assess the evaporative input of water vapor from savannah biophysical and hydrological components, the ET_a, at the beginning and at the end of the dry season, this parameter is compared with *LULC* types, hydrological units and tree density classes. The final part of the chapter is concerned with the application of the sap flow technique to estimate water use/transpiration of individual trees and whole stand vegetation in savannahs. Chapter 5 synthesizes the findings of the thesis. The first data set summarizes the biophysical and hydrological characterization of the savannah landscape, while the second examines the spatial distribution of the ET_a and the parameters relationships with the biophysical and hydrological units. Third data set gives conclusions and recommendations of the study.

2 STUDY AREA AND GENERAL APPROACH

2.1 General description of the Volta Basin

The Volta Basin in West Africa has an approximate area of 400,000 km^2, within the latitudes 15° N and 4° N and longitudes 5° W and 3° E (Figure 2.1). It covers six countries: Burkina Faso, Ghana, Togo, Mali, Benin and Côte d´Ivoire. Burkina Faso and Ghana occupy more than 80% of the watershed. The main rivers, the White and Red Volta, flow from north to south to the Gulf of Guinea. Exception comes from the Black Volta that flows first south to north, and then north to south. Important tributaries to the Volta rivers are the Sourou, the Pendjari or Oti, Tono and Sissili river.

The basin has a population of about 70 million with a mean annual growth rate of 2.79% and a mean density of about 40 inhabitants/ km^2. The population distribution is varied across the six countries. In Burkina Faso, 78% and 22% of the population lives in the rural and urban areas, respectively; about 90% of the labor force is engaged in agriculture. In Ghana, population distribution varies across the country with 68% and 32% living in the rural and urban areas, respectively. About 52% of the labor force is engaged in agriculture, 29% in services and 19% in industry. Agriculture contributes 54% of Ghana's GDP and provides over 90% of the food needs of the country (SRID, 2001 GDP). The average annual income in the region is estimated at US $800 per year. For the majority of the population, rainfed and some irrigated agriculture is the backbone in the largely rural societies and the principal source of income.

The climate in West Africa is influenced by the hot, dry and dust-laden air mass, the Harmattan that moves from the north-east across the Sahara and by the tropical maritime air mass that moves from the south-west across the southern Atlantic Ocean. This movement between continental dry and maritime humid air determines the climatic conditions in West Africa (Pallier, 1981; Fontès, 1983; Guinko, 1984). Broadly, the Volta Basin is characterized by a wet tropical climate in the coastal areas. Precipitation in the south is very high with more than 1500 mm per year and at least 10 humid months; in the tropical semi-humid climate further north with 6-9 humid months it decreases to 1000-1500 mm yearly, and in the semi-arid areas in the most northern area of the Volta Basin precipitation is only 500-1000 mm per year in 3-5 humid months (Knapp, 1973). However, inter-annual rainfall varies considerably between years, and extreme rainfall events and frequency of dry spells within the growing season increase with distance to the equator (Sivakumar, 1991).

The mean monthly temperature over most of the basin in Burkina and Ghana is 25° and 35° C, respectively; mean annual temperature averages between 18° C (Burkina) and 27° C (Ghana). The absolute maxima approaches 40° C, whereas absolute minima can be as low as 15° C (Dickson et al., 1988; Benneh, 1990). In the coastal areas, where the modifying influence of the sea breeze is felt, the annual range of temperature fluctuations is between 5 and 6° C. On the other hand, in the interior of Ghana this range is higher, i.e., about 7° to 9° C.

The vegetation of the Volta Basin is characterized by complex types of forested and savannah areas, which lie between the Sahel and the Gulf of Guinea. In Ghana, the main vegetation formations as described by Benneh et al. (1990) are the Coastal Strand and Mangrove, which form the evergreen vegetation along the coastline, around lagoons and estuaries of large rivers; the Coastal Savannah in the Accra Plains with rainfall of 700-800 mm that comes in two peaks; the closed forest divided into rain forest and semi-deciduous forest with heavy rainfall of 1500-2200 mm distributed throughout the year; the interior savannah zone, which has the largest extension through the basin and comprises typically tree savannah or a continuous grass cover interspersed with generally fire-resistant, deciduous, broad-leaf trees. The total precipitation averages about 1100 mm per annum.

The savannah areas in the Burkina part of the basin have been described by Guinko (1984) and Fontès et al. (1995). The interior savannah in Ghana splits into south and north vegetation types. The south is delimited by the isohyets 900 mm with a dry season of 5 to 7 months. The vegetation is composed of tree or shrub savannah, and a few sparse forests and perennial tree plantations. The north, with at least 700 mm rainfall, tree or shrub savannah is to be found. Upstream of the Volta watershed lies the Sahelian zone with an annual rainfall between 400 and 700 mm and a steppe domain varying from thorny bushes to *Combretum* and annual grasses.

In this study, the focus is on the interior savannah or Guinea Savannah or Sudanese Savannah, which is the dominating vegetation type in the Volta Basin. The research region is the Navrongo area of the Sudanese Savannah in Upper-East Ghana. The key geographical attributes of this site are given below.

2.1.1 Geographic settings

The Navrongo area is located on the frontier between Burkina Faso and Ghana and lies approximately between latitudes 12°00´N to 10°20´N and longitudes 0°16´W to 0°16´E (Figure 2.1), covering an area of about 13427 km^2. Navrongo, located in Upper East Ghana, is an old settlement known for trade between forest areas down south and Sudanese zones up north.

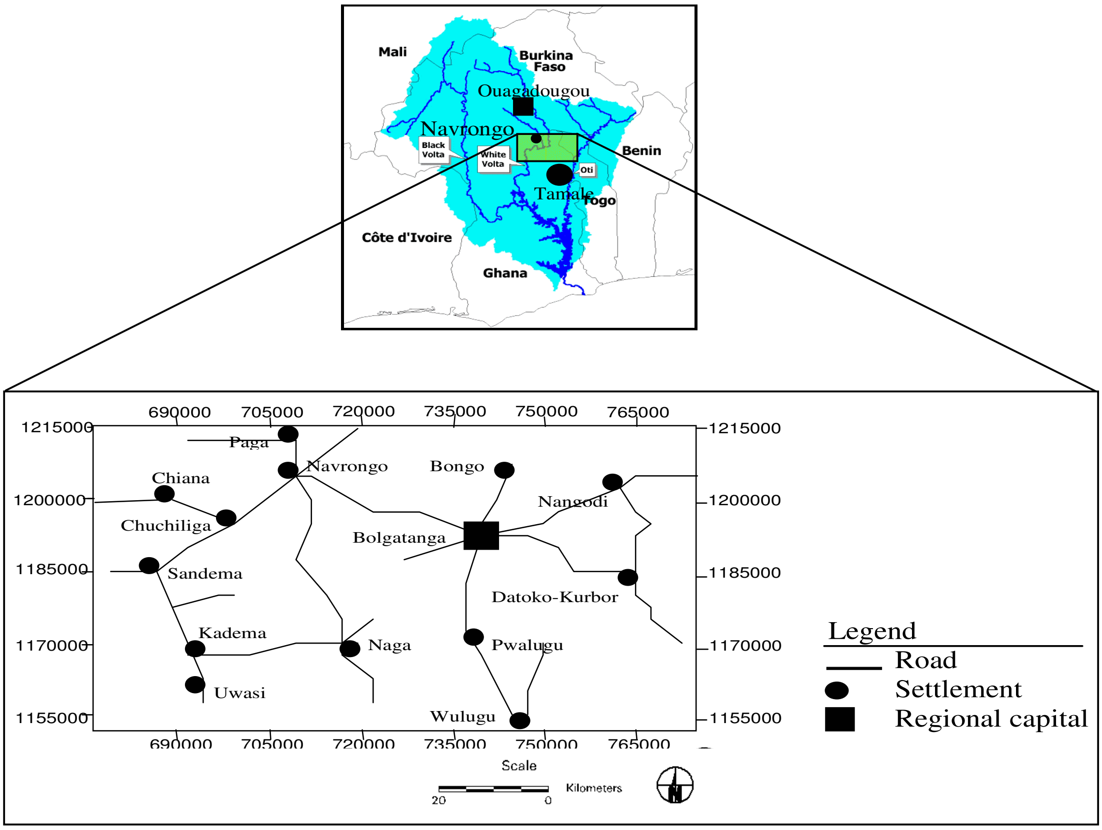

Figure 2.1: Location of the study area, Navrongo, Ghana

2.1.2 Climate

Like the entire Sudanese agro-climatic zone, the study site has a Sudanese climate, characterized by an annual precipitation level of about 1000 mm. Climate data for the Navrongo station dating back to 1961 and 2003 are shown in Table 2.1. During the last four decades, rainfall varied between 700 mm and 1100 mm annually (Meteorological Office-Ghana, 2003). Through the year, weather conditions change drastically: average monthly temperatures range from 26°C to 32°C, with the average minimum and maximum in the ranges 19°C to 26°C and 30°C to 39°C, respectively. The rainy season is mono-modal with a rainfall peak in August. The driest months are December and January; the lowest temperatures are experienced in December, while the highest temperatures occur in March. From 1961 to 2002, the potential evaporation was about 2.5 times the annual rainfall in the study area; monthly averages for relative humidity range from 16% to 95% (Navrongo Meteorological Service, 2005).

Table 2.1: Monthly climatic data in Navrongo 1961-2003

	Jan	Feb	Mar	Apr	May	Jun	Jul	Aug	Sept	Oct	Nov	Dec	Av
T (°C)	27.5	29.7	32.1	32.3	30.6	28.2	27.0	26.4	26.8	28.2	28.3	27.2	28.7
RF (mm)	0.7	3.2	15.0	50.6	102.1	129.5	188.0	273.1	168.2	51.4	3.8	2.3	986.7
WS ms^{-1}	2.2	2.3	2.2	2.5	2.4	2.0	1.8	1.5	1.3	1.3	1.4	1.8	1.9
ETp (mm)	273	312	307	248	186	134	104	89	100	151	245	269	2423

T is temperature; RF is precipitation; WS is wind speed; ETp is potential evapotranspiration; Av is monthly average (Source: Navrongo Meteorological Services)

The annual rainfall amount is marked by a high inter-annual variability that influences vegetative production. It is also characterized by a high variability that has a negative effect on crop production. In 1984, in Navrongo only 61% of the 852 mm annual rainfall fell during the cropping period June to September. In 1998, during the same period, 74% of 856 mm occurred with relative by good results in terms of production.

The Harmattan wind is an important climatic factor during the dry season in West Africa. This dry air flows from the north-east towards the south-west, coming from the high Saharan pressures or anticyclones of the Azores. This dry continental air, or boreal trade wind, is hot during the day and cold during the night. This wind is often charged with dust and is responsible for the quasi-permanent presence of dry fogs from December to March, with a concentration in aerosols from 15 to 20 mg cm^3 (Koné, 1992). This concentration can sometimes even reach 30 to 100 mg cm^3 due to violent dusts (Muller, 1985), with a visibility reduced to less than one kilometer (Kouda, 1982). Associated with the Harmattan are burning events that start with the dry season.

2.1.3 Hydrology, drainage and water resources

The White Volta, which crosses the southern part of the Navrongo area, generally flows in a north-west to south-east direction, and turns sharply west at the point where the river meets the Gambaga scarp. It is fed by a number of secondary rivers that include the Tono river in the west and the Red Volta in the north-east part of the study area

(Figure 2.2). In Navrongo, the Tono river flows north-south with the Tono dam located towards the north.

During the wet season, the vegetation, which is mainly composed of grasses, is dense and photo-synthetically active. Streams and rivers in the area are liable to sudden fluctuations in water level, suggesting that there is considerable surface run-off within their catchments during heavy rainfall. During the dry season, water flow decreases and finally stops in March. A common feature in the savannah is a series of disconnected pools in river beds separated by dry stretches of sand and rock. Humans as well as livestock suffer from shortages of domestic water that is mainly obtained from rivers, small dams, springs and boreholes. A water deficit in the soil also has an impact on the vegetation layer, which is essentially composed of deciduous tree species that shed their leaves to avoid water stress. The process is characteristic of the savannah areas, and it starts earlier in the drier Sahelian zones before reaching the more humid savannah. This situation of unbalanced spatial and temporal distribution of available water poses the crucial question of what management is best for regional development.

Hundreds of small dams have been constructed in Ghana to overcome water shortages in the dry season. In the Navrongo area, the Tono Dam is the main reservoir for irrigation water throughout the year, while small dams and groundwater from bore holes are mainly used as drinking water and for garden vegetables during the dry season.

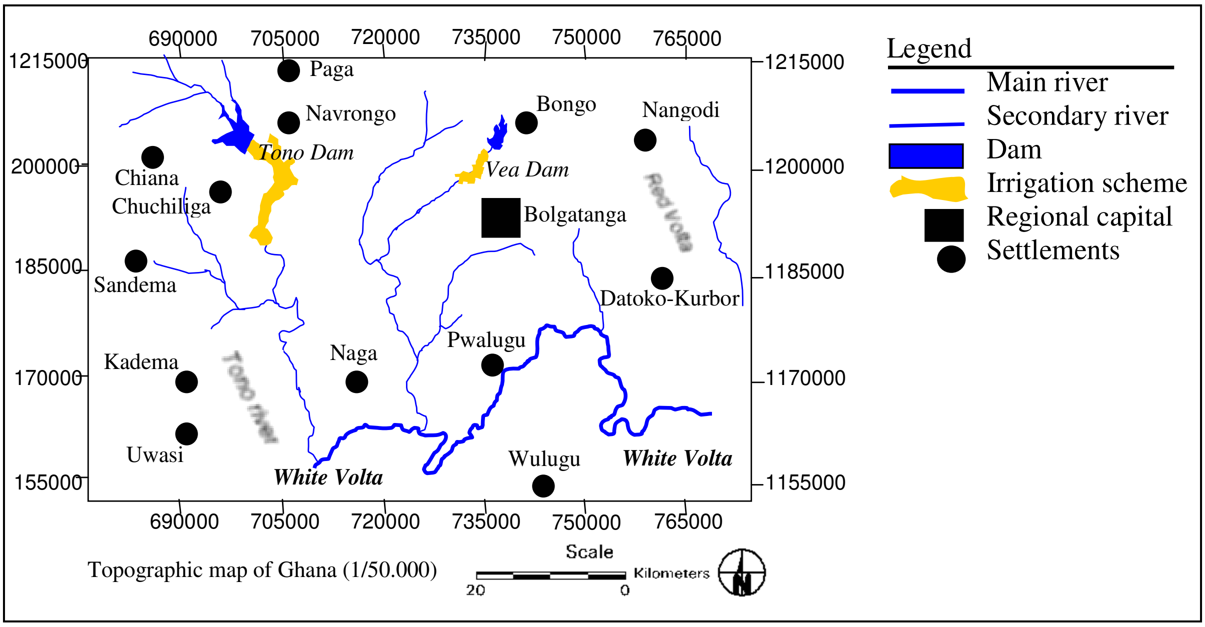

Figure 2.2: Hydrological network showing the drainage lines of Tono and the Volta river in the Navrongo area, Ghana

2.1.4 Geology and soils

The geology of the study area consists essentially of an old migmatized and granitized base with some Birrimian intrusions. Globally, the geology can be subdivided in Voltaian, Birrimian and Precambrian units as described by Adu (1969), ORSTOM (1976), Atlas du Burkina Faso (1993) and Obeng et al. (2000).

The Voltaian is represented by sandstones and shale locally confined along the White Volta river. The Birrimian is composed of metamorphosed sediments and volcanic rocks, but arenaceous conglomerates and argillaceous rocks are also to be found. The Precambrian in the area is dominated by granitic rocks described in the Navrongo as compound gneisses.

According to the geology, four main soil classes are observed. Soils derived from granites consist mainly of sandy soil in the series of Tanchera and Bongo associations. The topsoil is loose, porous, coarse textured and easy to cultivate; however, it is also easily eroded and poorly supplied with nutrients and with a low moisture retaining capacity. They are suitable for the cultivation of guinea corn, millet, groundnuts and beans (Adu, 1969; ORSTOM, 1976; Atlas Jeune Afrique, 1993; Obeng and CSIR-Ghana, 2000).

Over Birrimian rocks, the predominant soil association is the Bianya series. The topsoil is light grey silty or fine sandy clay colluvium, overlying quartz gravel and stones or weathering rock. It frequently supports sparse Acacia tree species with low covering capacity.

The Voltaian rocks are mainly covered by the Kintampo soil series, which is associated with lithosols that expose bare rock outcrops found along the Pendjari and the White Volta rivers. On these soils, the vegetative cover is poor and consists only of short grasses and shrubs.

Soils derived from Quaternary and Tertiary rocks consist of the Siare-Bonabi-Dagare series and occur extensively along the alluvial tracts of the major tributary rivers of the Volta rivers. They are deep to very deep fertile soils well suited for mechanized cultivation of rice, cotton, sugarcane and vegetables. They usually support rich woodland to gallery forests. Management of these soils is costly and example types in the area correspond to the rice irrigation schemes below the Bagré Dam in Burkina and the Tono Dam in Ghana.

2.1.5 Vegetation characteristics and land use

Different studies have analyzed the vegetation in the study area, usually with scales varying from local to regional levels. At a continental or regional scale (>1:100,000), the vegetation structure is homogeneous, whereas it becomes heterogeneous at watershed to local scale (≤1:50,000). At the regional level, the vegetation has been classified as the "transition zone between wet and dry savannah" (University of Maryland, USA), tall grass savannah (Yenik, 1994), tree savannah, savannah woodland or woodland (Letouzey, 1969), or simply as savannah (Belward, 1996; Loveland, 2000).

The original vegetation, mainly composed of deciduous trees in grassland, is largely influenced by human agricultural deforestation activities including livestock overgrazing and periodic bush fires. Moreover, this savannah is also prone to erratic climatic conditions dominated by high inter-annual rainfall variability (Nicholson et al., 2000; 1996).

The vegetation of the study area has been described by Taylor (1952 in Adu, 1969). The natural vegetation is basically composed of woodlands on varying soils. Common tree species are Anogeissus leiocarpus, (Loa in local in Mapprussi language), *Vitellaria paradoxa* (Sungu) and *Parkia biglobosa* (Dawa-dawa). *Acacia* species occur frequently and are usually found on heavy clay soils associated with old river alluvium, piedmont slopes and eroded sites. Riverain woodland fringes tenuously along the White and Red Volta, the Sissili and a few of the minor streams.

Around the populated areas of Navrongo and Bolgatanga, tree density is low as a result of land degradation and deforestation for new farms, fuel wood, building and other purposes. The main cultivated crops are cotton, tobacco, tomato, black pepper, sweet potato, millet, guinea corn, maize, cowpeas, bambara beans, cassava and yam. The agricultural landscape, composed of compound and bush farms, is an agro-forestry park with a few indigenous tree species left for their economic value. The most common tree species include *Vitellaria paradoxa, Parkia biglobosa, Acacia albida, Anogeissus leiocarpus, Adansonia digitata* (baobab), *Tamarindus indica, Mangifera indica* and *Ceiba pentandra*.

2.2 General approach

Two main steps are used in this research study. The first is a land classification of the study area using remote sensing and field data, and the second is the assessment of the actual evapotranspiration applying the surface energy balance algorithm for land ($SEBAL$). The sap flow technique was also used to assess individual tree water use. Figure 2.3 shows the details of the two approaches.

The $SEBAL$ model uses satellite images, and meteorological and field data to estimate the spatial distribution of the ET_a in the study area. In the land classification process, satellite images were successively used to map $LULC$ types, tree density and the spatial distribution of hydrological units. To estimate the hydrological role of the biophysical and hydrological components of the savannah landscape, the ET_a was extracted for each $LULC$ type, tree density and hydrological unit. To arrive at a reliable temporal integration of remote sensing method outcomes, the ET_a was related to the Penman-Monteith ET with an adjusted crop coefficient K_c for times where satellite data are not available. That allows comparison at spatial and temporal scales. To estimate the savannah vegetation cover transpiration at the land unit, individual tree water use was combined with tree density data for up-scaling. Furthermore, tree transpiration E_c was related to the reference evapotranspiration (ET_o) with an adjusted transpiration coefficient K_{bc} to estimate savannah vegetation transpiration for time without direct sap flow measurements.

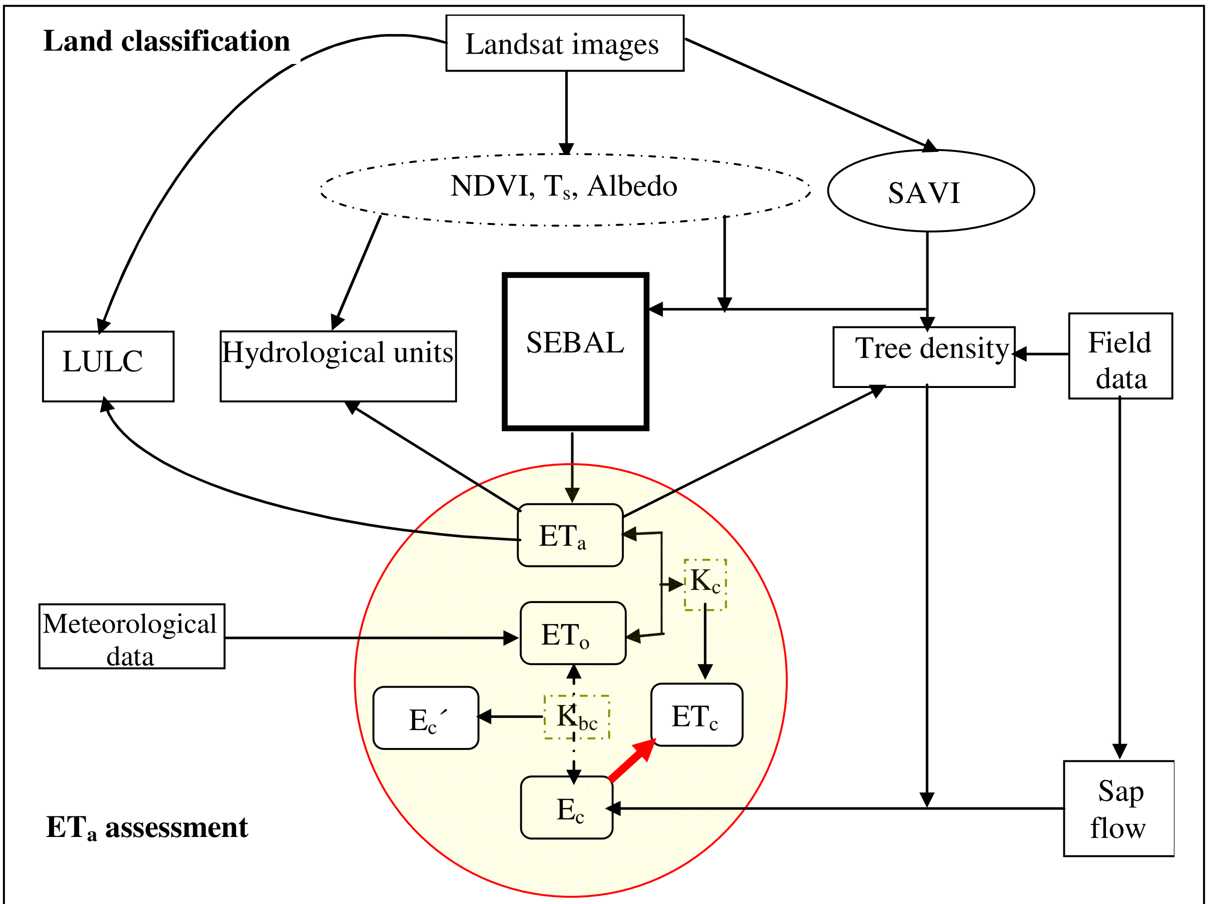

LULC is land-use and land-cover
NDVI is the normalized difference vegetation index
SAVI is the soil adjusted vegetation index
K_c is an adjusted crop coefficient
K_{cb} is an adjusted transpiration coefficient
SEBAL is the Surface Energy Balance Algorithm for Land model
T_s is land surface temperature
ET_a is the actual evapotranspiration
ET_c is the adjusted crop evapotranspiration
E_c is vegetation cover transpiration
$E_c´$ is the predicted vegetation cover transpiration
ET_o is the reference evapotranspiration

Figure 2.3: General approach followed for land classification and ET_a assessment

2.2.1 Land classification

The land classification procedure aims to spatially cluster the study area into homogeneous components, mainly considering cover types, hydrological units and tree density. Both satellite images and field data were used to achieve this goal.

Firstly, *LULC* classification was performed using high spatial resolution satellite images. Landsat images acquired for October, 2002 and March, 2003 were rectified and used for land classification. The hybrid classification approach was used to generate the *LULC* classes. In all, 11 *LULC* cover types were generated using the above method.

Secondly, a land delineation approach was used to cluster the savannah landscape into different hydrological units of similar wetness conditions on the basis of the vegetation index temperature trapezoid (*VITT*) concept. The process of hydrological unit delineation consists of combining remotely sensed spectral data of surface temperature (T_s), surface albedo (α) and normalized difference vegetation index (*NDVI*). The different maps were clustered using the unsupervised classification algorithm and the resulting maps were reclassified following the approach by Farah (2001).

Finally, an attempt was made to estimate tree density based on remote sensing and field data. The Soil adjusted Vegetation Index (*SAVI*) was used to characterize the study area into different tree density classes. The *SAVI* images were then calibrated using field data to estimate tree density for the whole study area.

The main objective of the land classification approach is to derive from remote sensing spectral data relatively homogeneous biophysical and hydrological land units in the savannah ecosystem. These land units will be later related to the Surface Energy Balance Algorithm for Land model (*SEBAL*) actual evapotranspiration (ET_a) spatial and temporal distribution in the Navrongo area.

2.2.2 Actual evapotranspiration (ETa) assessment

The ET_a and the potential evapotranspiration (ET_p) data are the two types of evapotranspiration required to estimate the real input of water from land surfaces to the atmosphere. Actual evapotranspiration can be defined as the quantity of water that is actually removed from a surface due to the processes of evaporation and transpiration, whereas ET_p is a measure of the ability of the atmosphere to remove water from the surface through the processes of evaporation and transpiration assuming no limitation on water supply. Such information is needed for the practical purpose of water resource management to determine the amount of water used by different cover types.

The ET_a assessment approach comprises two parts. First, a remote sensing technique is applied using the Surface Energy Balance Algorithm for Land (*SEBAL*) developed by Bastiaanssen (1998a, 2000). The aim is to derive actual evapotranspiration from selected satellite images from the dry season (2002-2003). The *SEBAL* was selected because of its robustness and its low demand for input data and routine weather station data. Furthermore, the remote sensing techniques compute evapotranspiration directly from the energy balance equation without having to consider other complex hydrological processes, which could mitigate calculation errors.

Due to extremely scarce ground meteorological data in the Volta Basin savannahs, utilization of high spatial resolution satellite imagery is an attractive approach. Advanced remote sensing sensors such as the Landsat7 ETM+ using thermal bands have a high potential to estimate hydrological processes at the land surface. However, a major limitation of remote sensing data is that the temporal distribution of satellite-based estimations is poor, and that interpolation techniques with reference station data are necessary to define evapotranspiration between satellite overpasses (Tasumi, 2000; Farah, 2001). Another limitation lies in the estimation of the surface temperature using the energy balance. While the energy balance approach has been found to be successful over surfaces with near full canopy cover with unstressed transpiration, its performance has been questioned over sparsely vegetated surfaces or bare land. This is because over such heterogeneous surfaces, remotely sensed surfaces temperature cannot be assimilated to aerodynamic surface temperature, which is the quantity needed to formulate convective fluxes (Chehbouni et al., 1997).

The *SEBAL* model minimizes some of these limitations and considers a linear relationship over the entire raster image by defining dry and wet anchor pixels for such analyze (Bastiaanssen, 1998a; 2000). Furthermore, the model has been applied in many areas of different climatic conditions, e.g., in Egypt, USA, Spain, and Pakistan but not yet in the West African savannah environment of the Volta Basin. The *SEBAL* model, due to its robustness, has been for this study selected and will be applied over an arid environment with sparse vegetation.

Another approach to obtain data on input of vapor water into the atmosphere is a method based on tree density and individual tree water transpiration measurements using the sap flow technique. The transpiration of the vegetation layer is a critical component in the physiology of plants, the hydrologic cycle, and the surface energy balance. The use of water by plants is linked to their growth and survival. In turn, the amount of water transpired directly affects a host of landscape processes related to the availability of water. Therefore, there is a need for management issues to accurately estimate the water use rate of the vegetation layer. Because of the need to know the role of the savannah vegetation in the variation of the atmospheric water content in the Volta Basin, the application of the sap flow technique may be the best way to assess individual tree transpiration at the local scale. The sap flow technique is a method to measure the ascent rate of sap in the sapwood (xylem) by estimating sap flow velocity and the flux of water through the plant.

For the past decade, several sap flow equipments have been marketed commercially (Smith and Allen, 1996). These include (1) heat pulse velocity (HPV; Green et al., 2003; Caspari et al., 1993); (2) trunk segment heat balance (THB; Cermàk and Deml, 1974; Kucera et al., 1977; Cermàk et al., 1973, 1982); (3) stem heat balance (SHB; Sakuratani, 1981, 1984; Baker and Van Bavel, 1987); (4) heat dissipation (HD; Granier 1985), (5) Heat field deformation (HFD; Nadezhdina et al., 1998; Nadezhdina and Cermàk, 1998).

The acceptance and utility of sap flow results beyond the research community has been limited due to different technical problems (Bauerle, 2002) such as the disruption of the normal flow of water through the xylem (Smith and Allen, 1996) or the presence of the heater probe that affect the quality of the measurements (Olbrich, 1991; Smith and Allen, 1996). Alternative methods of correction have been proposed for improving the outcomes of the sap flow technique (Do and Rocheteau, 2002). The sap flow methods can be used continuously for long periods of time and provide an accurate method for determining the vapor flux from the dry canopy in a forest stand (e.g., Cermàk and Kucera, 1987; Granier et al., 1990; Diawara et al., 1991).

The Granier method, which is considered to be easy to use and inexpensive, has often been used successfully in temperate and tropical countries in Australia and Africa (Botswana: Timmermans, 1999; Lubczynski, 2000; Ghana: Oguntunde, 2004). The Granier method will be applied in the present study to assess the hydrological role of natural tree species in the Volta Basin.

The main focus in the general approach, based on land classification and the ET_a assessment steps, is the development of meaningful relationships between computerized land units from remotely sensed products, results of the *SEBAL* model applying the energy balance, and ground truth data collected during field surveys. The ultimate goal will be to understand the relationships between the land units and the ET_a. Since it is cumbersome to utilize this approach for estimating water vapor loss to the atmosphere, the proposed methodology looks at the spatial and temporal distribution of the ET_a derived from the *SEBAL* model according to the biophysical and hydrological components of the savannah. For each of the remotely sensed spectral features, a statistical regression analysis will be run in order to identify a valid relationship between ET_a values and the computed land units.

3 BIOPHYSICAL AND HYDROLOGICAL CHARACTERIZATION OF THE SAVANNAH LANDSCAPE IN NAVRONGO, GHANA

3.1 Introduction

Landscape, under the ecological concept, can be seen as an interacting mosaic of patches or ecosystems relevant to the phenomenon under consideration (McGarigal and Marks, 1995). A landscape element is defined as the smallest discernible object in the observed environment such as trees, water bodies, towns as well as agricultural parcels, and forest stands (Forman and Godron, 1986). This definition is a very flexible one in the sense that landscape elements can be very different depending on the scale of the observed environment, e.g., landscape elements in a high resolution satellite image such as QuickBird differs greatly from landscape elements of Landsat TM imagery.

Landscape classification is the arrangement of land units into various categories based on the properties of the land or its suitability for some particular purpose. The purpose of the land classification is to distinguish land areas that differ from one another in ecological, hydrological or climatic characteristics. However, land classification may be qualitative with a much more subjective approach to determining the limits of landscape units that may not be suitable for ecological studies. Therefore, it is necessary to obtain quantitative information from landscape elements for several purposes, e.g., leaf area index (LAI), $LULC$, land-surface temperature, hydrological maps. The landscape element in this case is a spatial object with several parameters, which needs to be analyzed. However, in many applications not only the landscape elements are important but also the interaction between the landscape elements. Some examples are the nitrogen and phosphor cycle in a landscape, as well as the water cycle, which depends, for example, on the attribute "land-cover" of a landscape element.

A combination of physical and biological factors, such as climate, geology, topography, soils, water and vegetation are used to classify different landscape attributes. These factors are known to control or influence biotic composition and ecological processes. Together, they provide a useful approximation or estimation of ecosystem potentials. Remote sensing data provides an opportunity to study environmental issues at spatial scales ranging from local to regional (Barnsley et al., 1997). Remote sensing data are considered to be very effective and useful for classifying the complexity and heterogeneity in the landscape elements (Curran et al., 1997).

In this study, a remote sensing approach with integrated field data will be employed to classify the savannah landscape in the Navrongo area into relatively homogeneous biophysical and hydrological entities. Landsat images acquired for the years 2002 and 2003 were georectified and used in the classification procedure. For the adopted land classification approach, a pixel-based analysis using the maximum likelihood algorithm was employed. The results of the remote sensing approach were calibrated and tested using field data. The main approach used in the land classification considers the landscape components in terms of *LULC* types, tree density and hydrological units to study the role of the savannahs in the spatial and temporal variation of the actual evapotranspiration.

3.2 Materials and methods

3.2.1 Land-use and land-cover (LULC) classification

Remote sensing data preparation

Landsat7 ETM+ images of the dry season (October 2002) were used to map the *LULC* in the Navrongo area. The data were geometrically rectified and registered to Universal Transverse Mercator (UTM) projection to enable comparisons with other referenced datasets of the area. The UTM 30 north and WGS 84 spheroid datum were applied during projection. Georeferencing was done using image-to-image registration, with the Landsat7 ETM+ image from 30 October, 2002, used as the master image for the other Landsat images, 7 November, 1999 and 7 March, 2003, the ASTER image from 14 December, 2001, and the QuickBird subset image of 14 October, 2004. The resultant root mean squared errors (RMSE) in the geometric correction were about 6 m or 0.20 pixels for the images dataset. For all cases, the rectification results agree with the proposed acceptable values of 1.5 pixels or 0.20 pixel accuracy (Townshend et al., 1992; ERDAS Imagine, 1999).

To help the field survey, an unsupervised classification was run on a Landsat image for November 1999 to estimate the spatial distribution of the *LULC* types in the study area. The terms land-use refers to how the land is used by human beings, whereas land-cover refers to the biophysical materials found on the land (Jensen, 2000). A list of

17 *LULC* types was produced according to the United Nations Educational, Scientific and Cultural Organization (UNESCO) classification scheme (UNESCO, 1973) and examined in the field (Table 3.1).

Land-use and land-cover classification scheme

For the present study, it was necessary to develop a classification system or scheme to capture the whole vegetation organization of the study area. The classification scheme used in this study is derived from the Food and Agriculture Organization of the United Nations (FAO, 1997) land-cover classification methodology that comprises a dichotomous and a modular hierarchical phase. The dichotomous phase that describes the landscape structures was applied for the characterization of the natural terrestrial, aquatic and cultural cover. Then the UNESCO (1973) classification was modified and used (Table 3.2) to describe the savannah vegetation cover.

Table 3.1: Land-use and land-cover types defined during fieldwork in the Navrongo area, Ghana (Source: modified from UNESCO, 1973)

Land-use land-cover types	Description
1. Cultivated park land	Agricultural land under park savannah
2. Agricultural degraded land	Eroded bare agricultural land
3. Bare-land	Areas where vegetation cover is less than 5%; does not support any vegetative layer
4. Outcrop rocks and laterite	Exhumed stones and rocks on the land surface iron pans
5. Grassland	Areas dominated by grass, grass-like, or forb vegetation or shrub component with *Combretum glutinosum*
6. Shrub-land	Areas dominated by shrubs that generally exceed 0.5 m in height, and a canopy cover of 26% or more
7. Open savannah	Mixture of open and dense savannah
8. Fallow	Temporarily abandoned cultivated land
9. Woodland	Areas dominated by trees with a total canopy cover of 26-60% with a grass or shrub undergrowth layer
10. Closed woodland	Areas dominated by trees with a total canopy cover of 40-60% with a grass or shrub undergrowth layer
11. Reserves and plantations	Protected areas and crop tree areas
12. Forest	Continuous stand of trees with interlocking crowns; canopy cover of 61% or more
13. Gallery forest	Tree formations developed along the river banks in the middle of shrub or grass vegetation
14. Rice fields	Irrigated rice fields
15. Dams	Included small and large reservoirs
16. Rivers	Main and secondary streams
17. Built-up areas, towns	Settlements, roads

This classification scheme is used for two main reasons. First, it offers a concise hierarchical grouping that is based primarily on vegetation physiognomy in the landscape. This helps to understand the relation soil-vegetation-atmosphere. Secondly, the physiognomic classification as a quantitative approach is important for the present study, because there is a need to relate the vegetative structure of savannahs to the input of water into the atmosphere. In this study, the savannahs are classified according to vegetation structure and organization on one hand, and on the other to the hydrological component in terms of tree species composition, tree physiology, vegetation structure and climate. More information can be found in Mueller-Dombois and Ellenberg (1974) about the UNESCO classification scheme and the physiognomic approach to vegetation classification.

Table 3.2: Land-Use and Land-Cover Classification Scheme in the Navrongo area, Ghana

AFRICOVER dichotomous phase			Modified UNESCO (1973)	
Level 1	Level 2	Level 3	Description	LULC classes
Vegetated	Vegetated terrestrial	Cultivated terrestrial	Farms	1. Farmlands
			Farm bare soil	2. Bare-land
		Natural and semi-natural vegetation	Savannah and fallow land	3. Closed woodland
				4. Woodland
				5. Open savannah
				6. Park savannah
				7. Shrub-land
	Aquatic or regularly flooded vegetated land	Cultivated aquatic	Irrigation scheme	8. Rice fields
		Natural and semi-natural aquatic vegetation	Gallery forest, Forest, Reserves	9. Gallery forest/reserves
Non-vegetated	Terrestrial non-vegetated	Built-up and associated areas	Artificial cover	10. Built-up areas, towns and outcrop rocks
		Bare areas	Bare rock areas	
	Aquatic or regularly flooded non-vegetated land	Artificial water bodies	Reservoirs, canals, dams	11. Dams and rivers
		Inland water	Rivers, lakes	

Modified from UNESCO (1973) and FAO (1997)

Classification algorithm and accuracy assessment

After the classification scheme had been defined, the method of Combining an Unsupervised algorithm and Training data (CUT), also known as hybrid classification, developed by Chen et al. (1997) was adopted in order to classify the satellite spectral data and derive *LULC* types. The hybrid classification involves successive use of both unsupervised and supervised techniques for deriving *LULC* maps. Supervised classification technique requires training data from the land cover to be known (Mausel et al., 1990), while the unsupervised classification is essentially based on automatic clustering of the statistical characteristics of pixels (Chuvieco, 1996; Jensen, 1996). Supervised techniques are based primarily on much more input data from the analyst, essentially data collected during field surveys, and representative training samples, and the generation of graphic methods for feature selection (Lillesand and Kiefer, 2000). However, the supervised classification method using the maximum likelihood procedure has the underlying assumption of a normal distribution of the data within each class. Therefore, supervised classification may present some limits for multimodal classes (Richards, 1993). On the other hand, the unsupervised technique requires minimal input of information from the analyst, although knowledge about the study area is of importance for labeling spectral clusters into *LULC* classes (Landgrebe and Biehl, 1995). The assumption in the unsupervised technique is that each spectral class corresponds to one and only one *LULC* category and vice versa (Lark, 1995).

Hybrid classification approaches that improve the accuracy of an unsupervised algorithm by employing training data have been successfully used (Chen et al., 1997; Estes et al., 1983; Townshend, 1992). The hybrid classification is based on the unsupervised classification algorithm to generate spectral classes. The spectral classes are then carefully merged according to *LULC* categories by using training data. Prior to the final classification, the signature file is derived by applying the maximum likelihood algorithm and tested through class separability (Jensen, 1996). As the analyst has a relative freedom in this processing type, hybrid classification has been found appropriate for classifying complex landscapes (Lucas et al., 1998; McCracken et al., 1999) such as the mosaic of vegetation patches in the Volta Basin (Glowa-Volta Project Proposal, 1999). In this study, 11 *LULC* classes were produced for the Navrongo areas. Each land unit of the map was described using field data collected during field surveys in 2002-2003. The land use and land cover of the study area mostly consists of agricultural land and natural savannahs (Glowa-Volta Project Proposal, 1999; Ademola, 2004; Duadze, 2004).

The accuracy of the classification results was checked and validated using an error matrix. The error matrix compares the relationships between reference data of pre-selected sites visited during fieldwork and the spectral classified results category-by-category. Part of the field data were used first for a training area for assessing the validity of the maps, indicating either how accurate a given area in the landscape can be mapped (producer's accuracy) or how accurate a given pixel from the raster image can be related to the studied area (user's accuracy).

3.2.2 Vegetation characterization: field survey and remote sensing approach

Field survey for LULC type characterization

To collect field data on vegetation type characteristics, 204 sample points were selected according to stratified random sampling. This method was chosen to ensure that a certain number of sampling points are assigned to each vegetation class while maintaining a random element (Campbell, 1987). A total of 204 plots of 100 m x 100 m were sampled in October, November and December of 2002 for the *LULC* classification. Later in the dry season, an additional survey was conducted in March-April 2003 to record tree density. Furthermore, historical information on *LULC* was also obtained from interviews with local populations in Navrongo.

The following parameters were recorded for each sample plot in the field.

1) Density, abundance and species composition using quadrats and corridor methods. These two methods were used to estimate the abundance and species composition of single tree stems present in the sampling area. To determine quadrat density, the number of plants encountered in a given strata were counted and the average trees per hectare calculated. The samples were described and geographically located using a Global Positioning System (GPS) receiver.
2) Tree stand mean height was recorded using a Blume-Leiss altimeter (2.5 % error) and tree diameter at breast height (Dbh; 1.30 m) was measured using a caliper.
3) Canopy mean width was measured in two directions, i.e., north-south and east-west. Then the average width (D) was calculated by fitting a regular hemispheric shape to estimate crown area, as common tree species present this general shape. Crown area (CA) is expressed as follows:

$$CA = \pi * r^2 / 4 \quad (3.1)$$

where CA is crown area (m^2), r is mean crown array (m) vertically projected on the ground.

4) Root architecture of the main tree species was assessed in three other locations of the Volta Basin. A tractor excavation method that consisted of pushing down trees was explored on a road works in the Dano-Dissin area in June 2003. Because fine roots usually remained in the soil, the expression effective root distribution is used in the description. In Kompienga and Navrongo, roots were dug exhaustively to assess maximum lateral root length and tape root depth.
5) To account for phenological change of the principal tree species in the Navrongo study area, field measurements of leaf area index (LAI) were carried out using a plant canopy analyzer (LAI-2000, Li-Cor Inc., Lincoln, NE). Bi-weekly measurements of LAI were conducted from February to December, 2003, at the test

site to monitor temporal change in tree phenology. This may allow a better understanding of crop development stage during the dry season. For each sample tree, four LAI measurements were calculated by averaging the individual estimates of LAI to take into account sky condition and canopy architecture variation. Six to ten trees per species were selected for measurements.

Ground measurements of burnt traces in fallow vegetation

Identification and mapping of fallow areas are useful to estimate the impact of burnt areas on the actual evapotranspiration (ET_a). Detection of burnt areas could help identification and mapping of fallow areas. There are widespread fallow areas in the study area and field mapping of all will not be possible using standard methods of land classification. Difficulties arise as burnt traces exhibit properties similar to other land surface units (open water and laterite) in the visible, near-infrared and shortwave infrared bands. Methods based on visual and automatic classification have been used to map them, but some confusion still exists. There is a need to separate burnt traces from other landscape components as these play a singular role in the variation of the energy fluxes in general and the latent heat responsible for evaporation in particular. Utilization of remote sensing data (ASTER) could help facilitate such task. To calibrate the spectral values of burnt/fallow areas represented in the satellite images, representative fallow areas were visited in the field and GPS recordings were taken.

Field measurements of surface albedo and temperature of burnt traces

Field measurements of surface temperature and albedo were conducted for inter-comparison of the fallow areas visited between 9:00 am and 14:00 pm. This time period was chosen as it ensured a sufficient radiation level and overpasses of major satellite sensors over the area.

A silicon pyranometer was used to measure both incoming ($K^{\downarrow}$) and reflected radiation ($K^{\uparrow}$). The sensor was attached to the end of a 1-m-long steel tube that extended almost horizontally (about 1°) over the measurement point. The tube and sensor were supported by the operator and positioned close enough to the surface for efficient measurement of $K^{\uparrow}$. For the measurement of $K^{\downarrow}$, the sensor was immediately oriented upright and readings recorded. Based on these measurements, albedo (α) was calculated using the following expression:

$$\alpha = \frac{K^{\uparrow}}{K^{\downarrow}} \tag{3.2}$$

Surface temperatures were measured using a handheld infrared thermometer. At each target point, 4 measurements were taken around relatively homogeneous sites.

Remote sensing application to burnt traces

One scene of 60 km x 60 km ASTER Level 1B (calibrated radiance-at-the-sensor data) imagery was acquired on 14 December, 2001, from the Earth Observing System Data Gateway (EDG) (online search and order facility http://edcimswww.cr.usgs.gov/pub/imswelcome).

The high spectral resolution remote sensing data was applied to identify and map fallow/burnt areas. A false color composite (3-2-1) image of the ASTER was used to assess burnt traces in the Navrongo area. Because ASTER has large spectral extension in the shortwave infrared (SWIR) and thermal infrared (TIR) zones, principal component analysis (PCA) was applied for enhancing the data and for reducing the amount of redundant information among individual bands of the multispectral image. PCA comprises the linear transformation of a set of numerical variables to create a new variable set with principal components that are uncorrelated and are ordered in terms of the amount of variance explained in the original data without a priori physical interpretation of the principal components (Eastman and Fulk, 1993). Unlike the original bands on which PCA is performed, the resulting principal components (PC) or neo-bands show a different spatial structure from one another that may be useful in explaining a phenomena distribution.

Image enhancement techniques based on PCA resulted in three best neo-bands in the SWIR (PC_{SWIR}) and TIR (PC_{TIR}), which were used as input bands. From the three bands, the first two from each two (PCA1 of the SWIR and PCA1 of the TIR) from the spectral enhancement were converted to image files and visually inspected in relation to burnt traces distribution on the original image and in field information. The results of the spectral enhancement are presented in the Figure 3.1.

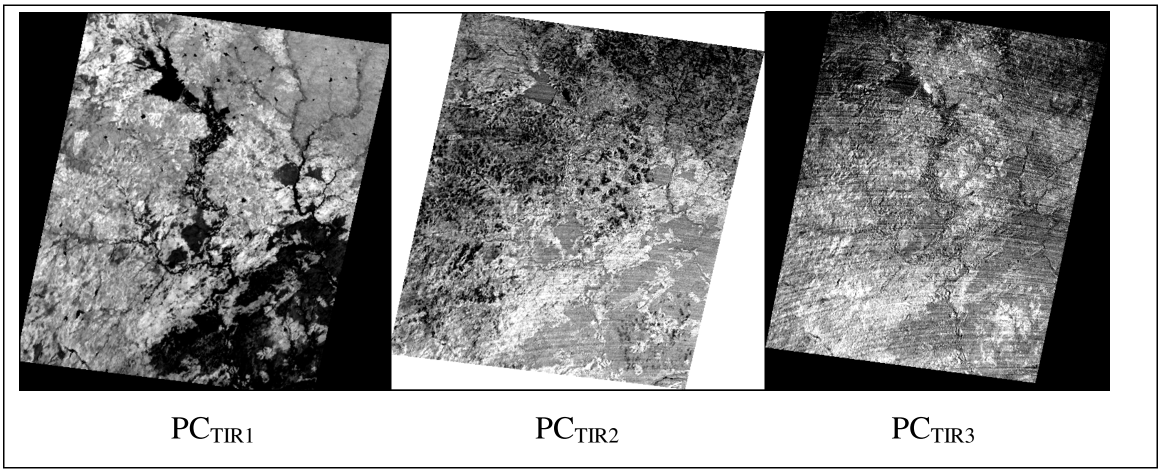

(a)

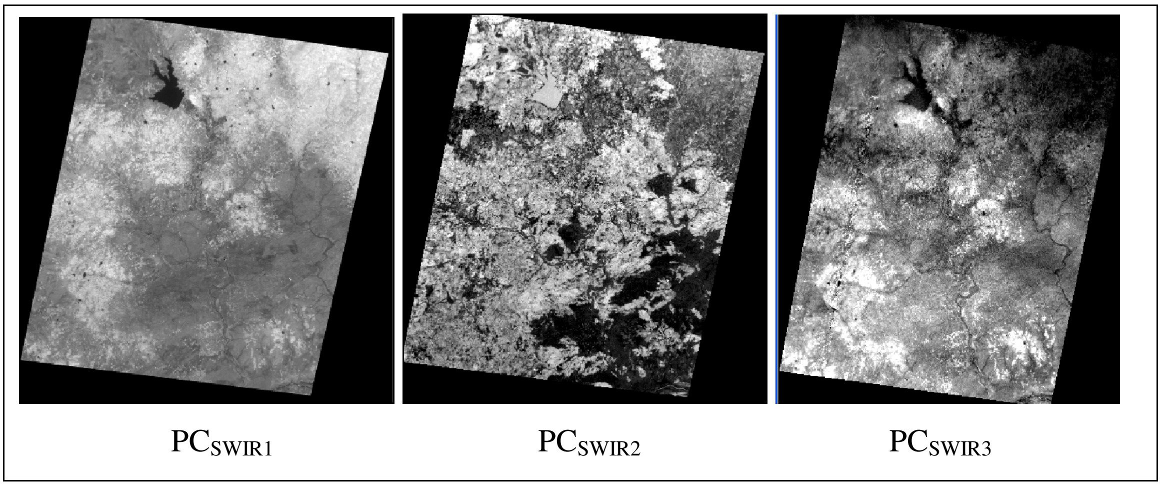

(b)

Figure 3.1: (a) Best neo-band images prepared using PC_{TIR}: three first PC_{TIR}-derived bands using ASTER bands 10-11-12-13-14;
(b) Best neo-band images prepared using PC_{SWIR}: three first PC_{SWIR} derived bands using bands 4-5-6-7-8-9.

In the PC_{TIR} neo-images, bright pixels are the thermal component of the ground layer symbolized by the burnt traces location, while the dark ones represent non-burnt areas such as bare-land and green vegetation. The PC_{TIR1} images, accounting for 95.5% of the raw bands, clearly shows clearly burnt areas, while the other PC_{TIR} images show artifacts of low quality data. The PC_{SWIR1} images, with 98.9% of the raw data, on the other hand enhances well the photosynthetic activity of green vegetation depicted by dark (including water bodies in black) and white pixels representing bare-land and farms. The best bands for burnt traces detection in both cases are therefore PC_{TIR1} and PC_{SWIR1}. On the other hand, the PC_{TIR2} and PC_{TIR3} and the PC_{SWIR2} and PC_{SWIR3} images displayed mixed responses with artifacts in the neo-images and were rejected from the analysis. Visual interpretation of the enhanced images also shows that PC_{TIR1} and PC_{SWIR1} depict better the distribution of burnt and vegetative areas. These improved neo-bands were subsequently combined with the original band in the NIR to build a burned areas false color composite image (Figure 3.1). The composite image was classified to detect burnt areas. Finally, the classified maps were compared with ground truth data.

3.2.3 Hydrological units delineation

Delineation of hydrological units in the study area is of great importance for studying the wetness conditions in the savannah landscape in general and especially the contribution of the vegetation layer in the spatial distribution of the ET_a. The process of delineating hydrological units consists of combining remotely sensed data of $NDVI$, surface albedo (α) and surface temperature (T_s) (Farah, 2001). Landsat7 ETM+ data acquired at the beginning of the dry season (October, 2002) and end of the dry season (March, 2003) were used for extracting vegetation indices, α and T_s for the landscape of the Navrongo savannah region through the $SEBAL$ model (Bastiaanssen, 2000).

Many studies have focused on the widely observed negative correlation between T_s and remotely sensed measurements of vegetation indices, such as the $NDVI$ (Nemani and Running 1989; Hope and McDowell 1992, and Moran *et al*. 1994). One hypothesis explaining this correlation is that the relationship between T_s and $NDVI$ is an indicator of evaporative cooling by plant transpiration. Studies have proven that under specific conditions, the radiative temperature (T_{rad}) can be related to $NDVI$ (Goward et al., 1985) and to α (Menenti et al., 1986). This finding was then developed into the concept of $VITT$, observing that the T_s gives a measure of evaporation, relative to maximum evaporation, in constant green vegetation (Moran et al., 1994). Lambin and Ehrlich (1996, 1997) used the combination of T_s and $NDVI$ in the $VITT$ diagram (Figure 3.2) to show the fractional vegetation cover, soil moisture condition, and evapotranspiration.

Figure 3.2 shows the relationships between T_s and $NDVI$ reflecting different land wetness conditions and vegetation cover as proposed by Lambin and Ehrlich (1996). A maximum vegetative cover and low T_s corresponds to a maximum moisture and transpiration, whereas a high vegetative cover associated to high T_s indicates vegetation under water stress; low vegetative cover associated to high T_s is related to warm dry bare soil. In contrast, a low T_s combined with a low vegetative cover is synonymous of saturated bare soil.

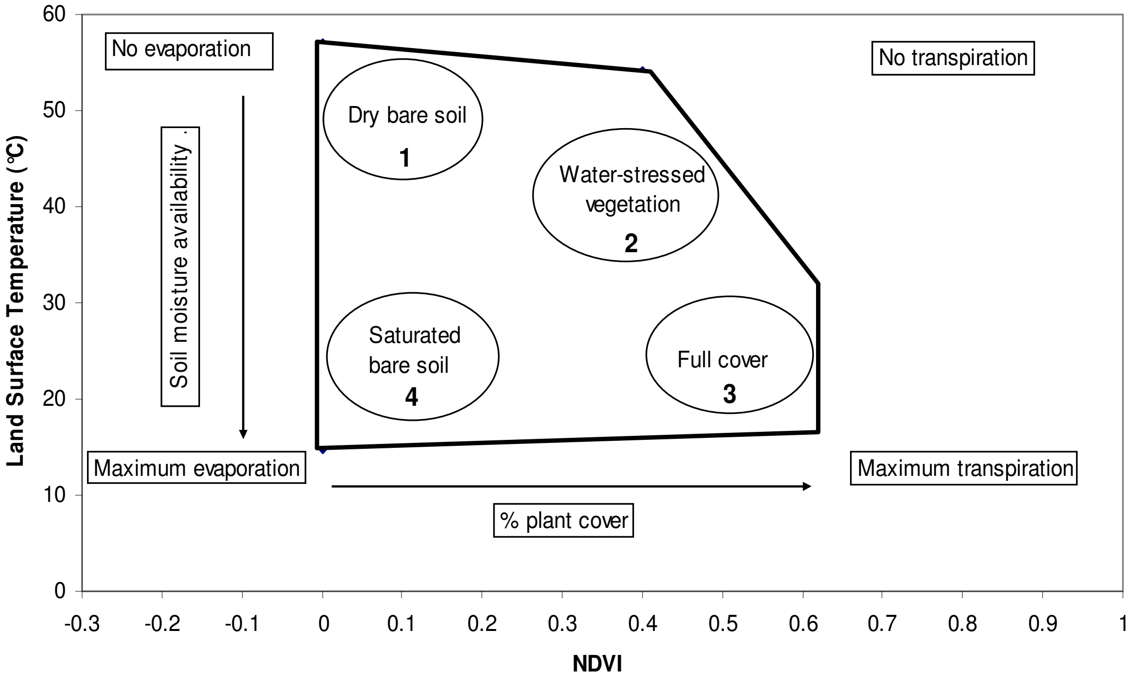

1. Dry bare soil with little evapotranspiration
2. Water stressed vegetation with variable evapotranspiration
3. Full cover vegetation showing maximum transpiration rate
4. Saturated bare soil with maximum transpiration rate.

Figure 3.2: Vegetation Index-Temperature Trapezoid diagram (Source: Lambin and Ehrlich, 1996)

Recently, Farah (2001) used the $NDVI$-α-T_s combination in a three-dimensional space to delineate homogeneous hydrological units in a heterogeneous watershed in Kenya. Figure 3.3 shows the relationships between $NDVI$, α and T_s, to reflect different land-wetness conditions and vegetation cover. Qualitative interpretation of the hydrological and vegetation status of sub-areas can be made such that low T_s, low $NDVI$ and low α indicate bare wet soils, whereas high T_s, low $NDVI$ and high α represent the warm dry bare soil pockets. Low T_s, high $NDVI$ and low α indicate healthy vegetation in good condition with unstressed transpiration, whereas high T_s high $NDVI$ and high α point to vegetation under water stress. As T_s, $NDVI$ and α can be derived from Landsat TM images, these biophysical parameters are combined and used to delineate the savannah landscape in Navrongo into hydrological units following the approach described by Farah (2001).

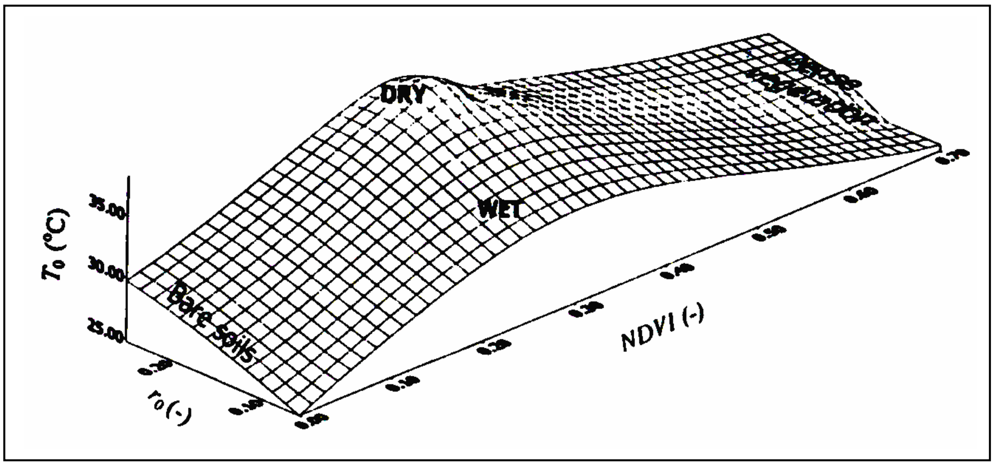

Figure 3.3: Relationships between NDVI, albedo and temperature (Modified from Farah, 2001)

The three spectral layers ($NDVI$, α, and T_s) were combined into one composite image that depicts the moisture conditions of the area. Before performing the clustering analysis, an exploratory diagram of the $NDVI$ and the T_s from field sample points was examined to obtain a preliminary insight of the moisture conditions in the study area (Figure 3.4). Because moisture training data were not taken, an unsupervised classification algorithm based on ISODATA was applied to generate spectral clusters. In order to conform to the number of $LULC$ clusters and generate representative hydrological units to each of the clusters, 11 classes of hydrological units were extracted. Description of the hydrological spectral clusters obtained by the unsupervised classification procedure based on the $VITT$ $NDVI$, α and T_s parameters enables assigning each cluster to one of the four moisture and evapotranspiration levels previously described.

Figure 3.4 shows the distribution of T_s and $NDVI$ data extracted from Landsat images acquired in October, 2002 and March, 2003 based on field sample points. The data representing October (Figure 3.4) are located towards the vertices point 3 indicating well watered and highly transpiring vegetation. In contrast, the data points collected from the Landsat image acquired in March (Figure 3.4) are mainly distributed around the vertices point 1, symbolizing the presence of more dry warm bare soil. This is in good agreement with the distribution shown in “trapezoid diagram” (Figure 3.2).

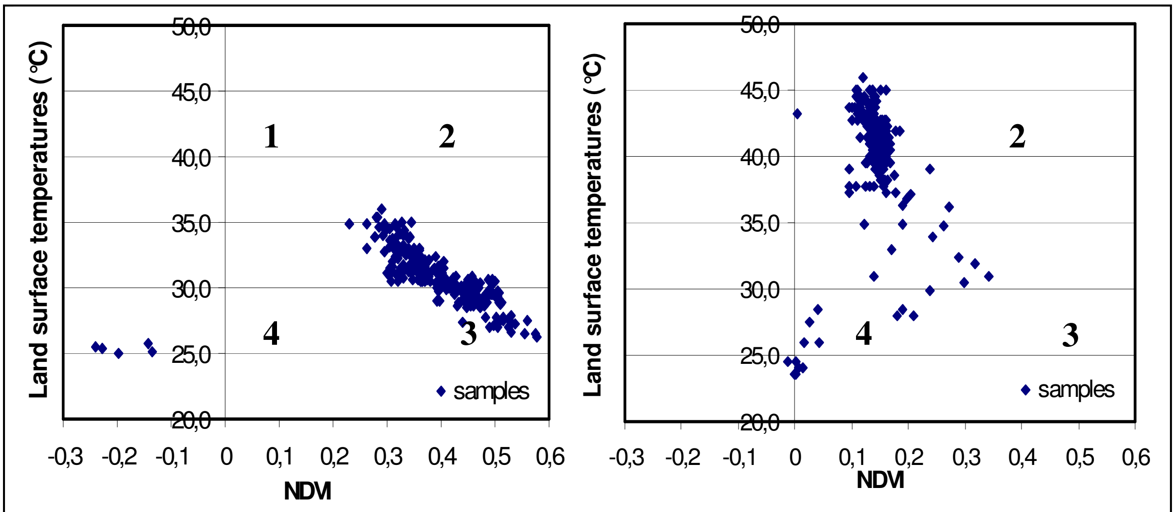

Figure 3.4: Evapotranspiration and moisture conditions during October and March for the Navrongo area, Ghana.

3.2.4 Tree density mapping

An accurate estimation of tree density in savannah areas is of great importance for studying the hydrological role of savannah vegetation in general and especially the spatial distribution of the ET_a. To map tree density in large areas, remote sensing has become a reliable technique based on satellite images with various spatial and temporal resolutions. The image interpretation usually consists of automatic or visual interpretation methods depending on the objectives, the scale and the accuracy required for the final map. The alternative approach used in the present study integrates a calibration method based on field reference data to map tree density from Landsat7 ETM+ spectral vegetation indices in the Navrongo area, except in the case of open water.

One major precondition for the study was the selection of a vegetation index that minimizes the influence of external effects such as soil background, atmospheric scattering, water vapor absorption, aerosols and view angles on the remotely sensed spectral data (Galvao et al., 2004). Vegetation indices have been shown to be positively related to biophysical variables such as leaf area index, absorbed photosynthetically active radiation, herbaceous net primary production (NPP), and crop yield (Tucker, 1979; Prince, 1991; Rasmussen, 1996). However, growing season vegetation indices may be highly correlated with photosynthetically active grasses (Hobbs, 1995; Hiernaux and Justice, 1986), which also exhibit some spectral greenness. Therefore, the use of images acquired during the growing season was avoided, and relatively drier condition images were selected to reduce the influence of non-woody plants in the data. Landsat7 ETM+ image acquisition from the beginning of the dry season (October 2002) was used in the present study. The Soil Adjusted Vegetation Index ($SAVI$) developed by Huete et al. (1988; 1992) was selected rather than the commonly used $NDVI$ to account primarily for soil-background effects (Huete et al., 1992). The $SAVI$ introduces a soil calibration factor, L, to the $NDVI$ equation to minimize soil background influences resulting from first-order soil-plant spectral interactions (Huete, 1988; Huete et al., 1992). The $SAVI$ has therefore been found useful to quantitatively characterize vegetation types in the sparsely vegetated savannahs of the Volta Basin. The $SAVI$ is determined as follows:

$$SAVI = (1+L)(\rho 4 - \rho 3)/(L + \rho 4 + \rho 3) \tag{3.3}$$

where L is constant, and ρ3 and ρ4 are spectral reflectance for Landsat bands 3 and 4, respectively.

It is usual to apply a value between 0.1 and 0.5 for $SAVI$ (Allen et al., 2002; Huete and Liu, 1994; Bausch, 1993). In this study, it was necessary to determine an appropriate L value as input for the savannah of the study area. For this purpose, three successive transformations were carried out on the original $NDVI$. Firstly, an L value of 0.8 was introduced for $SAVI$ to reduce external influences; secondly, a value of 0.5 was used for the computation, and finally, an L equal to 0.1 was used. The results of the successive transformations were then compared with field data, and roughness length and surface albedo values of similar cover types acquired from literature (Allen, 2001; Bastiaanssen, 2000). Based on roughness length, surface albedo and temperature values observed for rice fields in the Tono irrigation scheme, an L value of 0.5 was found to be realistic for the present experiment.

In order to evaluate the relationship between spectrally estimated vegetation indices and field-based tree density values, field surveys were conducted to assess tree density over the study area in Navrongo. Because of the financial implications of covering the entire study area, reference data were located and collected through a stratified random sampling. A total of 147 points were sampled and tree biometric characteristics including density at each land unit recorded. Each sample plot of about 1 ha was geographically located during the field campaign using a hand-held global positioning system (GPS). The reference samples were first assigned to 11 classes according to the spectral classes previously created, and in a final step, the best representative distribution of the sample data was adopted. A regression analysis was used to establish the relationship between tree densities (TD) and remotely sensed spectral vegetation indices ($SAVI$). The resulting linear regression equation was then used to calibrate the $SAVI$-based TD across the studied savannah landscape.

3.3 Results and discussions

3.3.1 Land-use and land-cover maps

Table 3.3 shows the $LULC$ types and their extent for the year 2002. The results show that shrub-land, open savannah, woodlands and gallery forest are the widest spread covering about 56% of the study area in 2002. The rice fields in the Tono and Vea irrigation schemes of about 5250 ha, or 1.16% of the area, were difficult to separate from the gallery forest. Possible explanations are their relatively small size (about 5250 ha) and similar radiometric responses. These land units were digitized and added to the automatic classification. Therefore, the agricultural lands, including rice fields, and park savannahs associated to farmland covers represent almost 35% of the study area. Water bodies and built-up areas are the smallest units in the study area with 0.68% and 0.19%, respectively.

Table 3.3: Percentage distribution of LULC types during the year 2002 in the Navrongo area, Ghana

LULC type	Area (ha)	%
Bare land	34805.3	7.68
Farmland	66453.1	14.67
Shrub land	56900.5	12.56
Park savannah	83145.0	18.35
Open savannah	61707.4	13.62
Woodland	61094.6	13.48
Closed woodland	57953.1	12.79
Rice fields	5250.2	1.16
Gallery forest	16614.2	3.67
Water body	3070.7	0.68
Built-up	852.5	0.19
Total	453128.4	100.00

The spatial distribution of the *LULC* types in the Navrongo area is shown in Figure 3.5. The spatial extent of park savannah, bare land and farmland is a good indicator of agricultural activities in the area. However, field observations indicate that confusion may arise as these *LULC* types look alike on the remote sensing images during the dry season. Indeed, in this period, most crops had been harvested, and most green vegetation cover has entered the senescence phase. Therefore, depending on the vegetative coverage and land-use techniques, there may be confusion between farmland, park savannah, bare-land and fallow vegetation.

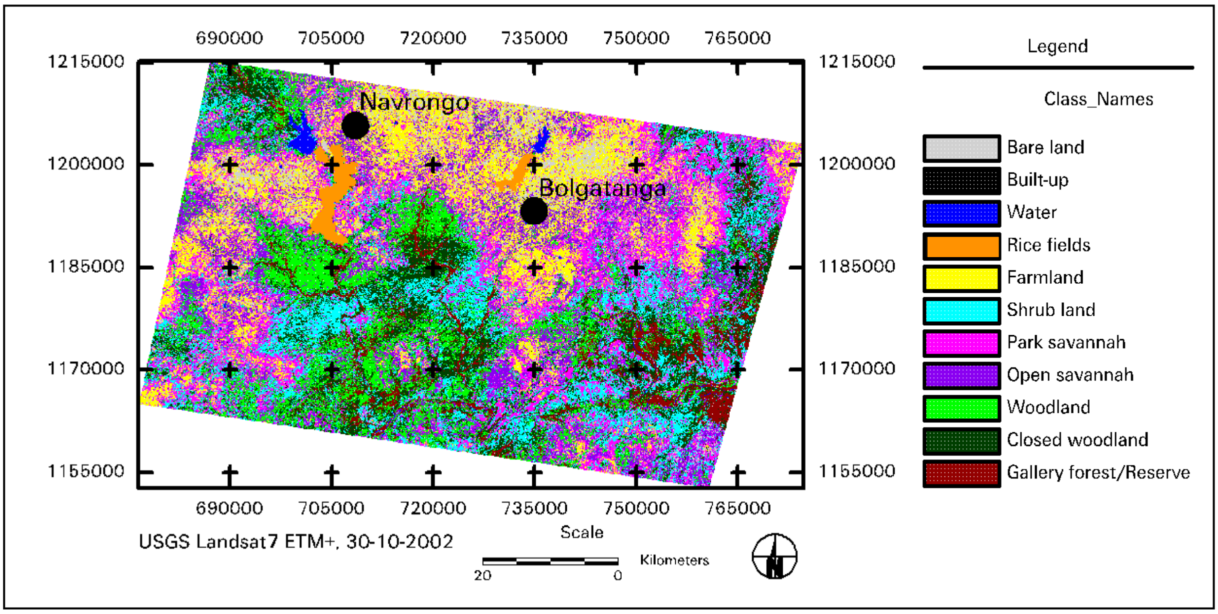

Figure 3.5: Land-use and land-cover map of the study area, Navrongo, 2002, Ghana

The use of training data collected in 2002 and 2003 on the different *LULC* types such as gallery forests, water bodies, shrub-land, farmland, built-up areas and outcrop rocks improved the satellite data classification. Based on the ground truth data and survey involving the Navrongo farmers, the satellite image-based *LULC* classification was a reliable source of information for the landscape dynamics during the 2002 period.

The accuracy of the *LULC* maps was tested using an accuracy assessment (error matrix) approach (Table 3.4). The method compares the relationships between ground-truth data and classified results category-by-category. Table 3.4 shows that the overall accuracy of the *LULC* classification is about 92%. The higher accuracy may be attributed to the relatively low number of classes and the fieldwork conducted in 2002 and 2003. Some specific misclassifications occurred in the mapping process, and pixels of burned areas have been confused with water. These misclassification problems have already been reported for the Volta Basin of Ghana (Duadze, 2004). Confusion between farmland and bare-land pixels may be expected, as most farmlands are bare-land in the dry season as they are poorly covered by a deciduous vegetation layer. Thus bare-land pixels have been interpreted as farmland or, on the other hand, farmland as bare or eroded land or outcrop rock. Some savannah patches were assimilated into farms or bare land due to an over-exposition of soil background reflectance. This is the case for cultivated areas, and also the response of underlying high reflective sandy soil types. However, the location, structure and shape of cultivated land allow separating farms from eroded lands or gravel areas.

Table 3.4: Accuracy assessment for LULC classifications in Navrongo, 30 October, 2002

Classified data	Reference data												
	A	B	C	D	E	F	G	H	I	J	Row total	PROD %	USER %
A. Gallery forest	17		2								19	89.4	89.4
B. Closed woodland		19	1								20	100.0	95.0
C. Woodland			24	2			1				27	85.7	88.8
D. Open savannah				14							14	77.7	100.0
E. Park savannah				2	17		1				20	89.4	85.0
F. Farmland	2		1			17					20	94.0	85.0
G. Shrub-land					2		18				20	90.0	90.0
H. Bare-land						1		22			23	91.6	95.6
I. Water									20		20	100.0	100.0
J. Built-up								2		18	20	100.0	90.0
Column total	19	19	28	18	19	18	20	24	20	18	205	91.8	91.9

Overall accuracy (%) is 91.8. PROD is producer accuracy; USER is user accuracy.

The studied area represents different landscape patterns due to long-term and diverse land-use practices mostly represented by agricultural activities. Human impact on the landscape is high and is primarily exerted around large rural settlements. This is the case with the continuous farms and park savannahs around the towns of Bolgatanga and Navrongo. The upper northern part of the area was found to mostly be affected by an intensification of permanent cultivation, whereas savannah land conversion to farms was taking place around densely vegetated areas such as north-west of Tono dam or south-east of the study area. Long-term natural changes in climatic conditions, human-induced alterations of vegetation cover and landscapes and the interannual climatic variability may be responsible for such *LULC* dynamics (Lambin and Ehrlich, 1996). Field observations, analyses of satellite images and climatic data also show that population growth, construction of micro-dams and droughts contribute significantly to the interannual changes in the landscape in the Navrongo area.

Characteristics of savannah vegetation in Navrongo area (2002)

Based on the classification scheme, the different vegetation classes were quantified and mapped using Landsat data. Tree characteristics such as composition, dominance, Dbh, mean height, and canopy size were recorded during the field campaign. A description of the vegetation types is given below.

Gallery forest and reserve

Table 3.5 shows the tree species composition of the gallery forest in the Navrongo area. These are found along temporary river banks due to the topography that allows floods and moisture. The main tree species are *Mangifera indica* (24.6%), *Azadirachta indica* (21.7%), *Anogeissus leiocarpus* (16.8%), *Camaldulensis spp* (9.6%), and *Tectona grandis* (3.3%). Most of these species are not riparian at all, but savannah or open woodland species that migrate towards the lower bed as rainfall progressively declines (FAO, 2001). Direct human impacts on the gallery forest are related to wild fire events in the dry season and fuel wood gathering.

Table 3.5: Tree species composition and dominance within gallery forest in the Navrongo area, Ghana

Tree species	Dominance (%)
Anogeissus leiocarpus	16.8
Cassia siamea	2.4
Camaldulensis spp	9.6
Diospyros mespiliformis	3.2
Mangifera indica	24.6
Azadirachta indica	21.7
Parkia biglobosa	3.5
Tectona grandis	3.3
Vitellaria paradoxa	2.6
Other	12.3
Total	100.0

Table 3.6 shows the biometric characteristics of the gallery forest trees. These trees can reach 12 to 25 m in height. The gallery forest in the study area supports relatively big trees with a Dbh size of about 50 cm, and a canopy diameter that reaches 10 m. Parts of the rich gallery vegetation in the Navrongo area have been replaced by open water (about 1400 ha). For management purposes, the up-stream relic gallery on the Tono River has been defined as a reserve by the Ghanaian forestry department,

while the down-stream gallery was converted into irrigation-based rice and vegetable farming over an area of about 3000 ha.

Table 3.6: Tree-biometric characteristics in gallery forest and reserves in the Navrongo area, Ghana

Trees number	Tree height (m)			Canopy diameter (m)			Dbh (cm)		
	mean	stdev	cv (%)	mean	stdev	cv (%)	mean	stdev	cv (%)
353	11.7	3.19	27.24	10.4	1.57	15.10	50.6	37.23	73.63

Woodlands

In the savannah landscape, woodland classes were found to mainly consist of large continuous patches (Table 3.7). The table shows that the dominating species are *Anogeissus leiocarpus* (29.8%), *Diospyros mespiliformis* (17.7%), *Balanites aegyptiaca* (12.0%), *Combretum glutinosum* (7.0%), and *Azadirachta indica* (4.4%).

Table 3.7: Species composition and dominance within woodlands in the Navrongo area, Ghana

Tree species	Dominance (%)
Anogeissus leiocarpus	29.8
Diospyros mespiliformis	17.7
Balanites aegyptiaca	12.0
Combretum glutinosum	7.0
Azadirachta indica	4.4
Lannea microcarpa	3.8
Combretum aeculatum	3.2
Cassia siberiana	2.5
Vitellaria paradoxa	2.5
Mytragina inermis	1.9
Ficus gnaphalocarpa	0.6
Vitex doniana	0.6
Other	14.0
Total	100.0

The tree-biometric characteristics in the woodlands are given in Table 3.8. Tree height is between 6 and 13 m and can reach up to 15 m depending on species composition and soil conditions. Relatively small trees are found in woodlands with a

Dbh of about 21 cm. Mean tree height was estimated at about 9.7 m, and the tree density was 166 trees per hectare according to canopy size and tree age.

Table 3.8: Tree-biometric characteristics in woodlands in the Navrongo area, Ghana

Trees number	Tree height (m)			Canopy diameter (m)			Dbh (cm)		
	mean	stdev	cv (%)	mean	stdev	cv (%)	mean	stdev	cv (%)
62	9.7	2.89	29.92	7.2	3.14	43.47	20.6	10.79	52.35

In 2002, about 10% of the Navrongo area was occupied by woodland vegetation. It was observed that the impact of agricultural activities based on conversion of natural savannahs to new farms is an ongoing process. Scattered newly created small farms were observed on the satellite images as small “white patches”.

Park savannah and farmland

Table 3.9 shows the percentage distribution of park savannah and farmland tree species compositions. Useful tree species such as *Vitellaria paradoxa* (55.5%), *Diospyros mespiliformis* (15.5%), *Acacia albida* (9.5%), *Bombax costatum* (2.5%), *Parkia biglobosa* (2.0%), and *Mangifera indica* (2.0%) are the dominant tree species in the cultivated areas. They are not cut down during land preparation and become more common over time, giving the impression of planted trees (Table 3.9). *Vitellaria paradoxa* is highly valued for its economical value and other social care functions. The fruit nuts are used by the local population to produce butter that gives the name “shea butter tree” to the *Vitellaria paradoxa*. Because of its ecological, economic and social values, *Vitellaria paradoxa* is one of the most protected species in West African countries. However, the changing agricultural practices are a danger, and increasing cultivation and lack of effective protection will threaten the natural population (Booth and Wickens, 1988). There is also a natural threat of reduction to the aging populations of *Vitellaria paradoxa* in the ecological zone that spreads from Senegal to Cameroon through to the drier parts of equatorial Central Africa and Uganda (FAO, 1994).

Table 3.9: Species composition and dominance within park savannah and farmland in the Navrongo area, Ghana

Dominant tree species	Dominance (%)
Vitellaria paradoxa	55.5
Diospyros mespiliformis	15.5
Acacia albida	9.5
Bombax costatum	2.5
Parkia biglobosa	2.0
Mangifera indica	2.0
Sclerocarya birrea	1.0
Other	12.0
Total	100.0

Most of the natural savannah is progressively being replaced by the park savannah vegetation due to the expansion of new farms. Park savannah classes are becoming highly degraded owing to prolonged traditional land management based on bush fires and forest clearing. Shifting agriculture is a rotational agro-forestry system in which a few years of crop production are followed by a short to long-term fallow period. Fields of about 1 hectare (observed in the study site) are cleared in the natural vegetation for millet, *Sorghum* or maize cultivation for several years, then the field is abandoned. This field may be converted again later for agricultural purposes.

Table 3.10 shows the biometric characteristics in park savannah and farmland. The mean tree canopy diameter in the study area was about 11 m, and tree Dbh of 66 cm. Tree density in the farmland was highly variable and varied between 0 and 24 trees per hectare depending on farming system. At the test site in Navrongo, the cultivated land vegetation was a climaxic stand of *V. paradoxa* trees of about 10 m in height (Table 3.10).

Table 3.10: Tree-biometric characteristics in park savannah and farmland in the Navrongo area, Ghana

Trees number	Tree height (m)			Canopy diameter (m)			Dbh (cm)		
	mean	stdev	cv (%)	mean	stdev	cv (%)	mean	stdev	cv (%)
244	9.3	1.66	0.17	11.6	3.96	0.34	66.0	40.33	0.61

Shrub-land

Shrub-land in the study area was a poorly vegetated layer because of hard soil conditions. Shrub-land usually covered narrow belts linked to exposed rock outcrops along river beds or confined to hill slopes. The shrub-land class covered up to 9.2% in the Navrongo area. Because of their poor vegetation cover, these areas are regularly subjected to annual bush fires that affect vegetation growth. Trees are rare (2 or 3 per hectare) and have a mean height of less than 5 m. Shrubs of *Acacia gourmaensis, Combretum glutinosum* and *Combretum nigricans* are the common shrub species of these vegetation units (Table 3.11). The grass layer is dense and basically composed of *Loudetia togoensis, Andropogon pseudapricus or Elionoris gracilis, etc*.

Table 3.11: Species composition and dominance within shrub-land in the Navrongo area, Ghana

Dominant grass and tree species	
Grass species	Coverage (%)
Elionoris gracilis	6.2
Andropogon pseudapricus	17.4
Loudetia togoensis	40.0
Other	36.4
Total	100.0
Tree species	Dominance (%)
Azadirachta indica	7.7
Tamarindus indica	2.6
Vitellaria paradoxa	25.6
Acacia spp.	10.3
Balanites aegyptiaca	33.8
Total	100.0

The *C. glutinosum* shrubs were located on degraded soil with underlying iron pan, the so-called "bowal". *C. glutinosum* greens up in the dry season immediately after bush fire events, but its covering capacity is low and it has been classified as bare or shrub-lands. These areas are less frequently converted to farming as they are unsuitable for agricultural and are mainly used for cattle grazing in the rainy season near the villages.

Tree-biometric characteristics are shown in Table 3.12. Shrub-lands are characterized by poorly vegetated areas with trees of less than 5 m in height, and a Dbh less than 10 cm. Furthermore, tree density is very low, as the substrate soil type is generally dominated by iron pan and gravel. Shrub-land at the beginning of the dry season is more representative of grassland, and may be confused later at the end of the dry season with bare-land units.

Table 3.12: Tree-biometric characteristics in shrub-land in the Navrongo area, Ghana

Tree number	Tree height (m)			Canopy diameter (m)			Dbh (cm)		
	mean	stdev	cv (%)	mean	stdev	cv (%)	mean	stdev	cv (%)
39	5.5	2.36	43.02	6.6	7.04	107.5	17.2	11.51	67

Built-up area

This *LULC* category in the study area is dominated by settlements such as the towns of Navrongo and Bolgatanga. The spatial area of these settlements is about 200 ha and 50 ha, respectively. Other land units such as rock outcrops and asphalt roads are also mapped in this category. Spectral confusion may be noticed between settlements, bare-land and some bush fire traces. Settlements that do not present a noticeable size in the Landsat image were omitted in the map result.

Fallow vegetation and burnt areas in Navrongo area

Seven burnt areas dominated by *V. paradoxa* tree stands were recognized in the field as representative fallow vegetation. The selected bush fire trace test sites are located on the ASTER scene presented in Figure 3.6 as a false color composite (*FCC*) of bands 3-2-1.

Biometric characteristics over fallows sites

Table 3.13 gives the biometric characteristics of the visited stands of fallow vegetation. The vegetation cover in these stands showed a discontinuous canopy of deciduous trees and a lower layer of *C. glutinosum* shrubs and grasses. Tree density over the fallow area was in the range of 16 to 40 stems/ha. *V. paradoxa*, the dominant species, showed a canopy of hemispherical shape with a mean diameter of 10 m. Tree mean height varied between 9 and 10 m, whereas trunk Dbh varied between 25 cm and 54 cm. The principal tree species of the fallow stands were *V. paradoxa, Adansonia digitata, Tamarindus indica, Bombax costatum, Balanites aegyptiaca, Sclerocarya birrea,* and *Ceiba pentandra* tree species.

Table 3.13: Tree-biometric characteristics of fallow vegetation in the Navrongo area, Ghana

Sites	Tree height (m)			Canopy diameter (m)			Dbh (cm)		
	mean	stdev	cv (%)	mean	stdev	cv (%)	mean	stdev	cv (%)
Pungu-Telania	8.0	1.6	20.0	7.9	2.6	32.4	42.1	9.7	22.9
Baweogo	7.9	1.9	24.3	8.8	2.5	29.0	36.7	13.4	36.5
Saboro	7.2	1.8	25.6	8.3	2.1	25.4	34.6	21.8	63.0
Tono	7.3	1.9	26.0	8.5	2.3	26.7	37.3	22.3	59.8
Boanea	7.9	2.0	26.1	9.3	2.1	22.9	38.0	35.4	93.2
Doba-Abalungu	8.4	2.1	25.7	7.7	1.7	22.4	59.3	38.8	65.5
Yagagnia	9.0	2.0	21.7	10.9	2.1	19.7	40.5	12.3	30.3

Fallow vegetation stands was developed on sandy or lateritic soil that supports grass species such as *Loudetia togoensis*, *Schoenefeldia gracilis*, *Andropogon pseudapricus, Schizachyrium exile* and *Andropogon pseudapricus*. The few farming activities were essentially based on ground nuts and represented 4% of the fallow zones.

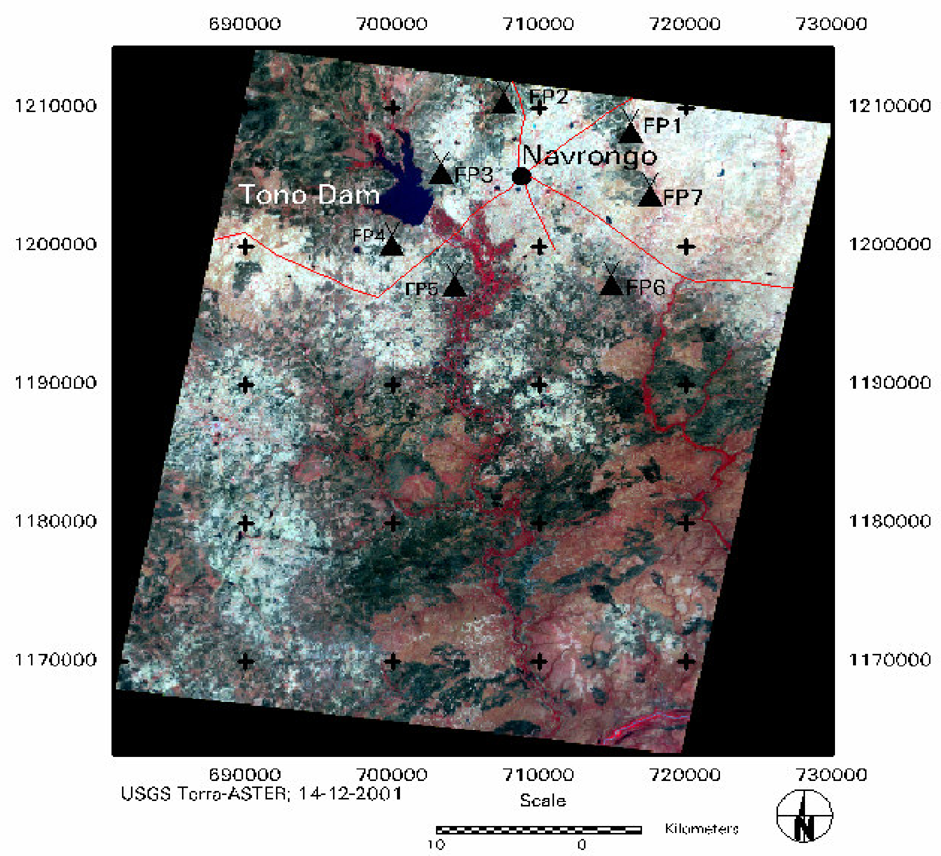

FP1- Test site Pungu-Telania
FP2- Test site Baweogo
FP3- Test site Saboro
FP4-Test site Tono
FP5- Test site Boanea
FP6- Test site Abalungu
FP7- Test site Yagagnia

Figure 3.6: False color composite image (3-2-1) of ASTER scene of the study area, 14 December, 2001. The test sites are located at homogeneous fallow vegetation around Navrongo area, Ghana. Burnt traces are displayed in a varying black color; the Tono Dam is displayed in a dark blue color.

Surface temperature and albedo over fallow vegetation stands

The results of the surface albedo measurements show that bare-lands are the most reflective elements in the landscape due to the high background reflectance of sandy soil. *V. paradoxa* (shea nut) leaves and iron pan (lateritic rock) show medium and generally declining albedo during the day. This may be due to a high absorption capacity inversely correlated to the diurnal course of solar radiation generally low in the morning and intense around noon. The higher absorption of solar radiation by mature *V. paradoxa* mature leaves may be explained by the need for energy in the photosynthesis process. On the other hand, mango leaves, farm bare-land and bare-land show relatively higher albedo with an asymmetric shape. This could be related to the reflective capacity proportional to the diurnal solar radiative variation. In contrast, water bodies and fire traces show relatively similar albedo and the lowest values. This may be attributed to the high absorption capacity of incoming radiation due to the black color of the ash from the burning, or to the development of green dark algae in pond water.

The results of land surface albedo measurements of different land surface units in early December, 2002, in the Pungu-Telania fallow vegetation are presented in Figure 3.7 for some comparative analysis.

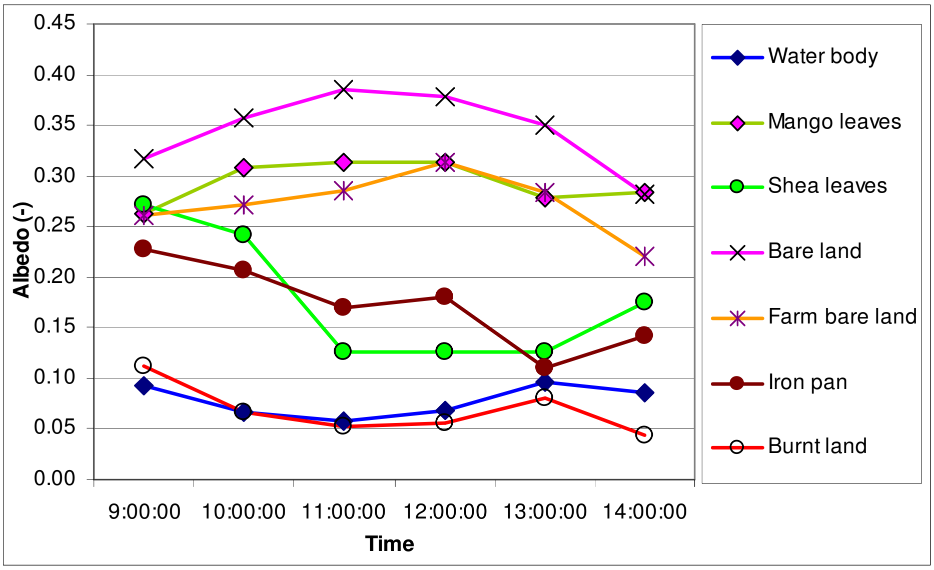

Figure 3.7: Albedo distribution in the Pungu-Telania fallow site, Navrongo-Ghana. Burnt areas and water bodies from small dams show similar albedo, while they are significantly different from other surfaces such as farm bare land, *Mangifera indica* (green mango leaves) and bare-land.

From Figure 3.7, it can be seen that most of the savannah landscape surface albedo values are generally different, which makes them separable; the only similarity in albedo is found between water bodies and burnt areas of the fallow. Burnt traces, iron pan and farm bare-lands are the four most important radiative elements in the fallow. The results of surface temperature measurements over burnt traces show high values up to 60°C, whereas lower values of about 30°C were recorded over water bodies and green leaves. The temporal distribution of surface temperature for the principal land-cover elements found in the Pungu-Telania test site is presented in Figure 3.8. The comparison of the absolute temperature absolute values between water bodies and burnt traces shows a significant difference of at least 20°C during the measurement campaign. This large thermal difference between water and burns could be a decisive parameter for spectrally discriminating burnt from non-burnt areas. Burnt areas present the warmest surface, whereas water is the coolest followed by the green vegetation cover made up of *M. indica* and *V. paradoxa*.

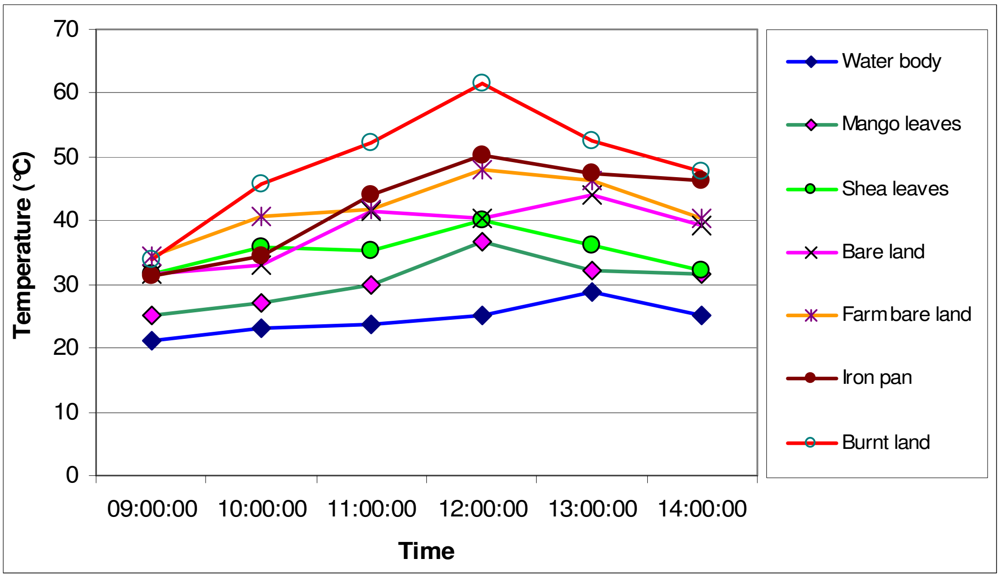

Figure 3.8: Surface temperature distribution of main land covers in the Pungu-Telania fallow site, Navrongo, Ghana

The surface temperatures of the burns in fallow and water bodies presented in Figure 3.7 and 3.8 are completely different, while both land units present similar surface albedo. Thus, while use of the visible, near infrared and shortwave infrared bands may confuse estimation of surface albedo, the application of the thermal infrared bands will be of great help to discriminate burns of *V. paradoxa* fallow vegetation from other features in the landscape and especially from open water features, since these land units show extreme differences in temperature values when monitored using TIR bands.

Mapping burnt areas using PCA images

Figure 3.9 shows the spatial distribution of burnt areas and other cover types. This false color composite (*FCC*) image was interpreted into burnt and non-burnt classes at 7 sites using supervised classification. Using the NIR, $SWIR_{PCA1}$ and TIR_{PCA1} images, 2 classes of burnt vegetation and 3 classes of non-burnt vegetation were mapped. Categories of burnt areas are depicted and classified here as old and recent fires. Green vegetation, bare land-and water classes with relatively low temperatures represent the non-burnt area. Major changes in the savannah vegetation phenology thus occurred with bush fires in the dry season but at different levels. Fallow stands were subjected to recent burns on 11.4% and old fires on 63.7% of the area, while non-burnt areas accounted for only 25%. Savannahs and gallery forests, mainly in the south-east, are the main vegetative layer left by the fires. Farms and bare-land are also not affected by fire because of the lack of readily burning biomass.

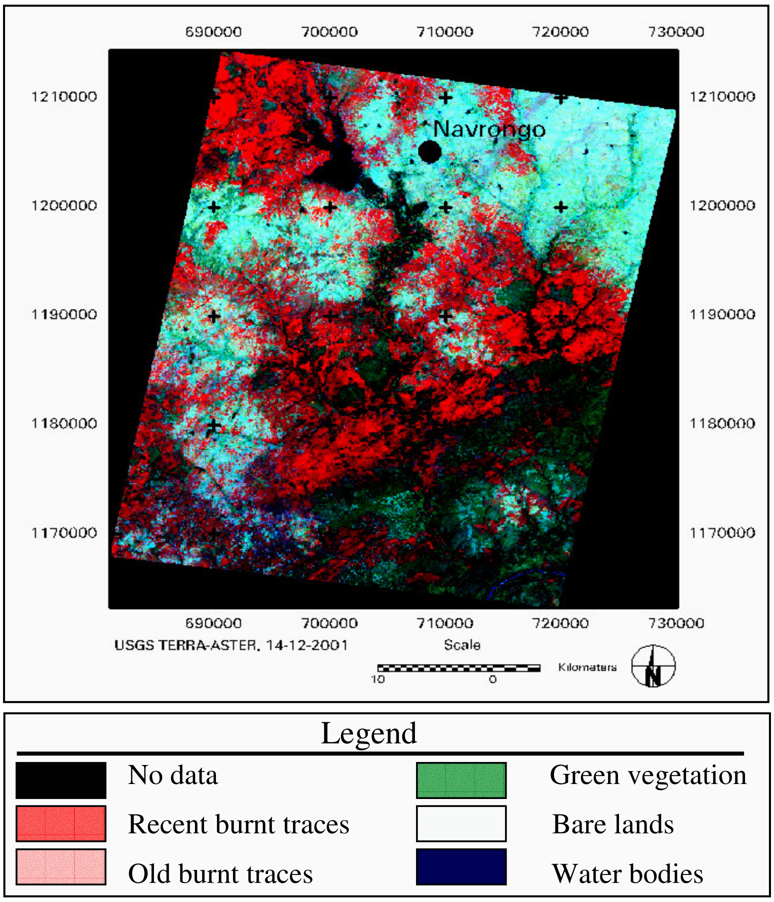

Figure 3.9: Composite NIR-SWIR$_{PCA1}$-TIR$_{PCA1}$ image depicting burnt traces in the Navrongo area, Ghana

In Figure 3.9, pink colors represent old burnt areas dating from November, 2001, the start of the fire events in the area. The lighter red colors on the image from 14 December, 2001, are the much larger savannah areas corresponding to recent and active fire traces. Dark blue colors symbolize water bodies, including small dams that are much deeper black. Green vegetation is represented by green colors, while bare-land and farms are light aquamarine.

Burnt traces are clearly displayed in variable forms, generally shaped in a north-east to south-west direction corresponding to the dominant Harmattan wind. These are well differentiated from the surrounding environment by their reflectance properties. This is basically explained by a high absorption of incoming radiation resulting in energy fluxes through soil and in sensible heat fluxes. These fluxes have the potential to intensify the evapotranspiration through the latent heat flux or evaporation, and the transpiration process.

Table 3.16 gives the results of the classification over the 7 selected fallow stands. At least 60% of the fallow areas were burnt in 2001, which confirms the occurrence of bush fire in savannahs areas. Among the visited stands, the Tono area was less affected by fire (59%), whereas Abalungu registered more impacts (91%) (Table 3.16). The predominance of the fire traces in the Abalungu area is primarily due to a larger extent of fallow areas with dry biomass from tree leaves and grasses that may burn easily; conversely, the Tono vegetation occurs more on sandy soils that do not support grass optimum development. Furthermore, the farming activities also limit the expansion of wild fires. In general, on the 14 December, the old burnt traces were already the dominant form of burnt traces detected by the satellite sensor. The proportions of burnt areas over the selected test sites are presented in Table 3.16.

Table 3.14: Spatial distribution of burnt areas in the selected fallow test sites in the Navrongo area, Ghana

Cover type	Pungu		Baweo		Saboro		Tono		Boanea		Abalungu		Yagagnia	
	ha	%	ha	%	ha	%	ha	%	ha	%	ha	%	ha	%
Old traces	882	74	748	66	607	63	989	49	947	65	824	49	495	79
Recent traces	57	5	89	8	45	5	191	10	134	9	716	42	11	2
Park savannah	53	4	130	11	122	13	294	15	170	12	0	0	54	9
Farms	207	17	174	15	186	19	471	24	209	14	154	9	62	10
Water	0	0	0	0	0	0	18	1	0	0	0	0	0	0
Gallery	0	0	0	0	0	0	18	1	0	0	0	0	0	0
Total	1199	100	1141	100	960	100	1981	100	1460	100	1695	100	622	100

Generally, the study demonstrates that ASTER data can be used to reliably map the savannah fallow vegetation stands (burnt areas) with 94% accuracy through appropriate spectral enhancement and image classification techniques.

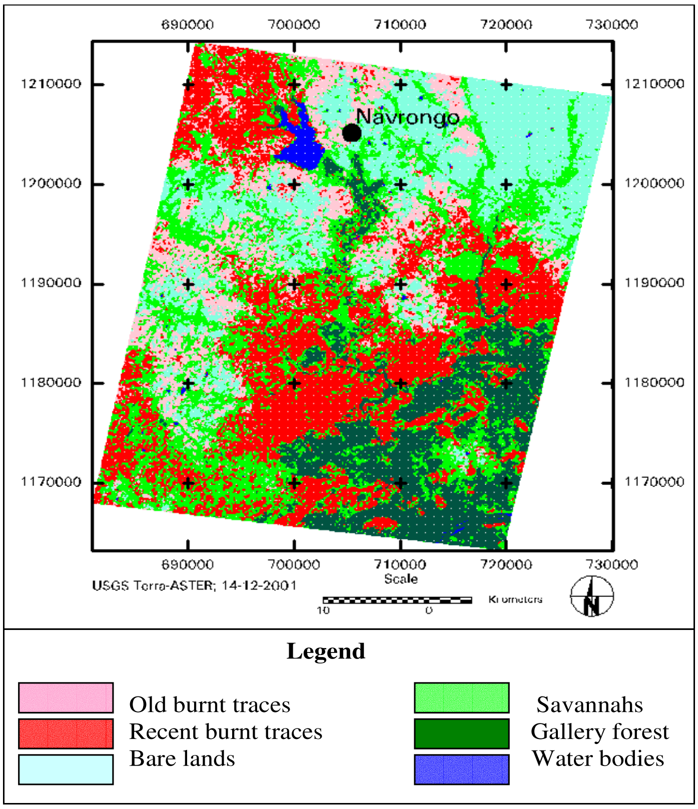

Figure 3.10: Fire traces of the study area, Navrongo, Ghana. Recent fires are the most extensively distributed in the area. Savannahs and gallery forests, mainly in the south-east, are the main vegetative layer left by the fires. Farms and bare-land are also left because of lack of readily burning biomass.

Leaf area index dynamics of main savannah tree species

The biweekly measurements of *LAI* of the studied tree species (Figure 3.11) were used to differentiate their phenological change in the dry season. The results show that mean *LAI* values were 1.05, 2.51, 2.56, 4.14 and 1.75 for *Acacia albida*, *A. leiocarpus*, *D. mespiliformis*, *M. indica* and *V. paradoxa,* respectively, measured at the end of the rainy season. The *LAI* of *V. paradoxa*, *A. leiocarpus* and *D. mespiliformis* reached its maximum value at the end of October, whereas *M. indica* and *A. albida* showed their maximum a month later (Figure 3.12).

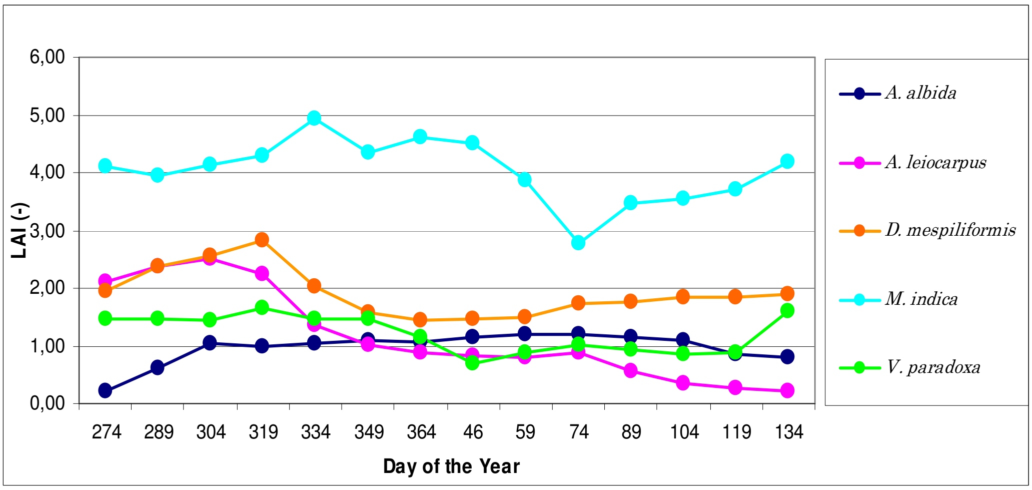

Figure 3.11: Temporal variations in the *LAI* of main savannahs main tree species in the Navrongo area, Ghana

Through the dry season, the principal *LAI* values decreased from between 57.0%, 48.3% 33.0% for *D. mespiliformis*, *V. paradoxa* and *A. leiocarpus,* respectively. In contrast, *M. indica* and *A. albida* showed slight increases in *LAI* values with 9% and 15% between October and December, respectively. The largest *LAI* decrease by 24.5% occurred between 30 December and 15 March for the *M. indica*, which may be due to the fructification period. A slight increase by 23% was observed from February to April for *D. mespiliformis*. Thus, three phases of evolution may be described for *D. mespiliformis:* from September-October, which corresponds to optimum phenology followed by a decrease in the *LAI* value between October and February and increased canopy activity between February and April. For the three tree species *D. mespiliformis*, *A. leiocarpus* and *V. paradoxa,* the decrease in canopy volume took place between 15 November and 15 February, which corresponds to the onset of the dry season marked by fire events. The deciduous tree species *V. paradoxa* and *A. leiocarpus* showed the greatest decreases, with values between 90% and 48% during the dry season. Leaf fall was accelerated for *A. leiocarpus* between 30 October and 15 February in response to water stress. However, the reverse phenology situation observed in *A. albida* may mainly be explained by water sources deep in the soil and the tree's physiological parameters such as great rooting depth. Indeed, it was observed that *A. albida* developed a tap root deeper than 2.5 m, whereas *V. paradoxa* and *A. leiocarpus* were limited to 100 cm soil depth. However, *V. paradoxa* was found to develop lateral roots up to 25 m away from the stem to secure its water and nutrient supply. *Mangifera indica* and *D.*

mespiliformis root distribution were site dependent, i.e., related to moisture availability, soil structure and type. From a deep river channel fringe, a root depth up to 3.5 m for *D. mespiliformis* was observed, while *M. indica* roots were found at 3 m in a deep well. These two species are mostly grown naturally or planted along riverbeds and depressions where the water table level is generally high.

3.3.2 Hydrological delineation

The remotely spectral data of T_s, $NDVI$ and α were used to characterize the landscape into different wetness levels (Table 3.15). In October, the derived hydrological units can be distinguished into two main groups according to their bio-physical parameters. The first group comprises units 1, 2, 3, 4, 5, 6 and 7 with $NDVI$ mean values of 0.42, T_s of 302.78, and α of 0.18. These pixels correspond generally to a higher $NDVI$ and lower α and T_s, and consequently represent the wet situation in the $VITT$ diagram. The second group displays lower average $NDVI$ values of 0.34, a higher T_s value of 305.87 and α of 0.21. The situation is more representative of relatively dry pixels. The comparison between classes in the hydrological units shows that the difference in the $VITT$ parameters was not significant at the 5% level. It may be seen that in October, there was a relative homogeneity in moisture and consequently evapotranspiration distribution in the savannah landscape. Table 3.15 shows the distributive radiometric characteristics of the 11 hydrological units.

Table 3.15: Surface temperature (T_s), normalized difference vegetation index ($NDVI$) and surface albedo (α) for hydrological units in October, 2002, in the Navrongo area, Ghana

Hydrological cluster	$NDVI$ (-)			α (-)			T_s (°K)		
	mean	stdev	cv (%)	mean	stdev	cv (%)	mean	stdev	cv (%)
1	0.38	0.292	76.98	0.16	0.022	13.76	300.00	0.877	29.23
2	0.46	0.031	6.74	0.18	0.012	6.80	302.00	0.193	0.06
3	0.47	0.030	6.44	0.17	0.008	4.69	302.73	0.174	0.05
4	0.43	0.033	7.62	0.17	0.006	3.43	303.15	0.196	0.06
5	0.46	0.025	5.37	0.19	0.004	2.56	303.64	0.178	0.06
6	0.38	0.021	5.59	0.18	0.006	3.56	303.70	0.133	0.04
7	0.35	0.031	8.91	0.19	0.011	6.30	304.22	0.201	0.07
8	0.37	0.027	7.44	0.20	0.010	5.29	304.67	0.269	0.06
9	0.35	0.026	7.42	0.21	0.008	3.85	305.13	0.248	0.08
10	0.33	0.022	6.82	0.22	0.014	6.37	306.04	0.274	0.09
11	0.30	0.029	9.58	0.22	0.016	7.18	307.61	0.599	0.19

Figure 3.12 shows the spatial distribution of the 11 hydrological units delineated based on their T_s, $NDVI$ and α value. Units 1 and 2 represent open water and flooded areas generally located at the Tono and Vea Dams and at some gallery forest and woodland sites. These units are also present in some depressions exhibiting the highest moisture conditions in the savannah landscape all year long. Other good water condition units are represented by the units 3, 4, 5, 6 and 7 associated to woodland, open savannah and park savannah vegetation types generally located around secondary streams.

Units 10 and 11 are likely found in farmland and bare-land of the study area. At the end of the rainy season they present the most dry conditions associated with a low $NDVI$ and a lower T_s and α. Unit 10 was found to be in fallow vegetation and degraded areas with some out-crop rocks, whereas unit 11 was generally located in the north-eastern part of the study area, where more bare farmland and bare-land was found. Units 10 and 11 show a higher average T_s of about 307°K and are likely the driest parts of the area. On the other hand, units 1 and 2 may transpire more than units 3, 4, 5, 6 and 7 due to the lower T_s and higher $NDVI$ value. This could be typically representative of the active riverbed vegetation stand. Relatively lower evapotranspiration rates in the area can also be seen in the drier units 10 and 11.

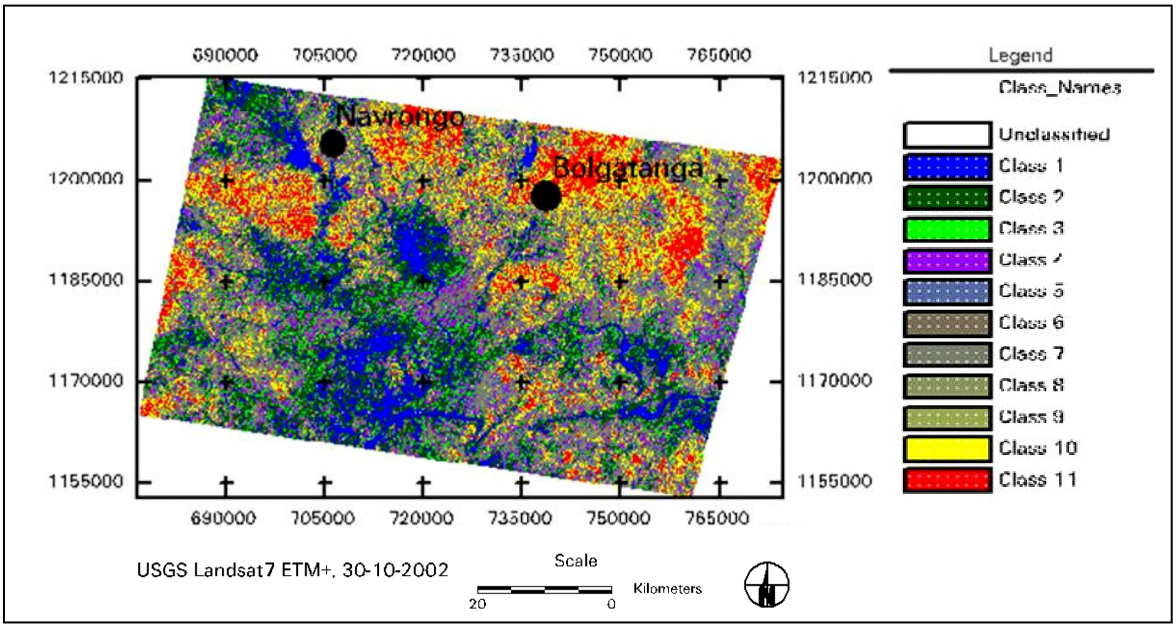

Figure 3.12: Land surface moisture distribution during 30 October, 2002, in the Navrongo area, Ghana

In March 2003, the climatic situation in the Navrongo area was different from that in October 2002. March is characterized by high radiation and temperatures, and more affected by more than 4 months of drought (after the last rains). The distribution of the $NDVI$, T_s and α values across the study area changed completely during this period as presented in Table 3.16. Relatively low $NDVI$ values are found in the different hydrological units and ranged from 0-0.36 compared to -0.27-0.6 registered in October 2002. On the other hand, high T_s and α values were observed over the whole area. The T_s values ranged from about 25-45°C compared to only 25-35°C in October, while α increased up to 0.17-0.37. However, the comparison between the hydrological units shows that the difference in $NDVI$ and α was not significant at the 10% level; the difference was only effective in T_s. This could be representative of the much drier situation in March.

Table 3.16: T_s, $NDVI$ and α for the hydrological units in March, 2003 in the Navrongo area, Ghana

Hydrological unit	$NDVI$ (-)			α (-)			T_s (°C)		
	mean	stdev	cv (%)	mean	stdev	cv (%)	mean	stdev	cv (%)
1	0.16	0.12	76.12	0.23	0.03	12.36	302.23	3.35	1.11
2	0.15	0.04	28.25	0.32	0.03	8.07	310.54	1.13	0.36
3	0.15	0.01	6.01	0.33	0.01	3.78	312.59	0.30	0.10
4	0.15	0.01	7.00	0.33	0.01	3.67	313.00	0.23	0.07
5	0.15	0.01	4.75	0.30	0.02	6.00	313.66	0.32	0.10
6	0.15	0.01	5.65	0.31	0.02	4.79	314.09	0.22	0.07
7	0.15	0.02	10.15	0.28	0.02	7.54	314.51	0.30	0.10
8	0.15	0.01	8.13	0.28	0.02	7.53	314.85	0.50	0.16
9	0.15	0.01	8.09	0.26	0.02	7.19	315.78	0.30	0.09
10	0.12	0.03	25.17	0.23	0.01	4.90	316.55	0.45	0.14
11	0.13	0.02	12.18	0.23	0.01	3.35	317.74	0.53	0.17

Figure 3.13 shows the spatial distribution of the moisture situation in the study area in March 2003. Unit 1 represents the aquatic system of open water located at the Tono and Vea dams. The irrigated rice fields and large riverbeds of the Tono are also found in unit 1. This unit depicts the wettest situation in the area with mean T_s values of 302.23, $NDVI$ of 0.16 and α of 0.23. On the other hand units 9, 10 and 11 are located in the woodlands with radiometric T_s values of 316.7, $NDVI$ of 0.13 and α of 0.24, and show a medium moisture status. Units 8, 7, 6, 5, 4 and 3 are located in the northern part of the study area, and they were generally observed in sparsely vegetated areas such shrub-land, park savannah, farmland and bare-land. These units are mainly characterized by a mean T_s of about 313.8, $NDVI$ of 0.15 and α of 0.30. The similarity in these 6 units may be explained by the presence of shed deciduous tree species during the dry season. Therefore, these units are heated by a relatively high solar radiation that easily dries out the uppermost soil layers. They are likely the driest parts of the study area. Unit 2 represents some clouds and cloud shade.

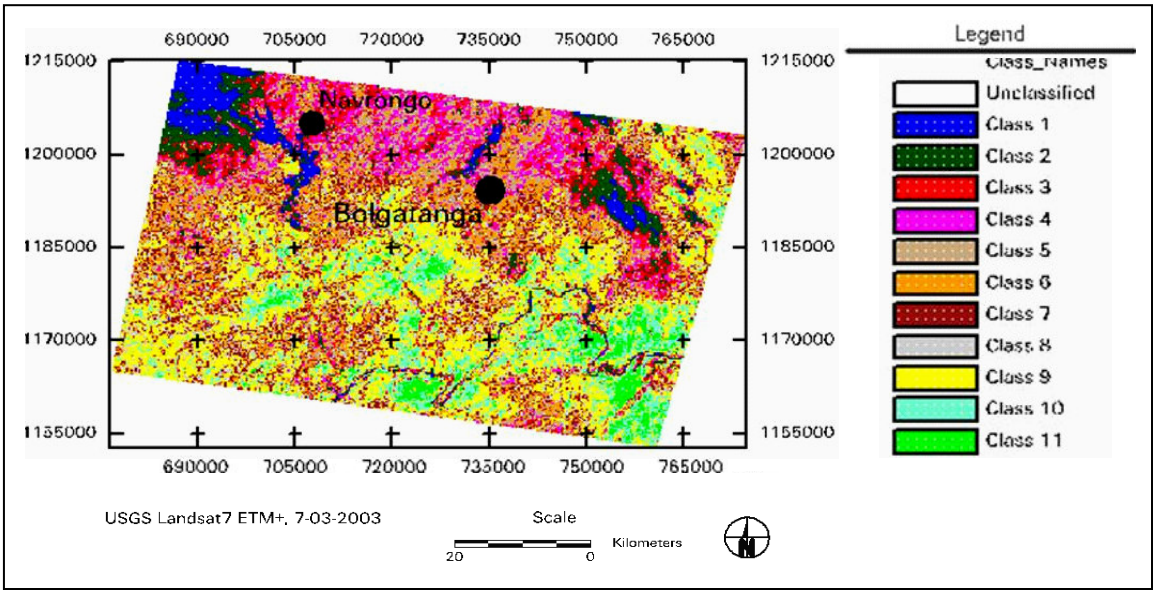

Figure 3.13: Land surface moisture distribution during 7 March, 2003, in the Navrongo area, Ghana

The *VITT* and statistical clustering present a quick technique for delineating the study area into hydrological units in terms of wetness conditions from very dry to very wet. However, extensive work in the field may be necessary for further measurements to compute the spectral estimation of the moisture conditions estimated from remote sensing methods.

3.3.3 Tree density mapping in the Navrongo area

In order to extract the tree density (TD) of the study area based on the vegetation indices of the different *LULC* classes, the *SAVI* values for each *LULC* were computed (Figure 3.14). Comparison of *SAVI* clusters with *LULC* data shows that sparsely vegetated areas such as bare-land and farmland were split into four different clusters. This may be related to difference in land management system, canopy density, and phenological development or performance of different vegetation types in each *LULC* category. Densely vegetated gallery forest and reserves areas with mean *SAVI* values ranging from 0.30 to 0.39 were divided into 2 different clusters. This may be because the gallery forest types are of mixed tree species that show different spectral reflectance characteristics. Differences in soil moisture conditions may also be the reason for the difficulty in digital classification.

Table 3.17 gives the relationship between $SAVI$ and TD derived for 147 representative samples. It can be observed that the vegetation index values of similar vegetation types within an area were not the same, indicating large within-site spatial variation among vegetation classes. The coefficient of variation within the vegetation classes for the $SAVI$ is on average about 15.2%. Vegetation indices also varied typically between sites. For instance, the differences in average values between gallery and bare-land sites were about 0.18 for the $SAVI$. The average difference between gallery and farmland sites was found to be about 0.13.

In Table 3.17, the densely vegetated savannah ecosystem, gallery forest and woodland show a $SAVI$ value between 0.28 and 0.35 that varies between 9.1 and 17.4%. The mean variation of the dense vegetation class is relatively low (less than 10%), which could be considered to not significantly influence the signal in the satellite sensor. The low variation is explained by the relative homogeneity of the vegetation cover. On the other hand, bare-land and shrub-land areas show the lowest mean $SAVI$ values ranging between 0.17 and 0.19, but these vegetative classes register the highest variation of about 16.3%. This is expected, as sparsely vegetated areas are more heterogeneous, showing patches of shrubs and trees in the middle of bare lands.

Table 3.17: Vegetation indices statistics for the different LULC classes in the Navrongo savannah, Ghana

LULC	*SAVI*		
	mean	stdv	cv (%)
Bare-land	0.17	0.04	24.5
Shrub-land	0.19	0.01	7.9
Farmland	0.22	0.03	13.4
Park savannah	0.22	0.03	13.1
Open savannah	0.27	0.03	11.1
Woodland	0.28	0.04	17.4
Closed woodland	0.28	0.02	9.1
Gallery forest/reserves	0.35	0.04	11.2
Water	-0.05	0.01	28.7

Considering the vegetation index values, the studied savannah may be divided into three categories: (1) dense vegetated zone comprising open savannah, woodlands and gallery forest; (2) medium-class that includes farmland and park savannah; (3) shrub-land and bare-land found in poorly vegetated areas.

Therefore, the hypothesis in the present study that higher tree density occurs with higher vegetative index and lower spectral vegetation index value with lower tree density is consistent with TD derived from $SAVI$.

Figure 3.14 gives the distribution of the ascendant cumulative $SAVI$ and TD sample data retained for the calibration analysis. It is a comparison between the $SAVI$ and the tree density data in the savannah vegetation. The cumulative $SAVI$ data can be represented by a linear function:

$$Y = 0.001x + 0.16 \tag{3.1}$$

with $R^2 = 0.95$; y is SAVI and x is tree number in plot. The cumulative tree density data can be fitted with a second-order polynomial function:

$$Y = 0.013x^2 - 1.00x + 16.63 \tag{3.2}$$

with R^2=0.87; y is tree density and x is SAVI value.

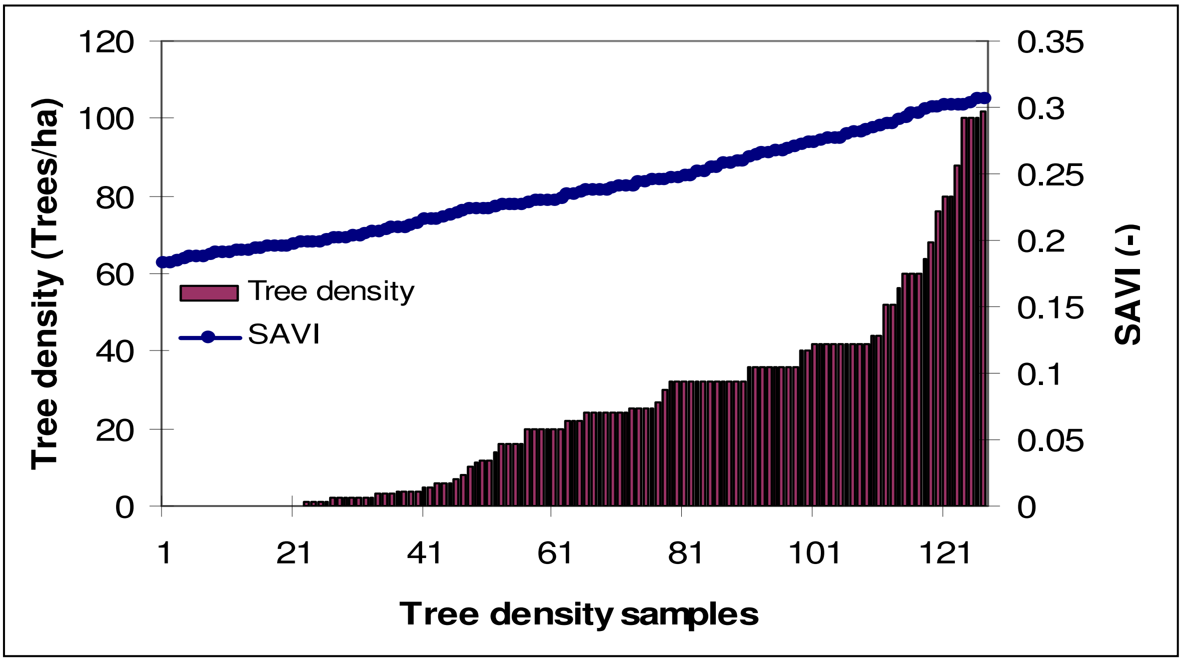

Figure 3.14: SAVI distribution compared to tree density in the Navrongo savannah, Ghana

Figure 3.15 shows the relationship between the representative reference TD and *SAVI* samples. Using the statistical relationship established between *SAVI* and TD samples collected in the field, a *SAVI* image was generated for the study area using Landsat images. The number of clusters was chosen to be relatively similar to the main *LULC* types of the area. The regression analysis gives a polynomial second-order function of the form

$$Y = -8E - 06x^2 + 0.002x + 0.196 \qquad (3.3)$$

and R^2=0.72; where y is SAVI and x is tree density in sample plot.

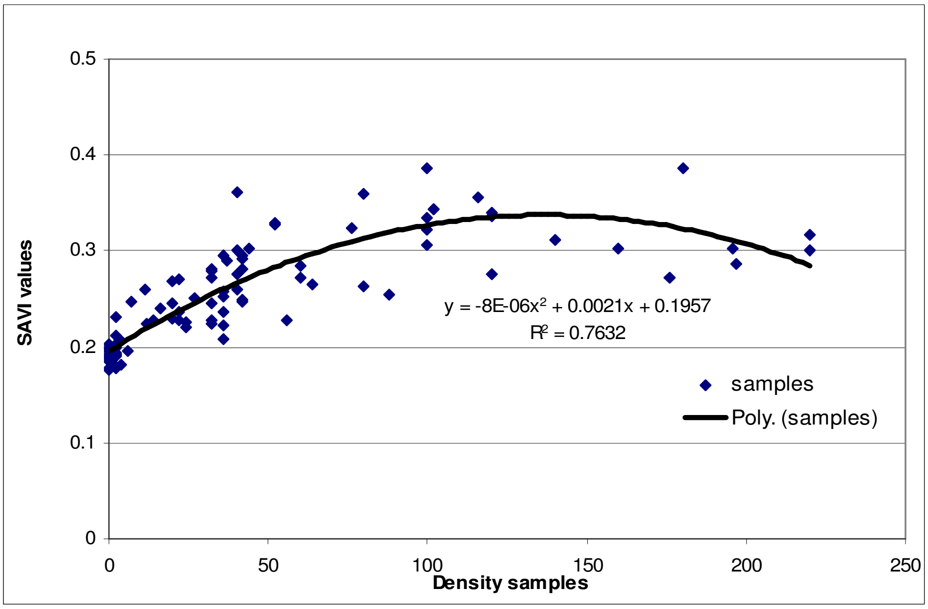

Figure 3.15: Relationship between tree density and SAVI data in the Navrongo savannah, Ghana

Table 3.18 gives the description of the 10 spectral classes. Farmland and bare-land areas characterized by relatively poor vegetation are represented by three clusters (2, 3 and 4). Because these classes present an overlapping range between 0.09 and 0.24, it may be difficult to classify them. To avoid confusion, they are merged to build one bare land class. Classes 6 and 7, though similar in their mean *SAVI* (0.28), are different because of their *SAVI* range values of 0.22 and 0.33 for the class savannah and 0.19 to 0.36 for woodland. On the densely vegetated areas, woodlands and gallery forest are well represented with distinctive *SAVI* mean values varying from 0.28 to 0.35.

However, the *LULC* unit gallery forest represented by two clusters is merged for consistency and further analysis.

Table 3.18: 10 spectral classes derived from *SAVI* in the Navrongo savannah, Ghana

Spectral classes	LULC	*SAVI*			
		mean	stdev	cv (%)	range
Class 1	Water	-0.05	0.02	28.78	0.07-0.04
Class 2	Bare-land	0.20	0.04	17.68	0.10-0.24
Class 3	Farm, bare-land	0.22	0.03	14.75	0.18-0.23
Class 4	Bare-land, built-up	0.18	0.07	23.01	0.09-0.24
Class 5	Farmland	0.23	0.03	11.40	0.17-0.28
Class 6	Savannahs	0.28	0.03	11.12	0.22-0.33
Class 7	Woodland	0.28	0.05	16.19	0.19-0.36
Class 8	Closed woodland	0.28	0.03	11.21	0.25-0.31
Class 9	Gallery/reserves	0.34	0.03	7.19	0.32-0.39
Class 10	Gallery/reserves	0.35	0.04	10.68	0.30-0.39

The graphical distribution of the 7 TD spectral clusters derived from field sample data is shown in Figure 3.16. The corresponding statistics are given in Table 3.19. The objective of the graphical analysis was to determine the acceptable number of classes that can be used to derive the spectral clusters in *SAVI* . Seven classes were defined varying from non vegetative (0) to sparsely vegetated (0-3) and medium (4-20); densely vegetated classes occurred in (21-40), (41-70) and (71-160); highly vegetated class corresponded to (>160).

A large spatial variation in tree density classes was observed. The coefficient of variation (CV) for tree density within class 1 (0-3) and class 7 (water) are low and do not represent the real variation of the class, because as previously discussed those classes were not considered as vegetation classes. The highest CV (99.6%) is found in class 2 (4-20) typically located in park savannah and farmland. The high variation can be explained by the farming system based on slash-and-burn, which reduces the number of trees in the cropping plot. The four other classes 3, 4, 5 and 6 show relative stability with a mean variation of 34.2%. Class 3, with a density varying between 21 and 40 trees ha^{-1} is mainly found in the *LULC* classes savannah and fallow vegetation. Class 4 is typical of open savannah with some patches of woodland. Tree density of this class varied between 41 and 70 trees ha^{-1} with a CV of 40.2% and a mean *SAVI* value of 0.2. Closed woodland and gallery forest and tree crop plantations such as mango reserve plantations are mainly found in class 5. Density is high with 71 to 160 trees ha^{-1} with a CV of 32.1%. Closed woodland occurs in class 6 and presents the highest value of 166 trees ha^{-1} and a CV of 31.9%.

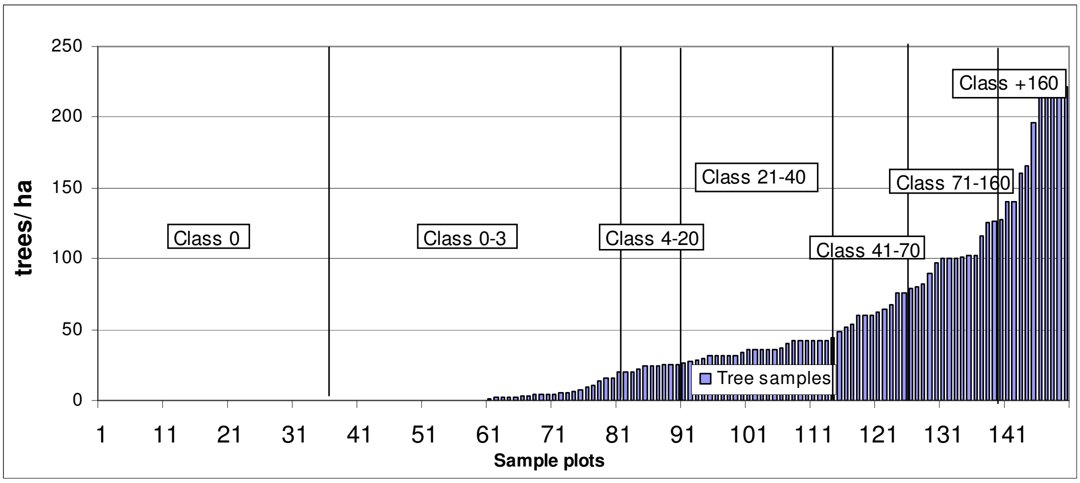

Figure 3.16: Graphical distribution of the TD classes from field data in the Navrongo savannah, Ghana

The tree density statistics in Table 3.19 show the distribution of the computed spectral tree density of the studied savannah vegetation. The table shows differences between classes. High differences are found between the sparsely vegetated class (class 1 and 3) and the densely vegetated classes (class 5 and 6). This large difference in vegetation indices is also reflected in highly different TD values. A comparison of absolute values in class 2 and classes 5 or 6, shows that the difference in tree density can be as high as 92 to 163. On the other hand, slight differences are found between class 3 and class 4, with a mean difference in tree density of 14 trees ha^{-1}. Unexpected is the higher density in closed woodland (166 t ha^{-1}) than in gallery forest (95 t ha^{-1}), which presents a higher vegetation index. This may be due to the fact that large trees with a large canopy are usually found in galleries in contrast to woodlands, which are characterized by relatively small trees. The environmental conditions may also play a role as seen in the case of rice fields with a very high vegetation index, although there are woody trees there.

Table 3.19: Tree density class statistics in the Navrongo savannah, Ghana

Spectral classes	Tree density			*SAVI*	
	class size	Mean (ha^{-1})	Stdev	Mean (-)	stdev
Class 1	0-3	0 (0)	0	0.20 (20.7)	0.04
Class 2	4-20	3 (99.6)	2.99	0.23 (11.4)	0.03
Class 3	21-40	30 (32.5)	9.76	0.28 (11.1)	0.03
Class 4	41-70	44 (40.2)	17.72	0.28 (16.1)	0.05
Class 5	71-160	95 (32.1)	30.52	0.34 (8.2)	0.03
Class 6	>160	166 (31.9)	52.98	0.28 (11.2)	0.03
Class 7	0	0 (0)	0	0.05 (28.7)	0.02

(20.7) Numbers in parentheses are coefficient of variation for tree density and SAVI

The tree density map of the Navrongo study area computed on the basis of continuous spectral vegetation indices using *SAVI* is presented in Figure 3.17. As expected, high variability in class density can be read in the spectral thematic tree density map. Higher tree densities are located in densely vegetated areas, while poorly covered savannahs features dominated by shrubs and grasses are characteristic of a lower tree distribution per ha.

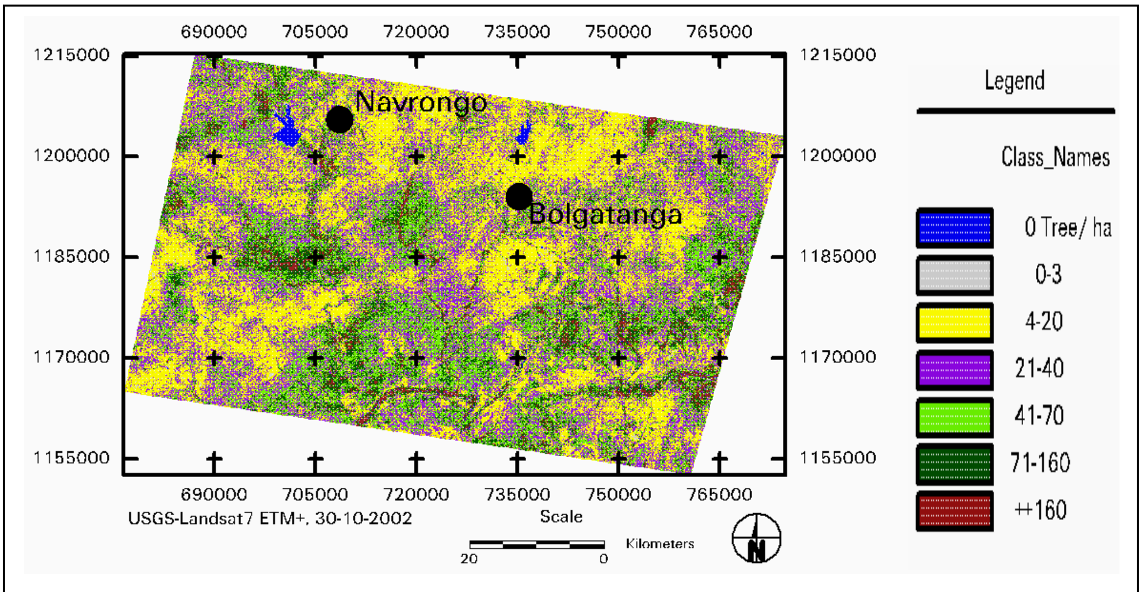

Figure 3.17: Tree density map of the Navrongo savannah, Ghana

3.4 Conclusions

The use of the high spatial resolution satellite images allows definition of an acceptable number of land classes in the savannah landscape. Landsat and ASTER images were used to cluster savannahs first into *LULC* types and then into burnt areas. The *LULC* map depicts 11 units based on their spectral characteristics. Densely vegetated areas are represented by the gallery forests and reserves, woodlands and open savannahs. Medium vegetated classes are represented by the agricultural park savannah and farmlands. Bare-lands and shrub-land represent the sparsely to bare-land areas. A non-vegetative class is represented by the open water bodies and some irrigated lands. The use of an appropriate classification scheme and classifier made it possible to obtain a successful land-use and vegetation cover map. This shall be used for assessing the hydrological role of each $LULC$ type in the study area.

The application of remotely sensed spectral data to map tree density classes in savannah shows some potential use of classification methods. Seven density classes including one non-vegetative class were derived using the $SAVI$ data calibrated with field data. The collection of exhaustive reference data may be a good indicator for the regression analyses. The present results may be improved with an intense survey on the ground for acquiring a larger dataset on tree density. The results encourage the use of the approach, which seems more efficient than direct measurements or visual interpretation of satellite images.

The land classification approach of the $VITT$ procedure resulted in the derivation of 11 wetness classes using remote sensing classifier. These results are more qualitative, and it may need a field survey to determine the limits of the moisture units in the landscape. An appropriate moisture map of the study area will be useful for hydrological studies. The interpretation of the present spectral moisture classes is based on the vertices indicated in the diagram. The approach delivers relatively quick results, which allow a better understanding of the moisture distribution that governs evapotranspiration mechanism.

The land classification approach was successful in deriving homogeneous land units in the savannah environment according to $LULC$ types, TD and hydrological units. These units will be used to estimate their relationship with hydrological processes in general and the spatial distribution of the ET_a in particular.

4 ACTUAL EVAPOTRANSPIRATION ASSESSMENT IN THE SAVANNAH VEGETATION

4.1 Introduction

Evapotranspiration (ET_a) is the process responsible for the transfer of moisture from soil and vegetated surfaces to the atmosphere. Changes in evapotranspiration are likely to have impacts on terrestrial vegetation, since the distribution and abundance of plant communities are controlled to a large extent by the quantity and seasonality of moisture.

The estimation of spatial variation of evapotranspiration is fundamental to many applications in water resources and climate modeling. Evapotranspiration, being the sum of interception, soil evaporation, open water evaporation and trees transpiration, is a key variable not only in water balance determination but also in estimation of the moisture, heat and CO_2 interactions between land and atmosphere (Sellers et al., 1996). As a result, information on the amount of evaporation from the land surface and transpiration from plants is essential to determine the amount of water used by different cover types and the implications for the local and regional climate change.

Generally, ET_a estimations can be made based on three approaches. One of the relatively best approaches is the remote sensing technique using the Surface Energy Balance Algorithm for Land (*SEBAL*) model developed by Bastiaanssen (1998a, 2000). *SEBAL* computes the ET_a at pixel level and is considered attractive because of its robustness and its low demand for input data and routine weather station data (Bastiaanssen (1998a, 2000). Furthermore, the *SEBAL* approach computes evapotranspiration directly from the energy balance equation without the need to consider other complex hydrological processes, which could introduce evaporation calculation errors.

Due to extremely scarce ground meteorological data in developing countries, utilization of high spatial resolution satellite imagery is an attractive approach. Advanced remote sensing sensors such as the thermal bands of the Landsat7 ETM+ have a high potential to estimate energy fluxes at the land surface. However, a major limitation of the remote sensing technique applying the energy balance method is that the temporal distribution of satellite-based estimates is poor, and that interpolation techniques are necessary to define evaporation between satellite overpasses (Allen et al., 1998; Mohamed et al., 2004) although this approach could be costly and time consuming. A solution in this study was to use two Landsat images to assess the ET_a distribution in two strategic periods of the dry season.

Another option to estimate the evapotranspiration is based on meteorological data using the most common Penman-Monteith (1948) method. The major advantage of the Penman method is the availability of data, their simplicity and easy computation. Because the result of the computation is a point measurement, it will be related to the ET_a derived from the *SEBAL* model by a crop coefficient. This will enable the computation of a crop evapotranspiration to alleviate the low temporal resolution of satellite data.

Finally, the contribution to atmospheric water by woody plants can be assessed by the use of the sap flow technique to measure individual tree transpiration (Granier, 1985; 1987). Further up-scaling approaches of sap flow based on tree density can be used to upscale to stand and to large stand vegetation transpiration (Oren et al., 1998; Vertessy et al., 1997). Such estimation of the temporal values of transpiration in savannah vegetation landscapes in the Volta Basin will be crucial for the assessment of stand and regional water balances. In addition, seasonal and diurnal dynamics of the sap flow rate could help to explain the behavior of tree species, which is important for the stability of these vegetation covers in the Sahel zone, an environment with high climatic variability.

In this study, *SEBAL* was used to estimate ET_a based on Landsat images for the dry season (2002-2003). Meteorological data of air temperature, relative humidity, wind speed, and solar radiation acquired from the GLOWA-weather station were used to calculate the FAO standard evapotranspiration used as the reference evapotranspiration (ET_o) for the study area. The sap flow technique was used to estimate water use or transpiration from individual trees and vegetation stands. Finally, the three measurements were integrated using an adjusted crop coefficient (K_c) to estimate the temporal variation of crop evapotranspiration (ET_c) according to the main landscape components governing the exchange land-surface-atmosphere. The significance of the ET_a estimation in semi-arid savannah landscapes and the benefits of temporal interpolation of the ET_a using meteorological data in developing countries are also discussed.

4.2 Materials and methods

4.2.1 Actual evapotranspiration computation using Surface Energy Balance Algorithm for Land

The $SEBAL$ is a remote sensing algorithm that computes the surface energy balance on an instantaneous time scale and for every pixel of a satellite image (Bastiaanssen et al., 1998a; Bastiaanssen, 2000). It has been applied for water balance estimations (Pelgrum and Bastiaanssen, 1996), irrigation performance assessment studies (Roerink, 1997), and for weather prediction studies (Van de Hurk et al., 1997). The scheme has found applications in different basins of the world, e.g., Snake River basin in Idaho, USA (Allen et al., 2002), the Lake Naivasha drainage basin in Kenya (Farah, 2001), all river basins in Sri Lanka (Bastiaanssen and Chandrapala, 2003) and the irrigated Indus Basin in Pakistan (Bastiaanssen et al., 2002).

The method is based on the computation of surface albedo (Zhong and Li, 1988), surface temperature and normalized difference vegetation index ($NDVI$) (Tucker, 1979) from multispectral satellite data. The surface albedo is calculated from Thematic Mapper bands 1-5 and 7; the surface temperature from band 6; the vegetation index from bands 3 and 4. The surface albedo is used to calculate net short wave radiation, and surface temperature for the calculation of net long wave radiation, soil heat flux and sensible heat flux. The vegetation index governs the soil heat flux by incorporating light interception effects by canopies and is used to express the aerodynamic roughness of the landscape.

The $SEBAL$ is a physically based analytical method that evaluates the components of the energy balance and determines the actual evapotranspiration (ET_a) rate as the residual (Bastiaanssen, 1995):

$$Rn = G + H + \lambda E \tag{4.1}$$

where Rn is net radiation at the earth's surface (W m^{-2}); G is the ground heat flux density (Wm^{-2}); H is the sensible heat flux density ($W\ m^{-2}$); λE the latent heat flux density (*W* m^{-2}), which basically is the ET_a rate. The ET_a derived from *SEBAL* includes not only bare soil evaporation but also canopy transpiration. The parameter λ is the latent heat of vaporization of water (J kg^{-1}) and *E* is the vapor flux density (kg m^{-2} s^{-1}).

The process to derive ET_a from remote sensing is based on the partitioning of the available energy (*Rn*-G) into λE and H. The net radiation *Rn* is estimated from the remotely sensed surface albedo, surface temperature, and solar radiation calculated from standard astronomical formulae (Iqbal, 1983). The ground heat flux *G* is determined through semi-empirical relationships with *Rn*, surface albedo, surface temperature, and vegetation index (Bastiaanssen, et al., 1998a; Bastiaanssen et al., 2002). The most critical factor in the physically based remote sensing algorithms is to solve the equation for the sensible heat flux:

$$H = \rho_a c_p \frac{T_{aero} - T_a}{r_{ah}} \tag{4.2}$$

where ρ_a is the density of air (kg m^{-3}), c_p is the specific heat of air (J kg^{-1} K^{-1}), r_{ah} is the aerodynamic resistance to heat transfer (s m^{-1}), T_{aero} is the surface aerodynamic temperature, and T_a is the air temperature either measured at a standard screen height or the potential temperature in the mixed layer (Brutsaert et al., 1993). The aerodynamic resistance to heat transfer is affected by wind speed, atmospheric stability, and surface roughness (Brutsaert, 1982).

Use of equation 4.2 to derive *H* could be difficult, since T_{aero} cannot be measured by remote sensing. Furthermore, remote sensing techniques measure the radiometric surface temperature T_{rad}, which is not the same as the aerodynamic temperature. The two temperatures usually differ by 1 to 5 °C. Unfortunately, an uncertainty of 1 °C in $T_{aero} - T_a$ can result in a 50 Wm^{-2} uncertainty in *H (*Campbell and Norman, 1998), which could be approximately equivalent to an evaporation of 2 mm per day. Although many investigators have tried to solve this problem by adjusting r_{ah}

or using an additional resistance term, no generally applicable method has been developed so far (Kustas and Norman, 1996).

The *SEBAL* overcomes the problem of inferring the aerodynamic temperature from the radiometric temperature and the need for near-surface air temperature measurements by directly estimating the temperature difference between T_1 and T_2 taken at two arbitrary levels z_1 and z_2 without explicitly solving for the absolute temperature at a given height. The temperature difference for a dry surface without evaporation is obtained from the inversion of the sensible heat transfer equation with latent heat flux $\lambda E = 0$, so that $H = Rn\text{-}G$ (Bastiaanssen et al., 2002; Bastiaanssen et al., 1998a; Bastiaanssen et al., 1998b):

$$T_1 - T_2 = \Delta T_a = \frac{Hr_{ah}}{\rho_a c_p} \tag{4.3}$$

where, T_1 is temperature measured at height z_1 and T_2 is temperature measured at height z_2, both temperatures measured in *(°K).* ΔT_a is air temperature difference between the two points (z_1 and z_2).

For a wet surface, all available energy *Rn-G* is used for evaporating water into λE so that $H = 0$ and $\Delta T_a = 0$. Field observations have indicated that land surfaces with a high ΔT_a are associated with high radiometric temperatures and those with a low ΔT with low radiometric temperatures. For example, in New Mexico and Idaho, moist irrigated fields have a much lower ΔT than dry rangelands. Field measurements in Egypt and Niger (Bastiaanssen, 1998), China (Bastiaanssen, 1998), USA (Franks and Beven, 1997), and Kenya (Farah, 2001) have also shown that the relationship between *Trad* and ΔTa is linear:

$$\Delta T_a = c_1 T_{rad} - c_2 \tag{4.4}$$

where c_1 and c_2 are the linear regression coefficients valid for one particular moment (the time and date the image is taken) and landscape. By using the minimum and maximum values of ΔT_a as calculated for the coldest and warmest pixel(s), the extremes of H are used to find the regression coefficients c_1 and c_2. Thus, the empirical equation 4.4 relies on differences in the radiometric surface temperature over space rather than on absolute surface temperatures to minimize the influence of atmospheric corrections and uncertainties in surface emissivity.

The ΔT_a and the aerodynamic resistance to heat transfer r_{ah} is affected by wind speed, atmospheric stability, and surface roughness. Several algorithms take a few field measurements of wind speed and consider these as spatially constant over representative parts of the landscape (Rosema, 1990; Hall, 1992). This assumption is only valid for uniform homogeneous surfaces. For heterogeneous landscapes, a wind speed near the ground surface is required for each pixel. One way to overcome this problem is to consider the wind speed spatially constant at a height of 200 m above ground level. This is a reasonable assumption, since at this height the wind speed is not affected by the heterogeneity of the local surface. The wind speed at this height is obtained by an upward extrapolation of a wind speed measurement at 2 or 10 m to 200 m using a logarithmic wind profile. The wind speed at each pixel is obtained by a downward extrapolation using the surface roughness, which is determined for each pixel using an empirical relationship between surface momentum roughness *z0m* and the *NDVI* or the Soil Adjusted Vegetation Index (*SAVI*) (Huete, 1988). The end result of all these calculations is the determination of r_{ah} and ΔT_a for each pixel, which allows us to find the sensible heat flux.

After defining necessary variables based on the above procedures and inserting R_n, G, and H into equation 4.1, the latent heat flux λE or ET rate can be derived for each pixel.

The *SEBAL* is considered to be more advantageous than other conventional methods that use T_{rad} and ΔT in estimating ET_a, because the *SEBAL* uses an internal auto-calibration process that eliminates the need for actual measurements of T_{rad} and/or ΔT as well as for atmospheric corrections (Bastiaanssen, 1995). The *SEBAL* is automatically calibrated for biases through the regression calibration of equation 4.4, which is based on a cold and warm pixel. Thus, the surface temperature T_{rad} is used as a distribution parameter for partitioning the sensible and latent heat. ΔT_a floats above the land surface as it is indexed to T_{rad} (through calibration equation 4.4), but it does not require actual measurements on the ground or atmospheric corrections.

The *SEBAL* yields an estimate of the instantaneous ET_a (mm/hour) at the time of the Landsat overpass around 10:00 am. This hourly ET_a rate needs to be extrapolated to the daily ET_a. The extrapolation is done using the evaporative fraction (i.e., the ratio of latent heat over the sum of latent and sensible heat) that has been shown to be approximately constant during the day. Therefore, multiplication of the evaporative fraction determined from the *SEBAL* with the total daily available energy yields the daily rate of ET_a.

4.2.2 Meteorological field data

The climatic data shown in Table 4.1 were collected from the Glowa-Volta micro-meteorological station located in the study area. Air temperature *Ta* and relative humidity *RH* were measured at two levels (0.3 m and 2 m) with temperature and humidity sensors having an accuracy of ± 0.2° C and 1% relative humidity. Wind speed *Wn* was measured at 2 m, while incoming solar radiation $K^{\downarrow}$ was measured with a pyranometer with a sensitivity of 1.5%. Rainfall was measured with a tipping bucket rain gauge. These measurements were collected automatically by data loggers and recorded as 10-minute averages.

Table 4.1: Climatic parameters at the Glowa-Volta weather station, in the Navrongo area, Ghana

Measured parameters	Height above surface level (m)	Measurement interval	Instruments	Type	Accuracy
Air temperature T°	0.3, 2.0	20 minutes	Thermocouple	Eijkelkamp	0.2 °C
Relative humidity RH	0.3, 2.0	20 minutes	Thermocouple	Eijkelkamp	1%
Shortwave incoming radiation $K^{\downarrow}$	4.0	20 minutes	Pyranometer	Kipp and zonen	1.5%
Shortwave reflected radiation $K^{\uparrow}$	0.5	1 hour	Pyranometer	Kipp and zonen	1.5%
Rainfall	0.3	1 hour	Tipping bucket	Eijkelkamp	1%
Surface temperature T°	0.3	1 hour	Thermal infrared radiometer	Eijkelkamp	0.1°C

The meteorological data collected at the site were used to calculate the reference evapotranspiration (ET_o) based on the FAO Penman-Monteih method as follows:

$$ET_o = \frac{0.408\Delta(R_n - G) + \gamma \frac{900}{T+273} u_2 (e_s - e_a)}{\Delta + \gamma(1 + 0.34u_2)} \quad (4.5)$$

where ET_o is reference evapotranspiration (mm day^{-1}), R_n *is* net radiation at the crop surface (MJ m^{-2} day^{-1}), G is soil heat flux density (MJ m^{-2} day^{-1}), T is air temperature at 2 m height (°C), u_2 is wind speed at 2 m height (m s^{-1}), e_s is saturation vapor pressure (kPa), e_a is actual vapor pressure (kPa), e_s - e_a is saturation vapor pressure deficit (kPa), Δ *is* slope vapor pressure curve (kPa °C^{-1}) and γ *is* psychrometric constant (kPa °C^{-1}).

The ET_o result based on equation 4.5, which integrates climatic parameters, was later used to relate to the ET_a computed through the *SEBAL* model.

4.2.3 Sap flow measurements

Transpiration consists of the vaporization of liquid water contained in plant tissues and the vapor removal to the atmosphere. The water, together with some nutrients, is taken up by the roots and transported through the plant. The transpiration process occurs predominately within the leaf, namely in the intercellular spaces, and the vapor exchange with the atmosphere is controlled by the stomatal aperture. Nearly all water taken up is lost by transpiration and only a tiny fraction is used within the plant.

Transpiration, like direct evaporation, depends on the energy supply, vapor pressure gradient and wind. Hence, radiation, air temperature, air humidity and wind terms should be considered when assessing transpiration. The soil water content and the ability of the soil to conduct water to the roots also determine the transpiration rate, as do water logging and soil water salinity. The transpiration rate is also influenced by crop characteristics, environmental aspects and cultivation practices. Therefore, different kinds of plants may have different transpiration rates. Not only the type of crop, but also the crop development, environment and management should be considered when assessing transpiration.

To evaluate the significance of vegetation transpiration and its role in the variation of atmospheric water content, the sap flow technique based on Granier's method (Granier, 1985; 1987) was used to measure individual tree water use. This method was chosen because of its simplicity, low energy requirement, reliability and low cost (Andrade et al., 1998; Braun and Schmid, 1999). The result from sap flow is supposed to be a great part of the actual evapotranspiration during the dry season when evaporation from soil and open water is lower than in the wet season.

Biometric characteristics of experimental stands

The vegetation of the sap flow experimental site was further characterized using transect methods to determine tree species composition. In this study, a tree is considered as a simple life plant form >5 m and a stem diameter ≥10 cm at breast height (Dbh; 1.30 m). Tree height, Dbh, and canopy size were estimated as presented in section 3.2.2. Tree sample trunks were visually described in situ based on healthy individuals with regular trunk shape. The result of the vegetation survey was used to select representative tree species for the sap flow measurements.

A tree water use experiment was performed for *V. paradoxa, A. albida, D. mespiliformis* and *M. indica* located in the fallow vegetation and in the cultivated area (Figure 4.1). To obtain robust estimates of water use in tropical savannah and enable appropriate scaling, samples of at least five trees are required (O'Grady, 2000). A total of 16 trees were used in the experiment. To ensure similar climatic conditions within the experimental site, sap flow measurements took place within 2 km radius around the Glowa-Volta Project meteorological station.

Estimation of tree water use using the sap flow technique

The xylem sap flow method developed by Granier (1985, 1987) was applied. The approach is based on the heat dissipation method and employs a pair of probes of 2 mm in diameter and 20 mm in length (Umweltanalytische Produkte, Munich, Germany) inserted in the conductive xylem area of the tree stem. A vertical distance of 10-15 cm separates the probes. The upper probe is continuously heated by a constant power (0.2

W), and the temperature difference between the heated and non-heated probe is monitored with thermocouples. Sap flow is calculated by the temperature difference between the thermocouples caused by sap velocity. Outputs were measured every 30 s with a DataHog2 datalogger (UP Umweltanalytische Produkte GmbH, Munich, Germany) and recorded as 10-minute averages. When sap velocity is minimal or zero, the temperature difference is the maximum, while the temperature difference decreases with increasing sap velocity. The expression to calculate sap flow is as follows (Granier, 1985):

$$Q = J * Ax \tag{4.6}$$

where Q $(l\ h^{-1})$ is sap flow; J $(cm\ h^{-1})$ is the average sap velocity; Ax (cm^2) is the conductive xylem area at the measuring point.

Sap velocity (J) is calculated by the dimensionless empirical factor (K) described by Granier (1985) based on the temperature difference measured by the thermocouples, (measuring 1 cm^2). In this study, the relationship between J and K is expressed as:

$$J = K * (\Delta T \max - \Delta T)^{1.231} \tag{4.7}$$
$$K = 0.714$$

where $T\max$ is the maximum temperature between the probes when the flow is zero or close to zero (at night), and T is the instantaneous temperature measured at the non-heated probe, ΔT is the temperature difference between the heated and non-heated probe.

Savannah fallow stand sap flow and transpiration prediction

Sap flux estimates for the different individual sampled trees were averaged by species to allow an estimate of mean sap flux (J_s) for a given species located in the study area. The averaged sap flux velocity was calculated as the mean of the maximum and minimum sap flux values (J_{smax} and J_{smin}) of given tree species water use during the hot dry season. Over the fallow vegetation stands, sap flow per unit ground area was calculated according to averaged sap velocity and stand sapwood area (which depends on mean tree sapwood area and tree density TD).

Individual tree transpiration E_c (mm day^{-1}) is calculated as the ratio of mean daily water use (l day^{-1}) and sapwood area per unit ground area (A_s/A_G mm^2 mm^{-2}) as follows (Oren et al., 1998; Evers et al., 1999):

$$E_c = J_s * A_s / A_G \qquad (4.8)$$

where E_c is stand transpiration (mm day^{-1}); J_s is mean sap velocity (cm h^{-1}); A_s is total sapwood area (individual tree mean sapwood area * tree density);A_G is ground area (ha).

The A_s for each species was obtained from increment cores taken between the two sap flow sensors at the end of the measurements. The cores were conserved in diluted alcohol at 70% and later analyzed in the laboratory of the Institute of Plant Nutrition, University of Bonn, Germany. The depth to active sapwood was visually determined by binocular examination of the core samples. A relationship between known A_s and trunk basal area (BA) and expressed as A_S / BA was used to estimate sapwood area at the Dbh from non-measured sample trees. Tree density data at the homogeneous stand were obtained from field survey at local scale, and from tree density mapping (section 3.2.4) at the watershed scale; tree transpiration of the fallow test site was calculated according to mean sap velocity and mean sapwood area at land unit (per hectare) using tree density.

In early February 2003, shortly before the end of the cold dry season, the first sap flow experiment campaign was carried out when *A. albida* was showing a full cover canopy, and individual *V. paradoxa* displayed yellowish and shed leaves as symptoms of drought stress. Indeed, the phenological events are timed with the changes of seasons, and leaf fall, flushing, flowering and fruiting are noted principally as dry season events (Jøker, 2000). The sap flow experiment was conducted on the *Acacia* plot (SFP7 *Acacia*) from 2 to 8 February and on the *Vitellaria* plot (SFP1 *Vitellaria*) from 8 to 10 February, 2003. The second measurements campaign was carried out in the late dry season from 18 March through 7 April, 2003. The *V. paradoxa* tree species were at the end of flowering and leaf green up phenological stage. For intercomparison, measurements were extended to *M. indica* and *D. mespiliformis* and other tree species found in the study area.

Two methods were applied to estimate the temporal change in transpiration in the dry season from February through March. The first was direct estimation of the sap flow rate during the two major periods in the dry season, February and March. The second method is more indirect and involves first the prediction of water use E_c from reference ET_o using the interpolation technique. Two time periods were defined for the interpolation (Allen et al., 2002): the first from 1 February through 3 March and the second from 4 March through 10 April, 2003. The prediction of water use with climatic parameters was done by multiple linear regressions. Sap flow data, considered as the dependent variables, were regressed with climatic data, air temperature, relative humidity, wind speed and solar radiation, assumed to be independent variables. These climatic variables were selected because they are the most commonly and easily measured parameters in weather stations. The regression model is as follows:

$$Q = a + b * T_a + c * RH + d * Wn + e * Rn \tag{4.9}$$

where Q is stand water use at time t; T_a is air temperature; RH is relative humidity; Wn is wind speed; Rn is solar radiation; a, b, c, d and e are the regression coefficients.

To predict fallow vegetation transpiration for times without measurements, an adjusted coefficient of transpiration, K_{cb}, was determined as the ratio E_c / ET_o. The temporal interpolation of E_c can be formulated as follows:

$$E_c = K_c * ET_o \tag{4.10}$$

where E_c is fallow stand transpiration (mm day^{-1}); K_c is a crop coefficient; ET_o is the standard Penman-Monteith evaporation (Allen et al., 1998).

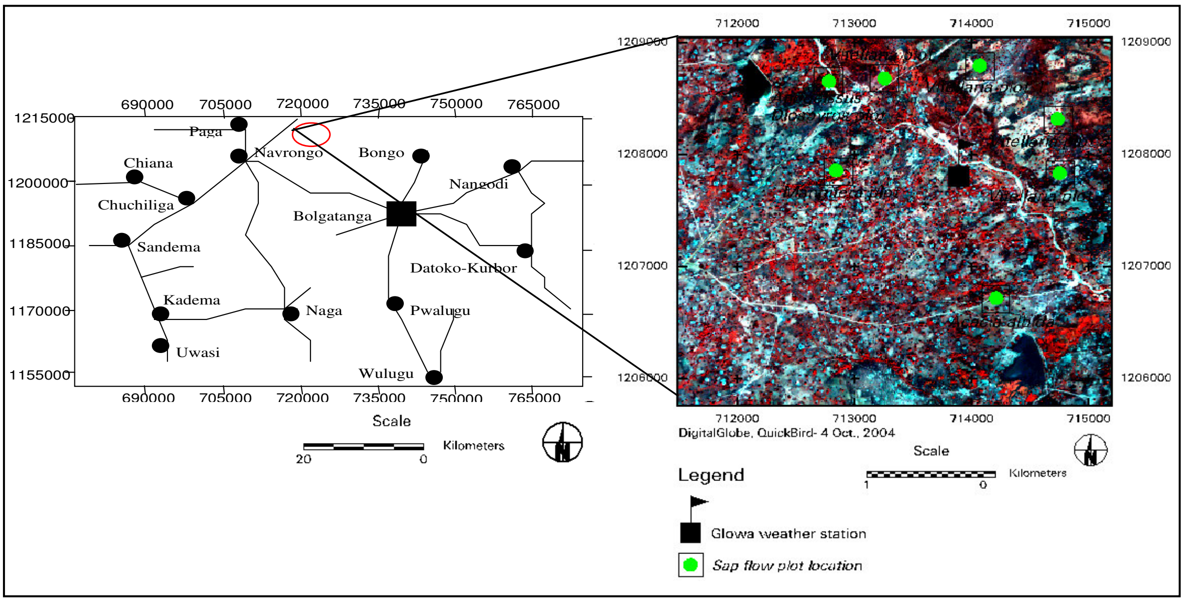

Figure 4.1: Location of the sap flow measurement sample plots test site of Pungu-Telania in the Navrongo area, Ghana

4.2.4 Temporal integration of SEBAL ETa with reference ET_o

To monitor ET_a flux over savannah vegetation during the dry season in the Volta Basin, two cloud-free Landsat7 ETM+ images acquired on the 30 October 2002 and 7 March, 2003, were processed using the *SEBAL* model. Between the consecutive satellite overpasses, ET_o was calculated at the weather station based on the FAO standard Penman-Monteith method (Allen et al., 1998) defined here as the reference evapotranspiration (ET_o). The concept of ET_o was introduced to study the evaporative demand of the atmosphere independently of crop type, crop development and management practices (Allen et al., 1998). As water is abundantly available at the reference evapotranspiring surface, soil factors do not affect ET_o calculation. Relating ET_o to a specific surface provides a reference to which crop evapotranspiration, ET_c, from other surfaces can be related. It obviates the need to define a separate ET_c level for each crop and stage of growth. ET_c values measured or calculated at different locations or in different seasons are comparable as they refer to the ET_o from the same reference surface. At this point the ET_p, the measure of the ability of the atmosphere to remove water from the surface through the processes of evaporation and transpiration assuming no limitation on water supply, differs from the ET_o. The main difference between ET_o and ET_p is the definition of reference crop surface characteristics, generally represented by an extensive surface of green grass of uniform height, actively growing and adequately watered. Indeed, the ET_o in opposition to the ET_p measures the ability of the atmosphere to remove water from a hypothetical crop with an assumed height of 0.12 m, with a surface resistance of 70 s m^{-1} and an albedo of 0.23.

To derive crop evapotranspiration (ET_c), a relationship is usually developed to relate the ET_o to a particular ET_c. Tasumi et al. (2000) used a similar approach to perform spatial interpolation of ET_a for periods where satellite data are not available. ET_c is determined by the crop coefficient (K_c) approach whereby the effect of the various weather conditions are incorporated into ET_o and the crop characteristics into the crop coefficient (Allen et al., 1998). Here K_c was computed for each land cover unit and used to extrapolate ET_a from the day of the satellite image to days between images. The assumption for the interpolation is that the ET_a ($SEBAL$) for the entire area of interest changes in proportion to the change in the ET_o at the weather station (Bastiaanssen, 2001). However, this homogeneous change in weather conditions is not always maintained (Farah, 2001), and the integration of the ET_o with K_c may suffer from cloud cover or haze situations affecting only the weather station or a part of the study area. These cases may be difficult to assess using optical satellite data. To carry out more accurate prediction of water transpiration over savannah vegetation, a cumulative 7-day crop evapotranspiration (ET_s) was defined for a short-term interval of 7 days covering the satellite overpass. The ET_s is the sum of the ET_c of 7 days when satellite images are not available. This should help to minimize the daily variability of the weather conditions in the final results for this study.

In order to compare ET_c between the two dates, two ET_a maps of the study area in the dry season were produced from two Landsat7 ETM+ images (30 October, 2002, and 7 March, 2003) using the $SEBAL$ model. These Landsat ET_a data were used as ground observed points to assist the computation of the ET_c for each $LULC$ class.

Calculating the adjusted crop coefficient K_c, and the 7-day crop evapotranspiration (ET_s)

To predict ET_a estimated from the *SEBAL* model, ET_a can be related to the ET_o through an adjusted crop coefficient K_c as follows (Allen, 1998):

$$ET_a = ET_o * K_c$$

$$K_c = \frac{ET_a}{ET_o} \tag{4.11}$$

For the time period when satellite images are not available, ET_a' for a given unit of the previously measured landscape can be predicted as follows:

$$ET_a' = K_c * ET_o \tag{4.12}$$

where ET_a'(mm day^{-1}) is daily simulated value for the real measured ET_a for the time period of satellite overpass.

The relationship for the short-term period ET_s is then computed by summing up all the daily simulated ET_a' values for the period*s* without a satellite image:

$$ET_s = \sum_s ET_a' \tag{4.13}$$

To calculate the ET_s (mm day^{-1}), it was necessary to define the beginning and the end of the dry season. For this study, the beginning of the dry season was considered to range from 27 October through 2 November, 2002, and the end of the dry season was from 4 through 10 March, 2003; these dates were defined considering satellite overpasses. Finally, mean daily ET_c was calculated for each *LULC* type, the summation of which gave ET_s.

4.2.5 Relationship between ET_c and biophysical and hydrological characteristics of the savannah

The relationship between ET_a and different landscape attributes (parameters) such as $LULC$, hydrological units and tree density was assessed using GIS-based analysis to extract respective information. ET_a data files were converted to grid files and automatically regressed with spatial data in the Arc-View GIS environment. About 5000 randomly selected points were used for the ET_a-based $LULC$ types, TD classes and hydrological units' analyses to derive the mean, coefficient of variation and standard error for each class. One way ANOVA was used to assess the significance level of the data variation within and between classes.

4.3 Results and discussion

4.3.1 SEBAL ET_a spatial distribution during the dry season

Daily SEBAL ET_a distribution at the beginning of the dry season October, 2002

Figure 4.2 presents the daily $SEBAL$ ET_a spatial distribution at the beginning of the dry season in the Navrongo area. High ET_a values are observed on the south-western sides of the study area, while low values are observed on the north-eastern sides. This may be possibly due to differences in land management practices and land cover-types. The north-eastern part is predominantly cultivated and therefore drier compared to the less cultivated and moist south-western part of the study site.

At the end of October 2002, which corresponds to the beginning of the dry season, high ET_a values are found in densely vegetated areas with mean values of 2.56, 2.80, 3.29 and 2.56 mm day^{-1}, for open savannah, woodland, closed woodland and gallery forest, respectively. The mean ET_a over these classes reached 3.18 mm day^{-1} with a mean variation of 20.2%. River beds and dams also show high ET_a values (Figure 4.2). Low ET_a values are located in bare land, shrub land and farmland, i.e., the sparsely vegetated $LULC$ classes. Mean ET_a in these classes is about 1.84 mm day^{-1} with 42.7% of variation in the data.

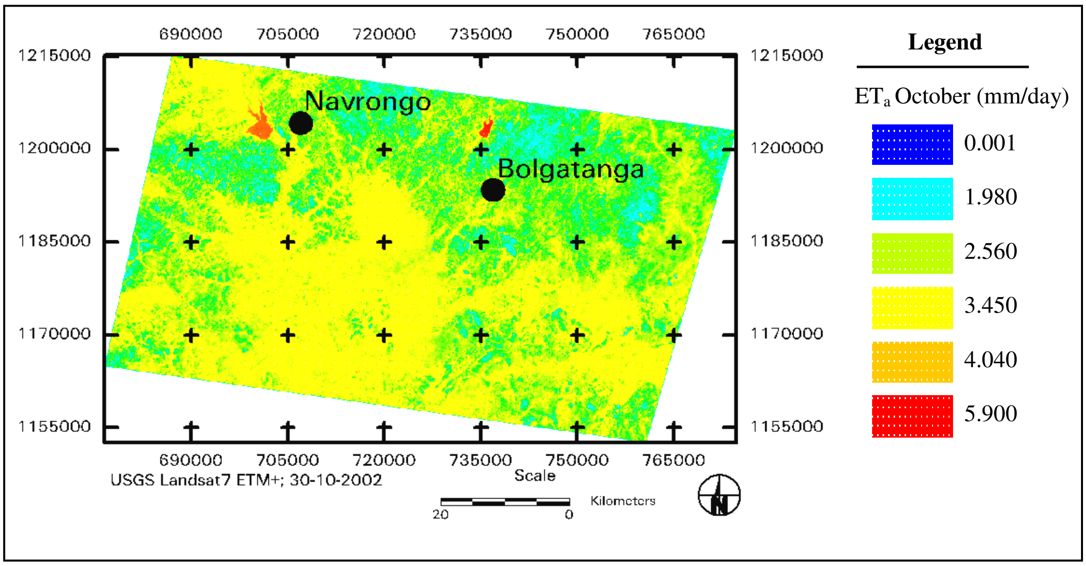

Figure 4.2: Daily ET_a spatial distribution in the Navrongo savannah on 30 October, 2002. High ET_a values are located in densely vegetated areas, river beds/dams and areas downstream of dams (depicted in red; bare lands, and poorly vegetated areas (depicted in blue) show low ET_a values.

The beginning of the dry season the savannah landscape was relatively moist, and most *LULC* classes were found to transpire water. However, due to the climatic conditions at the time (last rain occurred on 17 October), the ET_a values were relatively high and showed low variability, and all *LULC* classes were contributing to atmospheric humidity. Table 4.2 gives the daily ET_a spatial distribution by *LULC* classes at the beginning of the dry season (30 October, 2002). The higher variation in the ET_a for the *LULC* classes may be due to the role of biological activity in water transpiration in the landscape. This may be assessed through the correlation between vegetation indices and the ET_a patterns in savannahs.

Table 4.2: ET_a distribution by *LULC* classes at the beginning of the dry season (30 October, 2002), in the Navrongo area, Ghana

LULC classes	ET_a (mm day^{-1})		
	Mean	Stdev	cv (%)
Bare-land	1.29	0.8	59.2
Shrub-land	2.21	0.7	33.9
Farmland	2.04	0.7	35.1
Park savannah	1.89	0.7	41.7
Open savannah	2.56	0.7	28.6
Woodland	2.80	0.7	25.1
Closed woodland	3.29	0.5	15.3
Gallery forest/reserves	4.08	0.4	11.7
Rice fields	4.29	0.3	7.0
Water body	5.26	0.2	5.6
Built-up/outcrop rocks	1.48	0.2	18.9

Daily SEBAL ET_a distribution at the end of the dry season March, 2003

Figure 4.3 presents the ET_a spatial distribution at the end of the dry season in the study area. Very low ET_a values (close to 0) are found on bare-land, farmland and shrub-land. The low values may be primarily explained by the lack of moisture available in the upper soil layers and the leaf shedding of most deciduous savannah tree species, such as *V. paradoxa*, *A. leiocarpus*, *A. digitata,* to control water stress.

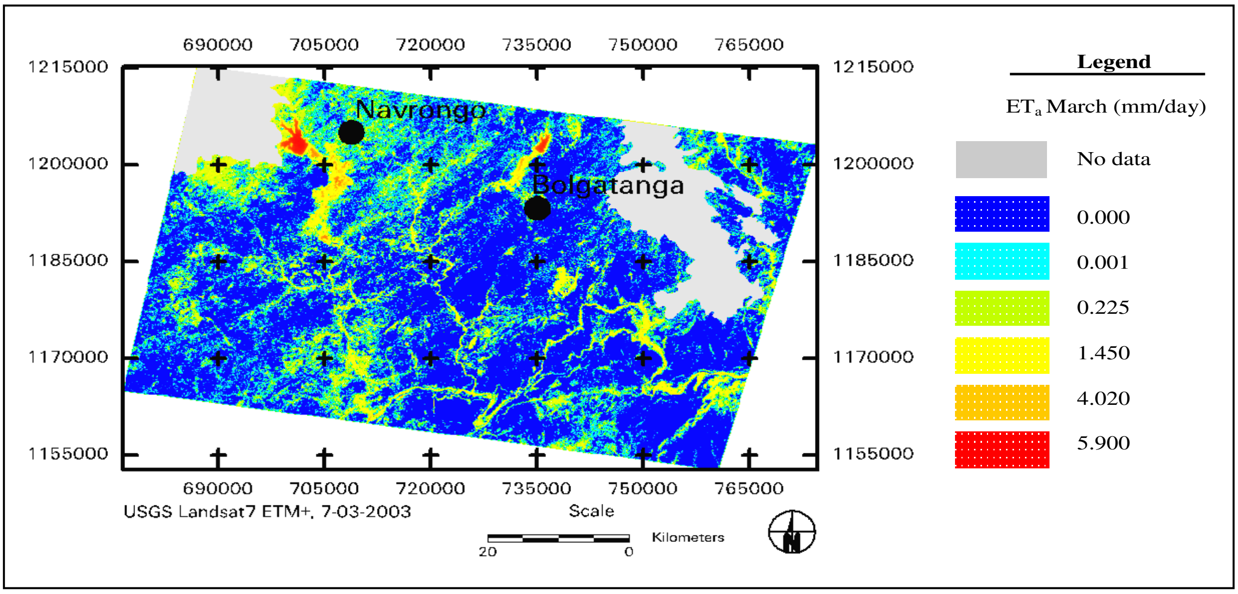

Figure 4.3: Daily ET_a spatial distribution in the Navrongo savannah on 7 March, 2003. During this season, the study area is dominated by dry patches depicted in blue. Grey patches represent some cloud cover (no data), while yellow structures represent riverbeds and gallery forests. Open waters are shown in red.

Table 4.3 shows high ET_a rates also over open waters and downstream of the Tono and Vea Dams, where rice and vegetable farming are produced in irrigated systems. Mean ET_a value was 4.86 mm day^{-1} with 29.7% of coefficient of variation. The high values may be due to high solar radiation and dry air conditions in the dry season. High ET_a values are also found in areas covered by dense vegetation. In gallery forests and reserves, mean ET_a values are estimated at 3.27 mm day^{-1}; variations reach the range of 40.9%. Table 4.3 shows the distribution of ET_a for each $LULC$ class during the warm dry season.

The mean ET_a for these $LULC$ classes ranged between 0.04 and 0.21 mm day^{-1}, and the calculated coefficient of variation was high (up to 154%), which denotes the heterogeneity of these classes. The very high variation in the ET_a distribution can be understood, as some patches of shrubs or trees may be found in some classes such as farmland or bare-land. Those relatively scattered plants are not spatially important enough to be remotely sensed at the scale of 30 m by 30 m (ETM+ sensor); however, they may be taken into account in the evapotranspiration calculation process as they nevertheless transpire vapor water. During the warm dry season, high ET_a values are found along riverbeds and in depressions. Hygrophilous trees usually grow in these areas, which are well adapted. Because of the topography and soil types, the groundwater level may be high along rivers, and thus water easily evaporates there. ET_a in those areas reached 3.27 mm day^{-1} with 40.9% of coefficient of variation.

Table 4.3: Distribution of the ET_a by $LULC$ classes at the end of the dry season, in the Navrongo area, Ghana

LULC classes	ET_a (mm day^{-1})		
	Mean	Stdev	cv (%)
Bare-land	0.14	0.1	135
Shrub-land	0.05	0.1	200
Farmland	0.21	0.2	126
Park savannah	0.04	0.0	156
Open savannah	1.00	1.1	117
Woodland	1.22	1.1	96
Closed woodland	0.60	0.8	134
Rice fields	3.19	0.7	22
Gallery forest /reserves	3.27	1.3	41
Water body	4.86	1.4	30
Built up/outcrop rocks	1.54	0.6	40

4.3.2 Temporal integration of SEBAL ET_a with reference ET_o

Relationship between adjusted ET_c and LULC types

The ET_o values were combined with ET_a from the satellite images to define an appropriate adjusted crop coefficient (K_c) that was more appropriate for savannah vegetation. This facilitated estimation of ET_c for each $LULC$ type. To extract ET_c values for each $LULC$ class, the K_c values were defined at the satellite overpass time periods (30 October, 2002 and 7 March, 2003). A mean ET_o value was calculated for a time period of 7 days to minimize variability of weather conditions before and after the satellite overpass day. Then the mean ET_o was multiplied with each $LULC$ class K_c to yield the ET_c spatial distribution over the study area (Table 4.4). Generally, the ET_c for the mean 7-day observation values were not significantly different from the ET_a. The variation between the ET_c and the daily ET_a were 3.14% and 1.61% in October and March, respectively. This implies stable weather conditions, and the use of ET_a or ET_c does not play an important role in the present study.

On 30 October, 2002, the highest K_c of 1.36 and 1.15 were found for water bodies and rice fields, whereas the lowest K_c of 0.33 and 0.38 were registered in bare-land and outcrop rocks, respectively. The high K_c values in water bodies and rice fields are certainly linked to more open water storage in lowlands and growing rice in depressions where water transpiration and evaporation is high. The results of the K_c and the adjusted crop evapotranspiration ET_c for each $LULC$ class are summarized in Table 4.4 for the time period October 2002, to January, 2003.

Table 4.4: Savannah crop coefficient K_c by $LULC$, October 2002 to January 2003, Navrongo, Ghana

LULC-weather station	ET_o	ET_a-SEBAL		K_c	Mean 7-day ET_o	ET_c
	(mm day^{-1})	mm day^{-1}	% ET_o		mm day^{-1}	mm day^{-1}
Park savannah	----	1.89	48.9	0.49	----	1.82
Open savannah	----	2.56	66.3	0.66	----	2.47
Gallery forest/reserves	----	4.08	105.7	1.06	----	3.94
Farmland	----	2.04	52.8	0.53	----	1.97
Closed woodland	----	3.29	85.2	0.85	----	3.18
Bare-land	----	1.29	33.4	0.33	----	1.25
Built-up/outcrop rocks	----	1.48	38.3	0.38	----	1.43
Water body	----	5.26	136.2	1.36	----	5.08
Shrub-land	----	2.21	57.2	0.57	----	2.13
Woodland	----	2.80	72.5	0.73	----	2.70
Rice fields	----	4.29	114.9	1.15	----	4.29
Weather station	3.86	----	100.0	----	3.73	----

On 30 October (end of the rainy season), the natural savannah in the area was estimated to have relatively good soil moisture conditions and full cover vegetation. At that time, early crop harvest had started for a few crops such as maize and ground nut leading to bare-land in the fields.

Throughout the area, ET_a values were high but unequally spatially distributed. The analysis of the K_c between $LULC$ classes demonstrates the heterogeneity of the savannah landscape in terms of its contribution to atmospheric water. The difference in mean K_c between $LULC$ classes was not significant at the 10% level, but the coefficient of variation was as high as 45%. This may be explained by factors such as soil moisture, vegetative cover or tree density, which will be studied in the next sections.

The estimated ET_c over the wettest areas (rice fields, water bodies, gallery forest/ reserves) was on average 19% higher than the ET_o, whereas ET_c was reducing over the drier parts (shrub-land, bare-land, farmland) of the landscape by about 52% (Table 4.4). This may be a significant ability of the *SEBAL* model to accurately predict ET_a over extreme soil conditions by selecting dry and wet pixels.

The calculated K_c values by *LULC* classes are given in Table 4.5 for the time period from January through April, 2003 in the Navrongo area. During the overpass of 7 March, 2003, the highest K_c values of 1.23, 0.86 and 0.83 were located in the wettest parts, i.e, water bodies, rice fields and gallery forest, respectively, but these values were lower than those found in October (Table 4.4). Lower ET_a values were recorded, and the lowest K_c values were found in park savannah, shrub-land and farmland. The mean variation in K_c between classes was very high, and was estimated at 109%, and the difference in K_c between *LULC* classes was not significant. The K_c values were generally decreasing as compared to the situation in October, and the only increase in K_c was noticed in the class built up/outcrop rocks of about 8%. This may be explained by the micro-climatic situation in towns during the dry season.

Table 4.5: Savannah vegetation crop coefficient K_c by *LULC*, January to April, 2003, in the Navrongo area, Ghana

LULC -weather station	ET_o	ET_a-SEBAL		K_c	Mean7-day ET_o	ET_c
	mm day^{-1}	mm day^{-1}	% ET_o		mm day^{-1}	mm day^{-1}
Savannah park	----	0.04	1.0	0.01	----	0.04
Open savannah	----	1.00	25.3	0.25	----	0.94
Gallery forest/reserves	----	3.27	82.9	0.83	----	3.08
Farmland	----	0.21	5.6	0.06	----	0.21
Closed woodland	----	0.60	16.1	0.16	----	0.60
Bare-land	----	0.14	3.8	0.04	----	0.14
Built-up/outcrop rocks	----	1.54	41.4	0.41	----	1.54
Water body	----	4.86	123.3	1.23	----	4.57
Shrub-land	----	0.05	1.3	0.01	----	0.05
Woodland	----	1.22	32.8	0.33	----	1.22
Rice fields	----	3.19	85.9	0.86	----	3.19
Weather station	3.73	----	100.0	----	3.71	----

On 7 March, the ET_a values for the savannahs were relatively low, which can be explained by the long drought. The savannah landscape at this time looked like a

uniform bare-land with leafless canopy trees. Vegetation greenness was low, as most deciduous trees were in either shedding their leaves or at the beginning of the greening phase (see section 5.1.3). Farmlands and bare-land are very similar, except that crop residues may be found on farms. Therefore, the high variation in the ET_a values among savannah landscape units during the dry season was not really expected, because of the vegetation development and the hotter weather conditions. However, the high ET_a values in areas with early vegetative growth such as river beds or depressions that had started their photosynthetic activity was expected. Figures 4.4 presents a comparison of the simulated daily course of ET_c by *LULC* computed using the *SEBAL* model and the reference ET_o at the beginning and end of the dry season of 2002-2003 in Navrongo savannah vegetation.

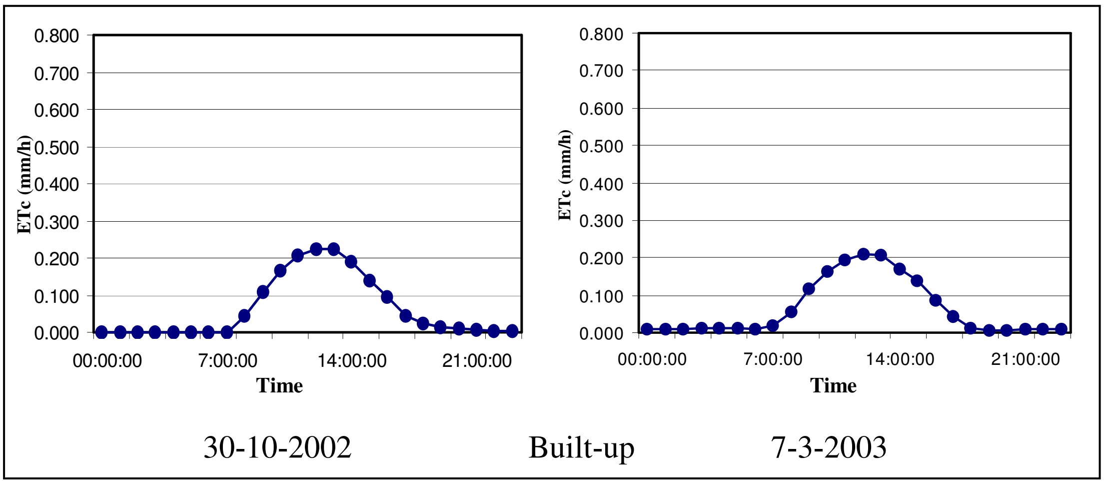

(a)

Figure 4.4: (a-j): Simulated daily course of ET_c by *LULC* at beginning and end of the dry season 2002-2003 in the Navrongo area, Ghana

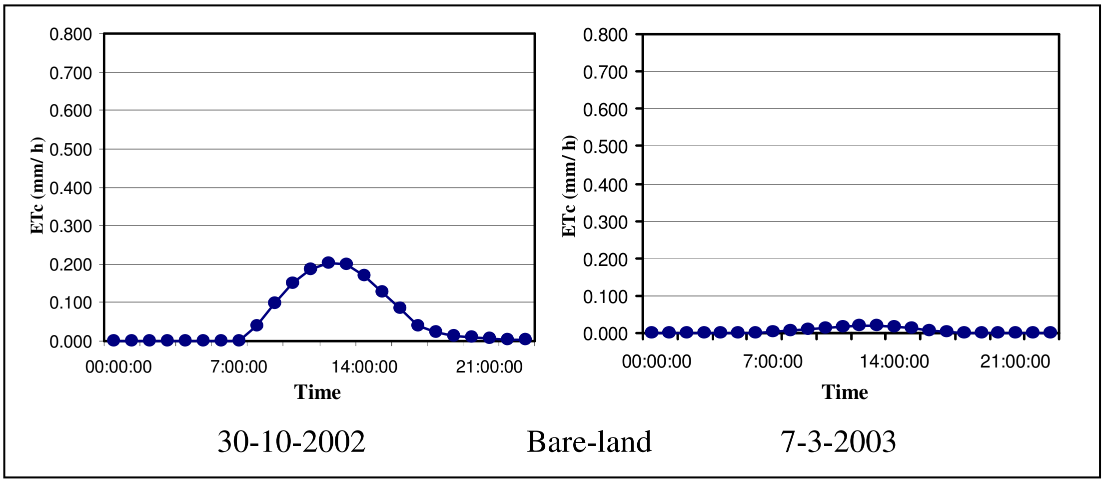

(b)

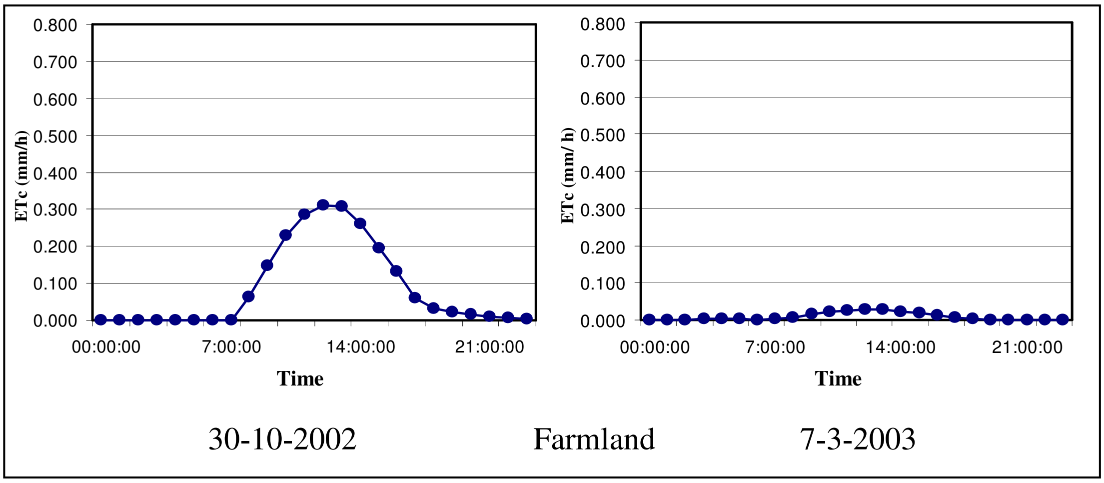

(c)

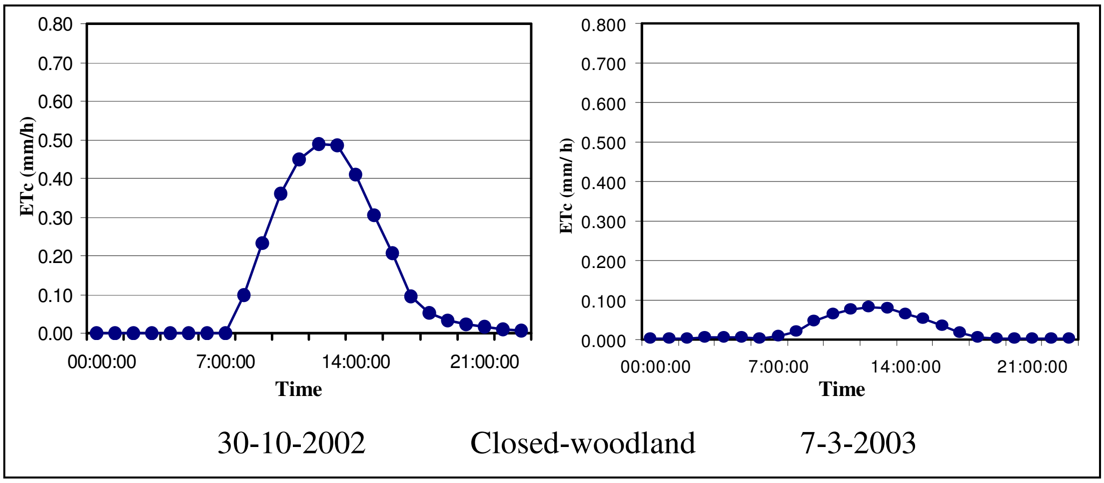

(d)

Figure 4.4: continued

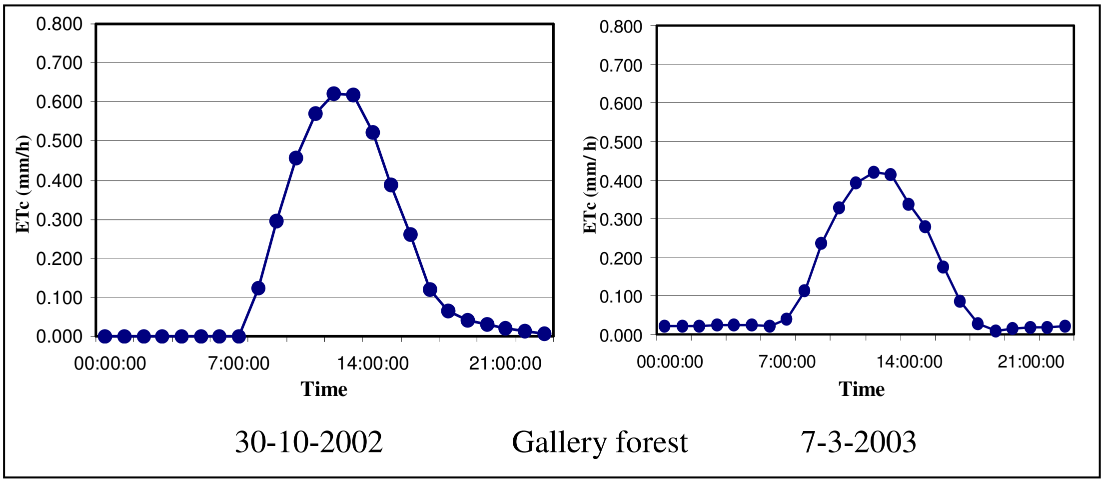

(e)

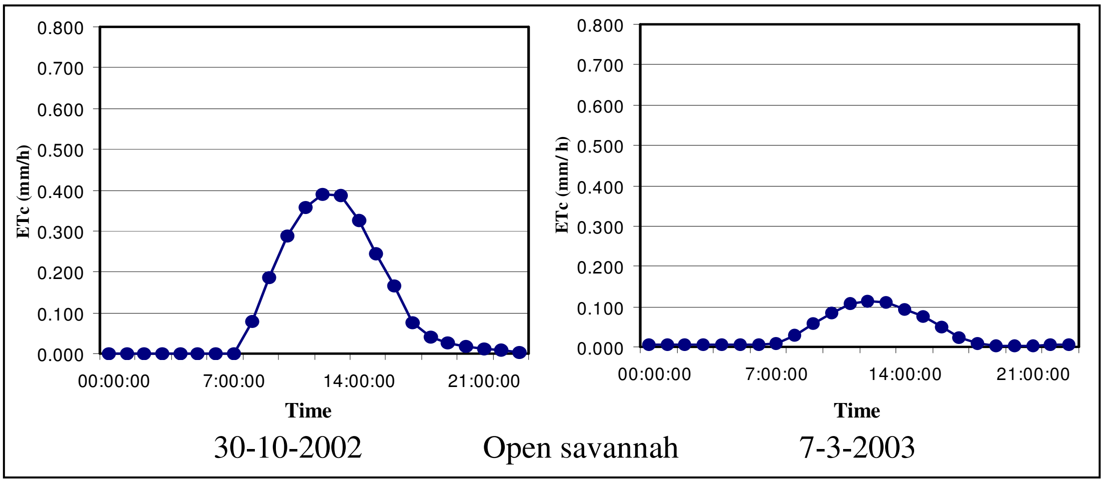

(f)

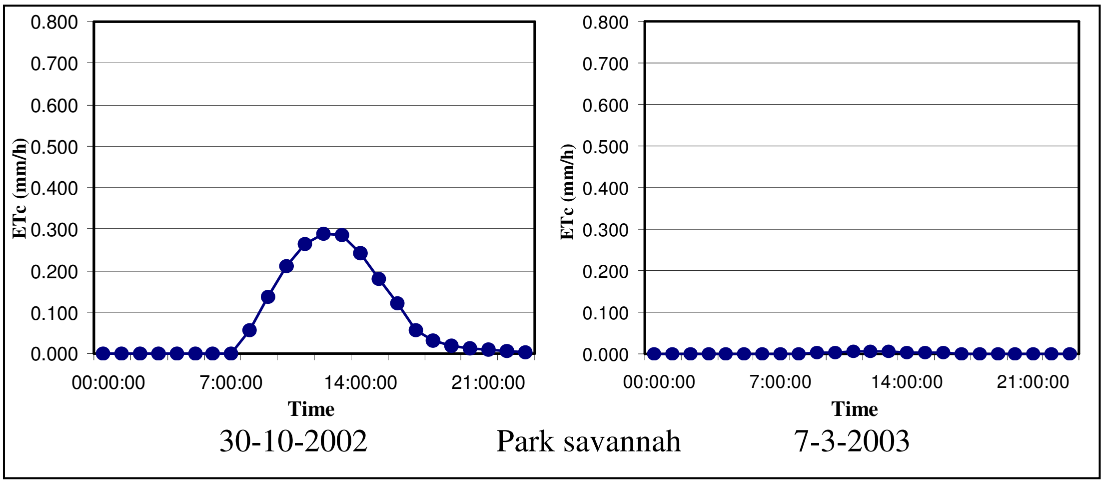

(g)

Figure 4.4: continued

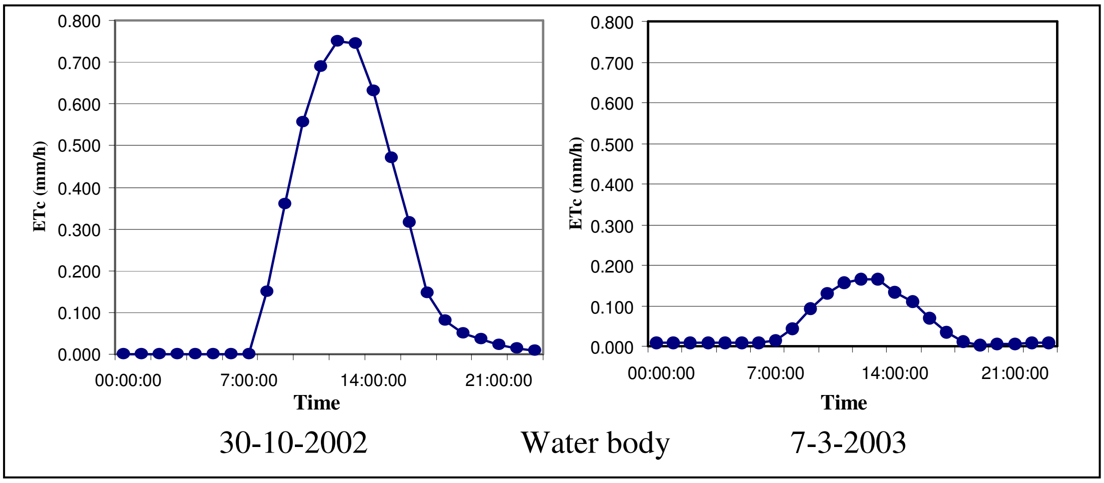

(h)

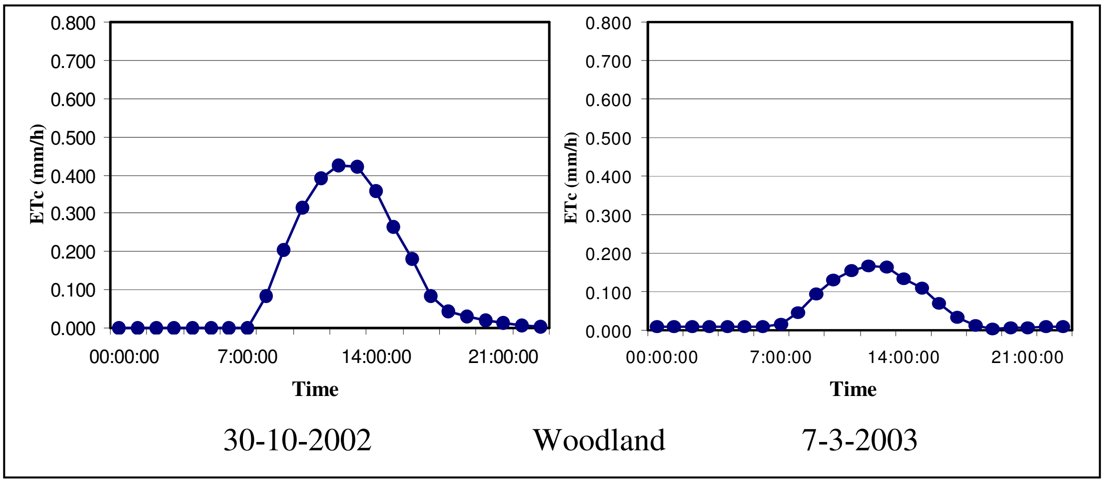

(i)

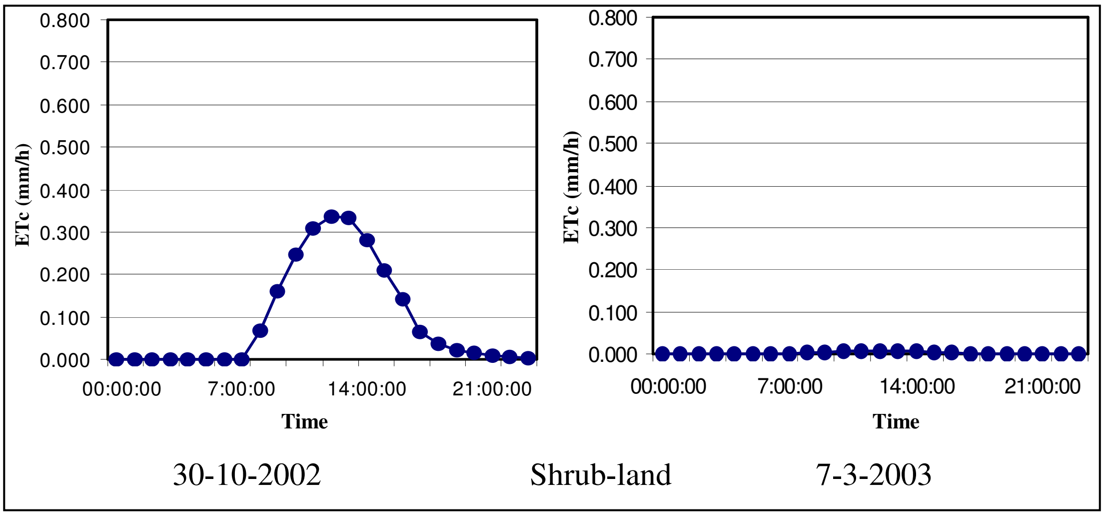

(j)

Figure 4.4: continued

Cumulative 7-day ET_s over the savannah vegetation during the dry season

The cumulative $7-day\ ET_s$ was calculated for each $LULC$ over the savannah landscape. During the beginning of the dry season, maximum ET_s values were observed over water bodies, rice fields and gallery forest/reserves. The $7-day\ ET_s$ values were 34.53 mm, 31.04 mm and 28.56 mm for water bodies, rice fields, gallery forest/reserves, respectively (Figure 4.5). The land unit types that contributed the lowest ET_s are bare-land, shrub-land and farmland with 9.03 mm, 15.47 mm and 14.28 mm, respectively. In those units, the ET_s is more linked to soil evaporation, as the green vegetation of the soil is lower.

At the end of the dry season, ET_s differed to that of the beginning of the dry season, where the values by $LULC$ were lower (Figure 4.4). At the end of the dry season, the highest ET_s rates were observed over water bodies, rice fields and gallery forest/reserves with 32.10 mm, 22.35 mm and 21.59 mm, respectively. The lowest ET_s values were recorded on bare-land, farmland and shrub-land with 0.98 mm, 1.47 mm and 0.35 mm, respectively. Figure 4.5 gives the cumulative $7-day\ ET_s$ by $LULC$ classes over the savannah vegetation at the beginning and end of the dry season 2002-2003.

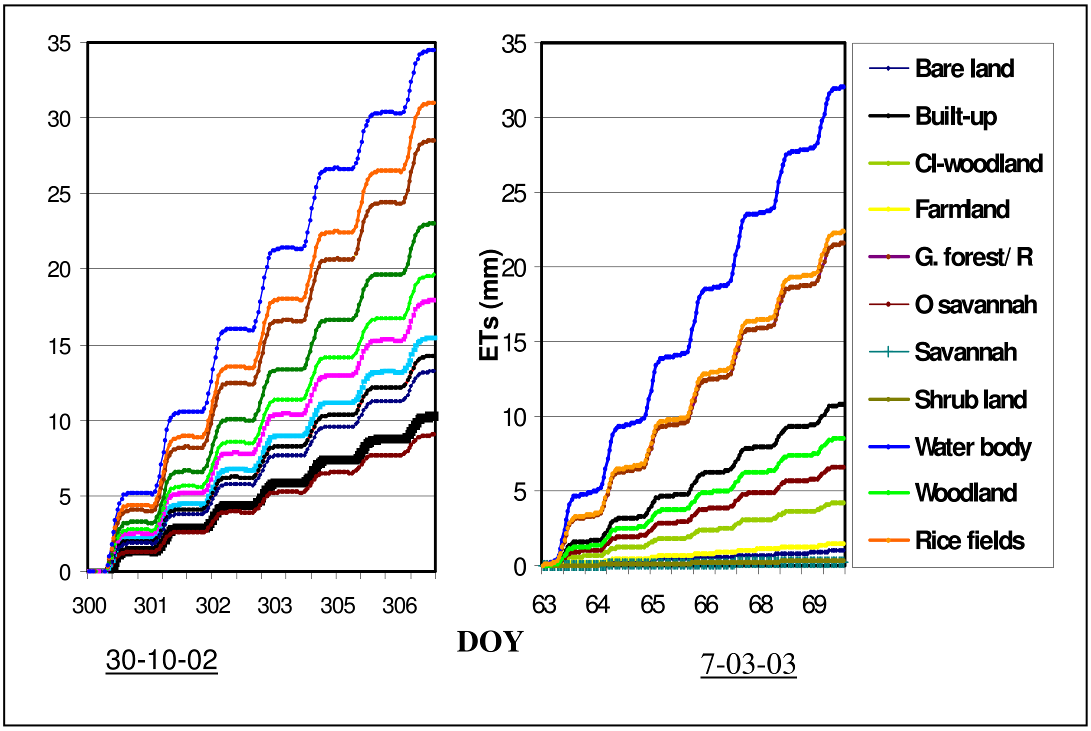

Figure 4.5: Cumulative $7-day$ ET_s by $LULC$ classes in the Navrongo area, Ghana

The ET_o values from 30 October satellite image were closer to ET_a for the $LULC$ units related to rice fields, woodland, water body, closed woodland, gallery forest/reserves and open savannah, and the moist areas in the savannah landscape. The higher ET_s rate is certainly explained by a high soil evaporation and transpiration from a luxuriant vegetation cover that is not short of moisture.

On the other hand, on 7 March, 2003, Landsat7 ETM+ image, ET_o and ET_a-$SEBAL$ values were totally different except for the wettest parts of the landscape. The ET_a-$SEBAL$ was only close to ET_o for the $LULC$ units related to rice fields, water body and gallery/reserves. The calculated K_c values over the savannah vegetation were generally <1, and thus the ET_a-$SEBAL$ values were lower than the potential ET_o. In fact, March presents the hotter and drier weather conditions in the study area, and this contributes to higher estimates of ET_o based on the energy balance equation. The conclusion is that the $SEBAL$ model and the Penman-Monteith equation closely predict ET_c for the wettest part of the landscape and preferentially at the beginning of the dry season when relatively moist conditions prevail in the savannah landscape.

4.3.3 Relationships between ET_c and tree density

Table 4.6 gives the ET_c by TD classes and their statistical characteristics in the Navrongo area for the time period of the October overpass. High ET_c values of 3.84, 3.31, 3.21 mm day^{-1} were recorded for TD71-160, TD+160 and TD classes 41-70, respectively, at the beginning of the dry season. The average rate of ET_c in these classes is 3.45 mm day^{-1}, with 9.80% of coefficient of variation (Table 4.6). This relatively low coefficient of variation indicates homogeneity in the ET_c distribution. The high ET_c values for the above TD classes may be linked to tree-biometric characteristics such as Dbh, root depth and phenological state. These vegetation classes are also located in the lowest part of the landscape that is characterized by higher soil moisture. However, the variation of the ET_c values in moisture classes was significant at the 5% level.

On the other hand, a second ET_c pattern was found in the TD classes TD0-3, TD4-20 and TD21-40 with a relatively lower mean ET_c value of 1.80 mm day^{-1}. But the variability and heterogeneity in ET_c was much more variable with a coefficient of variation of about 32%. Mean ET_c values of 1.30, 1.60 and 2.40 mm day^{-1} were registered for classes TD0-3, TD4-20 and TD21-40, respectively. The variability and heterogeneity may be explained by specific land management types with variable tree numbers on the farmland. They also may be due to the presence of ecotypes or specific groups of shrubs or trees linked with a particular soil type or moisture level at the site.

Table 4.6: ET_c distribution by tree density (TD) classes in October, 2002 (Landsat7 ETM+) in the Navrongo area, Ghana

Trees ha^{-1}	ET_c October, 2002				
	Mean	Stdev	cv (%)	Std error	Sig. level
0-3	1.30	0.56	43.35	0.06	0.003**
4-20	1.63	0.06	30.50	0.06	0.004**
21-40	2.36	0.34	14.45	0.04	0.002**
41-70	3.21	0.54	16.76	0.06	0.003**
71-160	3.84	0.67	17.40	0.08	0.004**
>160	3.31	0.30	9.25	0.04	0.002**

*** Significant at the 5% level*

The results presented in Table 4.6 are as expected. A higher TD class is associated with a higher ET_c and a lower TD to a lower ET_c rate in the studied savannah vegetation at the beginning of the dry season. The main explanation may be the availability of moisture at the beginning of dry season that allows equal evaporation from the soil layer. This shows how difficult it is to separate soil and water evaporation and tree transpiration from the actual evapotranspiration using the remote sensing approach.

Table 4.7 shows the calculated ET_c values by TD classes for the end of the dry season in the Navrongo area. At the end of the dry season, the three highest ET_c values 0.51, 0.73 and 1.14 mm day^{-1} were recorded in the TD41-70, TD71-160 and TD>160 classes, respectively. These values are lower than the values of the corresponding classes at the beginning of the dry season. The three other classes, TD0-3, TD4-20 and TD21-40, showed very low values of ET_c close to 0. The lowest ET_c values were 0.01, 0.04 and 0.06 mm day^{-1} in the classes TD0-3, TD4-20 and TD21-40, respectively. The ET_c rates were generally decreasing to very low levels as compared to the situation at the beginning of the dry season. For example, in the TD0-3 class, the ET_c at the end of the dry season was about 32 times lower than at the beginning of the dry season, while in class TD 71-160, the ET_c at the end of the dry season was about 4 times higher than at the beginning of the dry season. Globally, the ET_c in high TD classes at the end of the dry season was about 5 times lower than at the beginning of the dry season, while in sparsely vegetated classes the values at the end of the dry season were about 35 times lower than at the beginning.

Table 4.7: Landsat7 ETM+ ET_c distribution by tree density classes in March, 2003, in the Navrongo area, Ghana

Mean trees ha^{-1}	ET_c March, 2003				
	mean	Stdev	cv (%)	Std error	Sig. level
0-3	0.04	0.13	315.20	0.01	0.001***
4-20	0.01	0.01	557.00	0.01	0.001***
21-40	0.06	0.12	192.30	0.01	0.001***
41-70	0.51	0.50	99.50	0.05	0.003**
71-160	1.14	1.25	110.60	0.14	0.008*
>160	0.73	0.55	75.80	0.06	0.003**

**** Significant at the 1% level; ** significant at the 5% level; * significant at the 10% level*

Generally, two main patterns of ET_c were observed in the TD data. These are the densely vegetated classes (TD41-70, TD71-160 and TD>160) and the sparsely vegetated classes (TD0-3, TD4-20 and TD21-40) that were observed at both beginning and end of the dry hot season. However, there was a significant decrease in ET_c values between the two periods. The ratio between the classes TD0-3 (poorly vegetated) and TD71-160 (densely vegetated) was about 3 at the beginning of the dry season, and almost 28 at the end. The highest decrease between the two measurement times was observed in the sparsely vegetated class, which could be explained by a high evaporation from the soil layer. On the other hand, the densely vegetated class registered a higher ET_c value and the lowest decrease between the two periods. A possible explanation may be the good vegetative cover that was preventing direct evaporation from the soil layer.

Globally, it may be concluded that during the dry season (as we go further from the end of the rainy season) there is a higher decrease in the ET_c, and nearer to the end of the rainy season, there is a lower decrease in the ET_c. This may be due to drastic climatic conditions dominated by high solar radiation and the Harmattan wind. Furthermore, optical remote sensing may be less accurate for capturing the real extent of the savannah, as most tree species have shed their leaves. Therefore, the input of water vapor from the savannah vegetation may not be clearly identified, because of the mixing of soil layer evaporation and transpiration from the vegetative component.

4.3.4 Relationships between ET_c and hydrological units

Table 4.8 shows the ET_c values extracted for the different hydrological units (section 3.3.2) for the beginning of the dry season. Relatively higher ET_c values were registered for all the hydrological units varying from open water to bare lands. The ET_c values ranged between 0.91 and 4.46 mm day^{-1} with a mean value of about 2.7 mm day^{-1}. Generally, the mean ET_c values inside the hydrological units were significant at the 5% level assuming a high variability. However, the mean ET_c values between classes were relatively closed. This shows that each hydrological unit of the savannah landscape at the beginning of the dry season was contributing to the ET_c.

Generally, three main groups of hydrological units could be distinguished across the study area. Highest ET_c values of about 4 mm day^{-1} were observed for units 1 and 2, which correspond to the open water and irrigated areas found above the Tono and the Vea Dams. They are also found over small dams and the temporarily flooded zones of depressions and gallery forests. The Tono also shows a high rate of ET_c. The high ET_c values for this class can be understood, as they are the wettest part of the study area where storage and percolation are usually high. The availability of moisture allows the development of hygrophilous tree species such as *Vitex doniana*, *Mitragyna inermis*, *Daniellia oliveri* and *D. mespiliformis*, or simply some tree crop plantations.

In contrast, the lowest ET_c values of about 1.30 mm day^{-1} were registered in hydrological units 10 and 11 that were mostly located in farmlands and bare-lands. The low contribution of these units to ET_c may be directly linked to their low tree density ranging between 0 and 20 trees ha^{-1}. These land units are also generally characterized by high erosion and runoff and thus by poor to moderate infiltration.

Hydrological units 3, 4, 5, 6 and 7 showed medium ET_c rates ranging between 2.10 and 3.10 mm day^{-1}. These units are covered by the vegetation classes park savannah, farmland, and shrub-land. Farmland is also observed in this category due to the topographical location or the soil type. Hydrological processes in these units occur mainly in river fringes and depressions characterized by ephemeral streams to saturated overland flow.

Table 4.8: ET_c distribution by hydrological unit for the beginning of the dry season 2002 (Landsat7 ETM+) in the Navrongo area, Ghana

Hydrological unit	ET_c October 2002				
	Mean	Stdev	cv (%)	Std error	Sig. level
1	4.46	0.51	11.33	0.10	0.006*
2	3.25	0.98	30.29	0.20	0.012
3	3.07	0.65	21.11	0.13	0.008*
4	3.10	0.11	3.42	0.02	0.001***
5	2.72	0.11	4.08	0.02	0.001***
6	2.98	0.09	2.93	0.02	0.001***
7	2.78	0.15	5.26	0.03	0.002**
8	2.35	0.41	17.41	0.08	0.005**
9	2.19	0.13	5.96	0.03	0.002**
10	1.74	0.19	11.09	0.04	0.002**
11	0.91	0.45	48.87	0.09	0.006*

**** significant at the 1% level; ** significant at the 5% level; * significant at the 10% level*

At the beginning of the dry season, evapotranspiration was noticeable all over the savannah. The last rains had occurred about 10 days previously so that most of the vegetative layer was still benefiting from available soil moisture. However, the availability of water for ET_c depends on soil types and their capability to infiltrate or release water either through soil and open water evaporation or vegetation transpiration.

Table 4.9 shows the estimated ET_c values for the end of the dry season. Relatively lower ET_c values were registered in almost all hydrological units at the end of the dry season ranging between 0.9 and 0 mm day^{-1}. This may be explained by the fact that most tree species in the area are deciduous. By March (end of dry season), almost all trees have shed their leaves and are in a new greening phase with a mean LAI value of 0.20 for the main tree species *V. paradoxa*. However, high ET_c values could be observed in the unit representing the open water class (unit 1). In the hot dry season, ET_c variation in classes was significant at the 10% level at least for two classes. It could be assumed that the savannah vegetation at the end of the dry season was relatively homogeneous, but much drier than the beginning of the dry season. Only two main groups of hydrological units could be distinguished across the study area. The highest ET_c values of about 4 mm day^{-1} were observed in unit 1 which corresponds to open water bodies and some depressions. This may mainly be explained by the availability of surface water that continues to evaporate, and by the role of the groundwater table in lowlands or depressions that feeds deep-root riverine vegetation or leads to evaporation by capillary activity (Cole, 1986; Timmermans, 1999; Lubczynski, 2000).

Table 4.9: ET_c distribution by hydrological unit in March, 2003 (Landsat7 ETM+) in the Navrongo area, Ghana

Hydrological unit	ET_c March, 2003				
	Mean (mm day^{-1})	Stdev	cv (%)	Std error	Sig. level
1	4.48	0.98	21.80	0.21	0.03
2	0.88	0.61	69.67	0.13	0.02
3	0.12	0.16	128.10	0.03	0.01*
4	0.01	0.04	469	0.01	0.01*
5	0	0	0	0	0
6	0	0	0	0	0
7	0	0	0	0	0
8	0	0	0	0	0
9	0	0	0	0	0
10	0	0	0	0	0
11	0	0	0	0	0

** significant at the 10% level*

The hydrological situation at the end of the dry season is more complex and shows relatively low ET_c values. The main reason for these dry conditions is related to the deciduous vegetation layer that sheds leaves to minimize water loss. Indeed, the time period is characterized by the drastic climatic conditions of drought, high air temperature, solar radiation and relative humidity that contribute to high evaporation. As a result, the ET_c values are relatively lower at the end of the dry season for most of the hydrological units.

4.3.5 Sap flow and water transpiration in the savannah of the Navrongo area

Biometric characteristics of tree species in the sap flow experiment

The tree species composition found in the sap flow experimental site is given in Table 4.10. The results of the survey show that the Pungu-Telania fallow vegetation was mainly dominated by *V. paradoxa* (93%), *A. digitata* (2.3%), *Tamarindus indica* (1.6%) and *Bombax costatum* (1%), while *Acacia albida* (24.5%), *D. mespiliformis* (12.2%), *Parkia biglobosa* (10%), *Ceiba pentandra* (8.8%), *M. indica* (7.7%) were the most representative tree species in the cultivated area. Estimated tree mean distance ranged from 20.7 to 33 m and corresponded respectively to a mean tree density of 16 trees ha^{-1} in the fallow vegetation and 9 trees ha^{-1} in the cultivated area.

Table 4.10: Tree species composition in the sap flow experimental site in the Navrongo area, Ghana

Site area	Tree species	Frequency	Richness (%)
Fallow	*Vitellaria paradoxa*	238	93.32
	Adansonia digitata	6	2.35
	Tamarindus indica	4	1.56
	Bombax costatum	3	1.17
	Other	4	1.6
	Total	255	100
Cultivated	*Acacia albida*	22	24.49
	Adansonia digitata	12	13.33
	Diospyros mespiliformis	11	12.22
	Parkia biglobosa	9	10.00
	Ceiba pentandra	8	8.88
	Mangifera indica	7	7.77
	Azadichta indica	4	4.44
	Balanites aegyptiaca	3	3.33
	Ficus spp.	3	3.33
	Sclerocarya birrea	2	2.22
	Tamarindus indica	2	2.22
	Other	5	5.55
	Total	90	100.00

Tree species *V. paradoxa, A. albida, D. mespiliformis* and *M. indica* are the most representative over the site and were selected for the sap flow experiment during the dry season. The biometric characteristics of the selected trees are presented in Table 4.11. The canopy size of the selected trees was 7.90 m, 6.5 m, 11.8 m and 7.8 m for *V. paradoxa, M. indica, A. albida* and *D. mespiliformis*, respectively. The tree height was estimated to 8 m, 10.20 m, 10.50 m and 7.20 m for *V. paradoxa, M. indica, A. albida* and *D. mespiliformis*, respectively. The Dbh was 42.10 cm, 36.3 cm, 53.8 cm and 51.6 cm for *V. paradoxa, M. indica, A. albida* and *D. mespiliformis*, respectively.

Table 4.11: Biometric characteristics of principal tree species at Pungu-Telania site, in the Navrongo area, Ghana

Sample tree	Tree height (m)			Canopy diameter (m)			Dbh (cm)		
	mean (m)	stdev (-)	cv (%)	mean (m)	stdev (-)	cv (%)	mean (cm)	stdev (-)	cv (%)
V. paradoxa	8.0	1.6	20.0	7.9	2.6	32.4	42.1	9.7	22.9
Mangifera indica	10.2	0.7	6.7	6.5	1.5	23.5	36.3	21.3	58.7
Acacia albida	10.5	1.6	15.0	11.8	1.8	15.3	53.8	17.3	32.1
D. mespiliformis	7.2	2.4	33.7	7.8	2.0	25.5	51.6	19.0	36.7

The distribution of *V. paradoxa* Dbh size in the study site is given in Figure 4.6. Among the studied sample trees, the largest *V. paradoxa* tree-trunk size was about 3017 cm^2 and the smallest 314 cm^2. There was a variation of about 23% in tree-trunk size that may have lead to a high variation in water use.

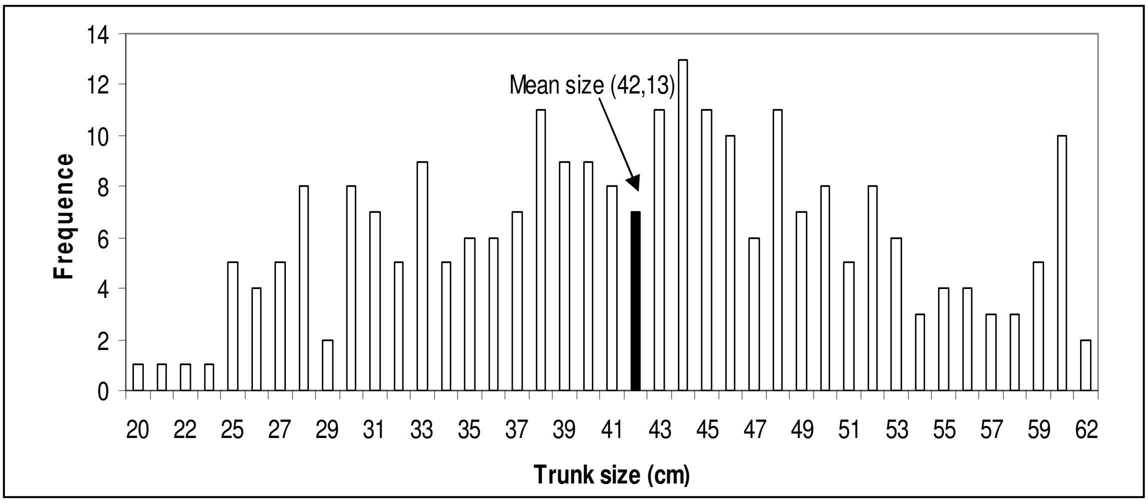

Figure 4.6: Dbh size distribution of *Vitellaria paradoxa* tree species in the fallow vegetation experimental site in the Navrongo area, Ghana

The relationships between sapwood area and basal area A_s / BA for the selected sample trees are given in Table 4.12. The determination of the average trunk size for the whole study area was necessary as sap flow estimation is largely dependent on the active sapwood area (Granier, 1985). The relationships between sapwood area and basal area were found to be 0.55, 0.79, 0.77 and 0.89 for *V. paradoxa, M. indica, D. mespiliformis and A. albida,* respectively (Table 4.12).

Table 4.12: Relationships between tree sapwood area and basal area in the Navrongo area, Ghana

Sample tree	Basal area (BA)	Sapwood area (A_s)	A_s /BA	Coefficient Mean	stdev (-)	cv (%)
Vitellaria paradoxa	1470.7	890.5	0.60	0.55	0.06	9.98
	660.2	298.2	0.45			
	2122.6	1174.4	0.55			
	1300.7	772.9	0.59			
	2189.0	1276.3	0.58			
	2550.5	1421.3	0.56			
Mangifera indica	1519.7	1213.2	0.80	0.80	-	-
Acacia albida	1017.3	916.0	0.90	0.89	0.03	3.55
	56.3	52.2	0.92			
	47.7	40.6	0.85			
	38.5	34.7	0.90			
Diospyros mespiliformis	40.5	29.9	0.74	0.77	0.06	7.99
	36.3	26.1	0.72			
	77.2	56.3	0.73			
	40.7	30.6	0.75			
	34.2	27.7	0.81			
	38.4	31.9	0.83			
	50.2	37.7	0.75			
	94.6	85.1	0.90			

Based on the above and taking into account Dbh size distribution, sap flow was measured from the mean *V. paradoxa* tree, considered as the reference for tree transpiration. Sample trees among *M. indica*, *D. mespiliformis*, and *A. albida,* the four principal species of the study area, were also measured for sap flow.

Estimation of water use of savannah tree species by sap flow technique

During sap flow measurements (day of year 77 (DOY 77) to (DOY 79)), weather conditions were hot with good atmospheric conditions. Sap flow was observed to begin at around 9 h in all *V. paradoxa* trees (Figure 4.7). The maximum sap flow rate reached about 10 l h^{-1}, which occurred between 12 and 15 h. Sap flow was observed to continue late after sunset at 19 h.

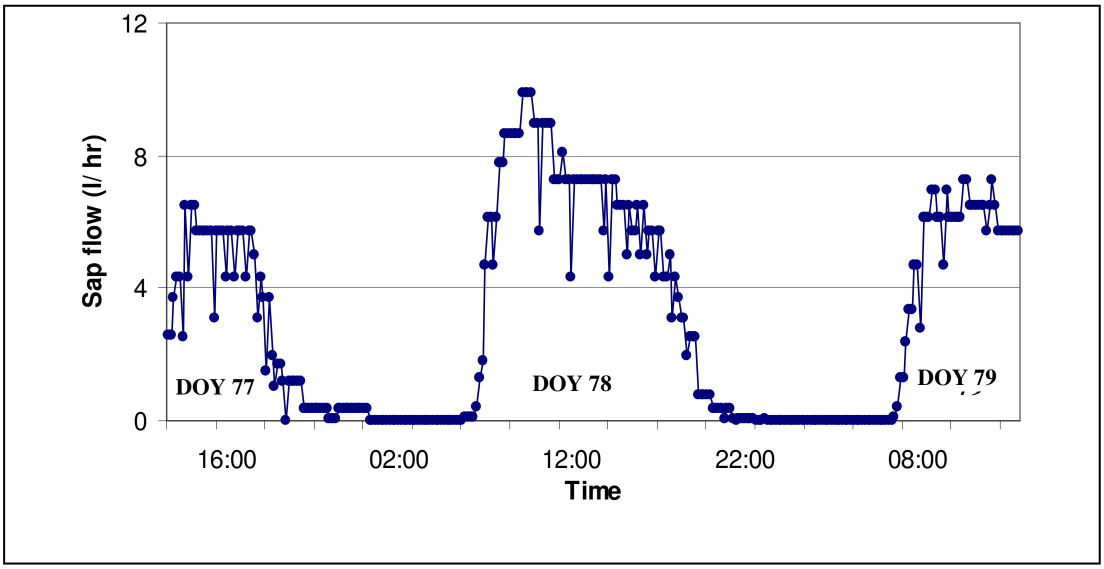

Figure 4.7: Diurnal courses of *Vitellaria paradoxa* water use for the DOY 77 to 79 in the Navrongo area, Ghana

The variation of sap flow rate in *V. paradoxa* according to sapwood area is presented in Table 4.13. The maximum daily water use of the largest *V. paradoxa* tree during the hot dry season was over 84 l day^{-1}, while that of the smallest tree was about 23 l day^{-1} (Table 4.13). The mean water use by the reference *V. paradoxa* was estimated at 32.4 day^{-1}. Daily sap flow daily rates in *V. paradoxa* varied largely according to biometric parameters including trunk size at Dbh level.

Table 4.13: Sap flow rate variation versus sapwood area in *Vitellaria paradoxa* in the Navrongo area, Ghana

Samples number	1	2	3	4	5	6	7	9
Q (l day^{-1})	23.3	84.1	32.4	40.2	45.6	77.5	25.9	74.7
A_s (cm^2)	368	368	847	926	1183	1183	368	1421

Sap flow variation reached 49% between trees of different sizes. This high variation suggests the need for a larger sampling campaign of the study site to capture all the landscape parameters that influence water use processes. Most importantly, tree transpiration is a function of the physiological and phenological characteristics of a species such as root depth or *LAI* (see section 3.3.1), or sapwood area (conductive xylem). A low sap flow associated with a larger sapwood area leads to a higher sap flow volume; a low sap velocity combined with smaller sapwood area leads to a lower water flow. On the other hand, a high sap velocity in a larger sapwood area leads to a higher sap flow volume, whereas a high sap velocity in a smaller sapwood area results in a relatively lower water flow.

The average sap flow for the monitored tree species in the Navrongo site during the dry season is shown in Table 4.14. Though sap flow rates are related to tree conductive xylem size, it is also dependent to tree species. The highest mean daily water use was observed in *A. albida* with about 110 l day^{-1} while the lowest water use was observed in *V. paradoxa* with 32.40 l day^{-1}.

Table 4.14: Daily sap flow (Q) in principal tree species in the hot dry season, 2003 in the Navrongo area, Ghana

Tree species	A_s (cm^2)	Q (l day^{-1})		
		Minimum	Maximum	Mean
Vitellaria paradoxa	847.26	5.77	91.34	32.40
Mangifera indica	1213.22	15.21	216.20	64.14
Acacia albida	1909.10	29.16	554.16	109.68
Diospyros mespiliformis	445.73	3.65	145.78	36.55

Transpiration, like evapotranspiration, is affected by climatic variables solar radiation, air temperature, humidity and wind speed, the principal weather parameters (Allen et al., 1998). The diurnal course of the sap flow is compared with the corresponding air temperature and solar radiation during the experiment days (Figure 4.8). During DOY 86 and 87 (27 and 28 March, 2003), there was a noticeable decrease in water use by *V. paradoxa* according to weather condition variations. On DOY 86, characterized by a clear and sunny sky, the daily sap flow rate was estimated to be 54 liters, while for the cloudy DOY 87 it was only 30 liters. This corresponds to a flux of about 56% (24 liters), which is primarily related to changes in the diurnal solar radiation between the two days.

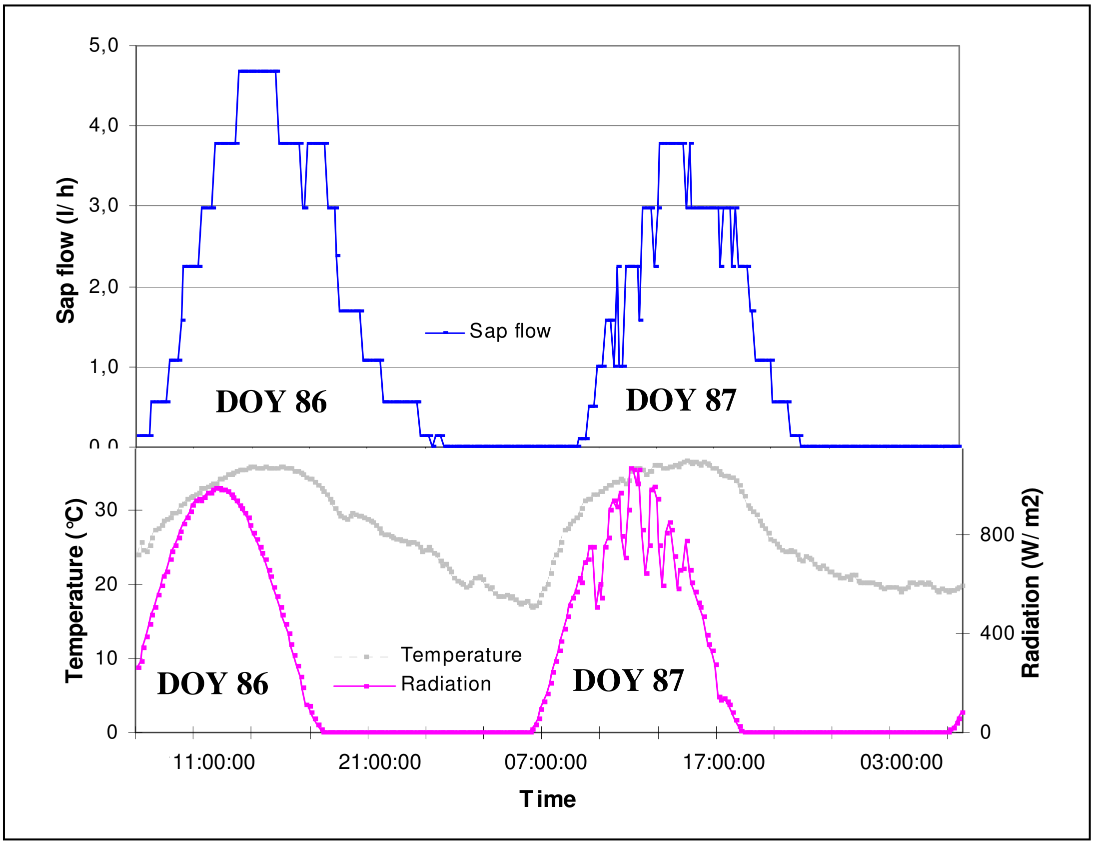

Figure 4.8: (Top) Diurnal variation of sap flow in *Vitellaria paradoxa* during DOY 86 clear sunny and DOY 87 cloudy weather
(Bottom) Diurnal variation of solar radiation and air temperature during DOY 86 and 87

The results of the estimation of the sap flow technique confirm that the technique can be used to assess the water use of savannah tree species. The sap flow distribution according to tree size shows consistency in the estimations. Tree sap flow varies according to sapwood area (Table 4.13) and species (Table 4.14). The results of the sap flow measurements in the selected species in the dry season confirm the ability of the technique to depict differences in water use. The present study gives insights into water transpiration in savannah natural vegetation in general and into the socio-economically important tree species *V. paradoxa* in particular especially during the dry season, which is characterized by drought stress.

Relation of fallow transpiration to climatic variables

The sap flow experiment shows that the water use of the principal savannah tree species was highly correlated with climatic factors (Figure 4.7). The sap flow rate relationships to climatic variables are shown in Table 4.15. During the hot dry season, *V. paradoxa* sap flow was positively correlated with *Rn* (R^2=0.58), *T* (R^2= 0.86), and *Wn* (R^2=0.73), but was negatively correlated with *RH* (R^2=0.74). A study on the tree species *Anacardium occidentale* in Edjura, Ghana has shown that the diurnal sap flow rate was correlated with the main climatic factors solar radiation *Rn,* air temperature *T*°*,* relative humidity *RH,* vapor pressure deficit *VPD* and wind speed *Wn* (Oguntunde, 2004). Because of its strong correlation with *Rn* and *T*°, sap flow is usually close to zero at night, while it increases at sunrise. Water transpiration of the savannah tree species *A. albida*, *M. indica* and *D. mespiliformis* was also strongly correlated with climatic parameters with a R^2 ranging from 0.91 to 0.32.

Table 4.15: Sap flow rate correlation with climatic variables in the hot dry season in the Navrongo area, Ghana

Savannah tree species	Climatic variables				
	Temperature (*T*°)	Relative humidity (*RH*)	Wind speed (*Wn*)	VPD	Solar radiation (*Rn*)
V. paradoxa	0.86	-0.74	0.73	-0.42	0.58
Acacia albida	0.62	-0.52	0.53	-0.06	0.75
Mangifera indica	0.35	-0.43	0.74	0.30	0.61
D. mespiliformis	0.52	-0.32	0.41	0.32	0.91

From Table 4.15 it can be seen that the climatic parameters *T*°, *RH*, *Wn* and *Rn* influence the sap flow rate. *T*° is more correlated with the *V. paradoxa* sap flow in the hot dry season (R^2=0.86) compared to (R^2=0.80) the cool dry season (data not shown). *Rn* also has a strong impact, which may exert more efficiently during the cool season when the green leaves need more energy for photosynthetic activity. In the hot dry season, the *Rn* impact on *V. paradoxa* sap flow dropped (R^2=0.58) as the leaves were shed by the semi-deciduous and deciduous trees. *RH* has a relatively constant impact through the dry season, and is negatively correlated with sap flow. *Wn* correlation with sap flow is more variable between the cool and hot dry season, and its correlation with the sap flow of *V. paradoxa* and *M. indica* becomes very obvious during the hot dry season with a correlation of up to 0.70.

Table 4.16 presents the relationship between *V. paradoxa* water use and the influencing climatic parameters, and *T*°, *RH*, *Wn* and *Rn* are considered as valuable determinants to predict water use.

Table 4.16: Determinants of water use for *Vitellaria paradoxa* in March, 2003 in the Navrongo area, Ghana

Variables			Coefficients
Air temperature	*T*	(°C)	1.840***
Relative humidity	*RH*	(%)	0.989***
Wind speed	*Wn*	(m/s)	0.217***
Solar radiation	Rn	(W/m^2)	-0.266***
Constant			----

**** Significant at the 1% level; R^2=0.86*

All determinants of water use in *V. paradoxa* are significant at the 1% level, and the R^2 value shows that at least 86% of the variation in water use in the monitored tree is explained by the climatic variables listed in the table. A 1°C increase in temperature increases water use by 1.84 l day^{-1}; a 1% increase in humidity increases water use by 0.99 liter day^{-1} in water use; an increase of 1 watt m^{-2} in radiation brings a reduction of water use by 0.27 l day^{-1}. Water use by *V. paradoxa* in the cool dry season can be predicted by the following equation:

$$y = 196.355 - 2.6T - 6.846RH + 7.727Wn + 0.176Rn \qquad (l\ h^{-1}) \qquad (4.14)$$

However, a linear relationship may not be adequate to predict water use, as the climatic variables radiation, temperature, and relative humidity are all interdependent. However, previous studies on sap flow measurements have shown that linear equations were best predictive of water use in comparison to other non-linear equations including quadratic or collinear models (Diane E. Pataki et al., 2000; Oguntunde, 2004).

Table 4.17 gives the functional relationship between the sap flow of the principal savannah tree species and climatic factors during the March-April period. Water use by different tree species is highly variable according to climatic parameters. During the experiment, *T, RH, Wn* and *Rn* were the parameters most highly correlated with *V. paradoxa* water use of the test site. The assumption considers climatic factors as independent variables while water use is the dependent variable.

Table 4.17: Relation of water use of principal savannah to climatic factors in March, 2003 in the Navrongo area, Ghana

Tree species	Regression models	R^2	SE	N
Vitellaria paradoxa	Qt = a+b*Rn+c*RH+d*T+e*Wn	0.86	13.6	285
Diospyros mespiliformis	Qt = a+b*Rn+c*T+d*RH	0.89	14.4	297
Acacia albida	Qt = a+b*Rn+d*RH+c*T+e*Wn	0.71	97.3	736
Mangifera indica	Qt =a+b*T+c*RH+d*Wn	0.63	40.8	391

R^2 for estimation data (n=285), SE is the standard error of estimate, N is the estimation data (285) and a, b, c, d and e are fitted model parameters.

Differentiation in water use of savannah tree species

Figure 4.9 shows the comparative diurnal course of sap velocity for *V. paradoxa*, *A. albida*, *M. indica* and *D. mespiliformis.* It illustrates the difference in sap velocity during the hot dry season. During the late dry season, the mean sap velocity for *V. paradoxa* trees ranged between 1.59 and 2.90 cm h^{-1}. This corresponds to a mean sap velocity of 1.91 cm h^{-1} over the fallow vegetation. However, the velocity among the measured trees showed a relative variation of about 26%. This suggests high variation of tree response to the bio-physical and climatic environment to access to water for transpiration.

Among all measured tree species, *A. albida* showed the highest velocity compared to all other tree species during the dry season. *A. albida* samples showed a mean sap velocity of about 4.8 cm h^{-1}, reaching 220 l day^{-1} for an individual of 52 cm Dbh. This is expected, as *A. albida* trees develop leaves in the dry season. The ratio of *A. albida* mean sap velocity to other species was high with 1.5, 2.2 and 1.1 respectively for *V. paradoxa, M. indica* and *D. mespiliformis* during DOY 86 to 88, 62 to 65, and 92 to 94. These differences in sap velocity suggest different water use by savannah trees.

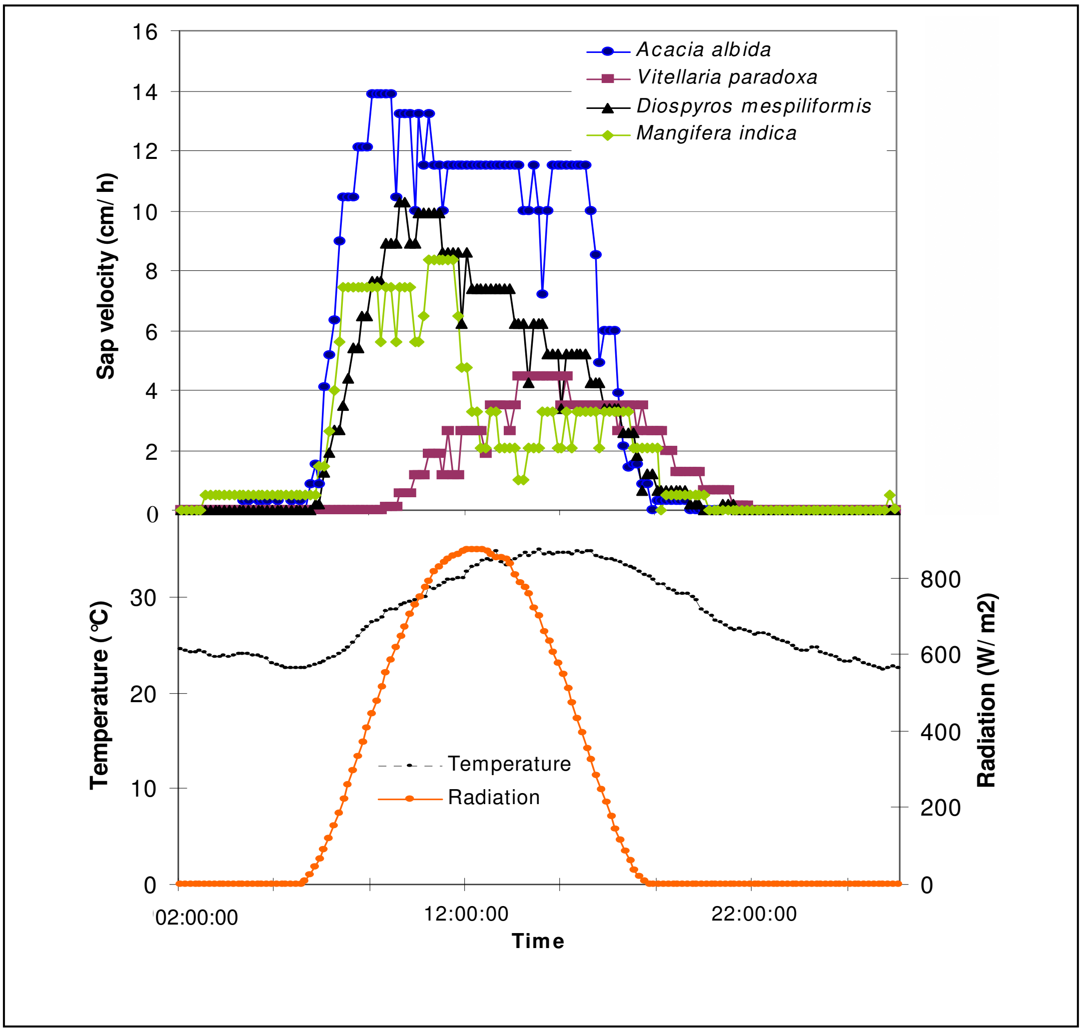

Figure 4.9: Water use (l day^{-1}) of savannah tree species in the hot dry season between 18 March and 7 April, 2003 in the Navrongo area, Ghana

Table 4.18 gives the mean sap velocities for the monitored trees showing that the highest sap velocities were observed in *A. albida* (13.06 cm h^{-1}) and *D. mespiliformis* (9.71 cm h^{-1}), while the lowest was observed in *V. paradoxa* (3.54 cm h^{-1}) samples. The immediate assumption is that with the same Dbh size, *A. albida* and *D. mespiliformis* are the highest consumers of water, while *V. paradoxa* individuals need little water during the dry season. The high water use in *D. mespiliformis is* not surprising as the natural ecotype of this plant is generally located in depressions and riverbeds where the groundwater table is high.

Table 4.18: Average sap flow velocities for savannah tree species during the hot dry season 2003 in the Navrongo area, Ghana

Tree species	Minimum (cm h^{-1})	Maximum (cm h^{-1})	Mean (cm h^{-1})	Stdev
Vitellaria paradoxa	0.28	4.49	1.91	1.54
Mangifera indica	0.52	7.61	4.06	2.63
Acacia albida	0.86	13.06	6.96	5.43
Diospyros mespiliformis	0.53	9.71	5.12	3.44

V. paradoxa tree species show the lowest sap flow velocity compared to the other species. However, the sap flow velocities mean values of the different tree species are relatively closed. It could be assumed that the savannah tree species at the site had a similar sap flow velocity during the experimental period. In conclusion, the studied stand vegetation transpiration is primarily dominated by the water use characteristics of *V. paradoxa* species (93% of the tree species).

Temporal variation of *Vitellaria paradoxa* water transpiration

Absolute sap flow data were compared on the basis of measurements for *V. paradoxa* and *A. albida* sample trees between the cool and hot dry season. Figure 4.10 presents the comparative sap flow rate change in *V. paradoxa* and *A. albida* in the two time periods. In *V. paradoxa*, there was an apparent decrease in sap flow rate in the late dry season in March-April. The mean sap flow rate in February was estimated as 86 l day^{-1}, while this value dropped to only 32.4 l day^{-1} in late March. This represents a large decrease in water use by about 61% during the observation period. This difference may be related essentially to physiological and phenological adaptation to the 5 month drought. Leaf shedding is a common phenomenon in semi- and deciduous tree species under water stress and is regarded as a mechanism of adaptation to occasional or periodic drought (Oppenheimer, 1960; Kramer, 1983). The phenological reaction of *V. paradoxa* consisted essentially of a reduction in *LAI* through leaf shedding from the end of January through February by about 50% (see section 3.3.1).

Conversely, the diurnal sap flow of *A. albida* in February was estimated to 80 l day^{-1}, which increased up to 104 l day^{-1} in March. This corresponds to a water use increase of nearly 30% in merely 2 months and a decline in soil moisture (section 3.3.1) in the layers 0-50 cm. The higher water transpiration is obviously correlated to its inverse phenological behavior in the dry season with a *LAI* increase by 15% between October and December. Green up usually occurs in October-November, and a full vegetative cover is reached in late February-March. The important quantity of water used by *Acacia* in the dry season is also related to a high physiological capacity to develop deep roots (see section 3.3.1) tapping deep groundwater.

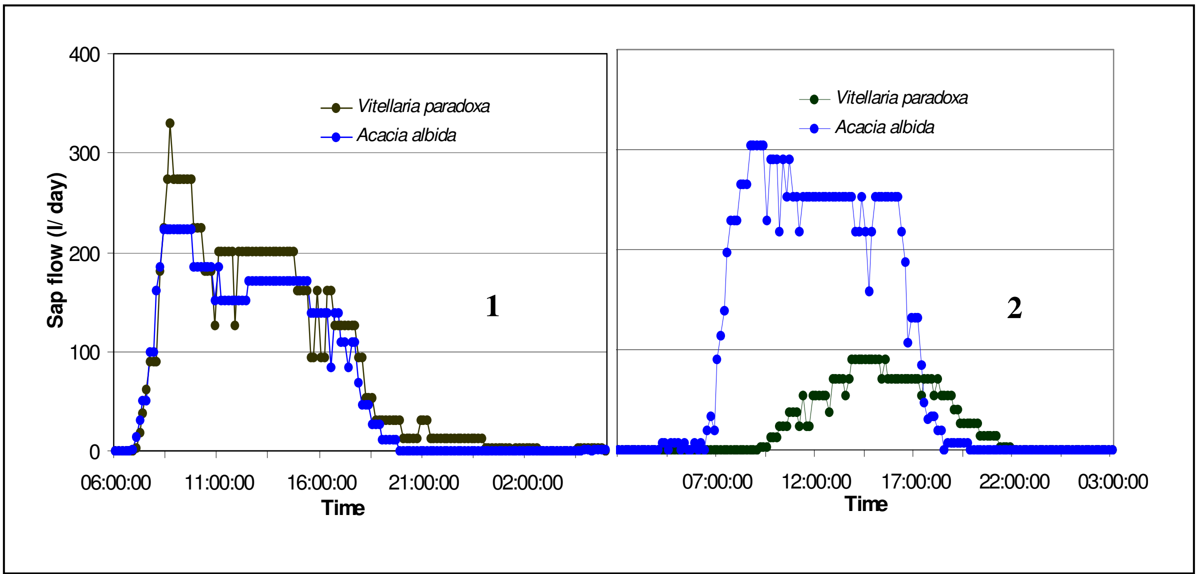

Figure 4.10: Diurnal sap flow rate in *Vitellaria paradoxa* and *Acacia albida* during the cool (1) and hot (2) dry season in a savannah fallow vegetation stand in the Navrongo area, Ghana

Compared to the cool dry season, the hot dry season was characterized by drastically drier environmental conditions requiring specific biological and physiological adaptation by the savannah tree species. The change in water use rate is related to sap velocity, which moves the sap from the roots to the leaves for photosynthetic processes. The monitored velocity for the *V. paradoxa* trees was estimated at 4.20 cm h^{-1} in February, dropping to 1.91 cm h^{-1} in the late dry season. In contrast, sap velocity of *A. albida* increased from 3.60 cm h^{-1} to 6.96 cm h^{-1}. These temporal adaptations to drought followed the phenological change of *V. paradoxa*.

Temporal integration of fallow vegetation transpiration using reference ET_0 data

The results of the water transpiration measurements during the dry season are presented in Table 4.19. The water transpiration E_c (mm day^{-1}) of the fallow vegetation was calculated from equation 4.8 for both cool (1 February through 3 March) and hot dry (4 March through 7 April) season. Tree density data, necessary for the spatial extrapolation from individual estimation, were acquired from the remote sensing analysis (see section

3.3.3). Mean water transpiration from the fallow vegetation was 0.14 mm day^{-1} in the cool dry season, while it decreased to only 0.05 mm day^{-1} in the hot dry season. For the cool dry season, a K_c value of 0.03 was estimated, which dropped to 0.01 in the hot dry season. This corresponds to a K_c change of about 67% between the two time periods.

The absolute evapotranspiration changes between the two periods based on the FAO Penman-Monteih method increased to an ET_o of 0.55 mm day^{-1} and a decrease of 0.13 mm day^{-1} based on the sap flow technique. For the cool dry season, the cumulative 7-day measurements (from 27 October to 2 November, 2002) of the ET_o and the E_c from the sap flow estimations amounted to 30.50 mm and 0.96 mm, respectively. In the hot dry season, the cumulative 7-day measurements (4 to 10 March, 2003) of the ET_o and the E_c were 62.00 mm and 0.67 mm, respectively. It is interesting to note that water evapotranspiration keeps increasing when estimated by the FAO Penman-Monteith method while it decreased with the sap flow method. This is explained mainly by the fact that the ET_o is the result of the energy-balance-based calculation that resulted in high values in the hotter weather at the end of the dry season. In contrast, the hotter weather conditions are not suitable for deciduous trees, which have to adapt by stomata closing and leaf shedding. These reasons may play a big role in the reduction of tree transpiration rates.

The increase in ET_o through the Penman-Monteith estimation is better explained by the use of the energy-balance terms. Any increase in energy supply through air temperature or radiation should result in an increase in water evaporation. This is not always the case in the tropical conditions in general, and especially the savannah conditions of Navrongo site, where droughts of about 4 to 5 months can reduce soil moisture and thus plant evapotranspiration. Indeed evapotranspiration may decrease over the dry season as the topsoil dries out, and the deciduous vegetation canopy sheds out. A reduction in the ET_a is likely expected, and the decrease registered from the sap flow measurements agrees well with common experience.

Table 4.19: Savannah fallow vegetation transpiration in the dry season 2002-2003 in the Navrongo area, Ghana

Time period in the dry season	ET_o (mm day^{-1})	Sap flow estimate		Transpiration coefficient K_{cb}
		mm day^{-1}	% ET_o	
Daily cool dry season	4.35	0.14	3.15	0.03
Daily hot dry season	4.90	0.05	1.08	0.01
7-days ET_c February	30.49	0.96	----	----
7-days ET_c March	61.90	0.67	----	----

The observed difference in the monitored transpiration between the early and late season is in accordance with phenological development of the savannah vegetation. Indeed, most of the deciduous or semi-deciduous trees including *V. paradoxa* generally suffer from water stress starting from the dry season (October-November), while leaf shedding occurs later in the middle of the dry season (February-March). The high tree transpiration difference between early and late season as observed by direct estimation of sap flow confirms the robustness of the sap flow technique to assess natural tree water use.

The water vapor input of the fallow vegetation to the atmospheric water is greatly reduced during the dry season. This is largely due to the plants´ ability to adapt to exterior factors, i.e., primarily drought conditions. However, the reduction in tree transpiration over the fallow vegetation can also be explained by the reduction in the soil moisture in a drier environment, and the transpiration reduction of other understory herbaceous green vegetative elements that disappear partially or totally during the dry season. Human-induced impacts such as wood cutting or bush fires could also play a large role in the reduction of water recycling capacity of natural savannah vegetation. This reduces the functional capacity of the green vegetative component to transpire water.

4.4 Conclusion

The use of the *SEBAL* model and the sap flow technique in this study to measure water use of the savannah vegetation gives successful results. Water transpiration was relatively low, and corresponds to the expectations. However, comparison with other similar results may be difficult, as most of the studies related to vegetation water transpiration were done in temperate forests and to a lesser extent in semi-arid and arid areas (Köstner et al., 1998; Oren et al., 1998; Vertessy et al., 1997; Philips et al., 1996).

However, the application of the techniques gives some information about the water transpired by natural tree species in the fallow vegetation of Navrongo area. These results may improve with further short- to long-term measurements of tree water use. The proximate estimates from the sap flow technique measurements and from the $SEBAL$ model validate the ET_a method and encourage the use of the techniques for monitoring evapotranspiration in the future. This is a first application of the techniques in the study area, and the methods need more tests on other tree species and in other areas. The relationships between biophysical and hydrological components were also highlighted. There was a decreasing rate of ET_a associated with decreasing tree density. However, ET_a varies between $LULC$ types and moisture distribution according to different hydrological units. On the other hand, the sap flow technique enables differentiation of water transpiration variation between biometric characteristics and tree species. Furthermore, both $SEBAL$ and sap flow methods allow estimation of the reduced water loss in the savannah environment during the drought stress conditions of the dry season. This shows the potential application of both methods in general for studying the hydrological role of savannah vegetation at local and regional scales. The sap flow technique in particular has advantages over other methods, as the assessed values reflect the direct water use by plants (Hatton et al., 1994) and are not mixed with evaporation values coming from diverse sources such as soils or water bodies, which is certainly the case with the $SEBAL$ ET_a.

5 SUMMARY AND CONCLUSIONS

5.1 Introduction

Actual evapotranspiration (ET_a) is an important component in applications related to hydrology, agriculture and meteorology. ET_a at the landscape level displays large variations both spatially and temporally due to differences in land surface parameters. Remote sensing is a powerful tool to estimate ET_a at local, watershed and entire river basin levels. However, the practical use of remotely sensed spectral data in hydrological management of the land surface has been limited by the non-availability of spatial ET_a data to support biophysical characterization of land surface parameters.

In developing countries in general, and in the arid and semi-arid areas of the Volta Basin in particular, the ET_a data are mainly point data acquired at meteorological stations and not representative of large areas. In this study, the Surface Energy Balance Algorithm for Land ($SEBAL$) model was applied over a savannah landscape to estimate the spatial and temporal distribution of ET_a. This is of importance to adequately determine the water budget at local and regional scale. The aim of this thesis is to quantitatively characterize the biophysical and hydrological components of the savannah landscape and to relate them to the ET_a variability.

In the Volta Basin, rapid population growth of about 3.1% yr^{-1} combined with increasing urbanization and expansion of irrigation systems will lead to rapidly growing water demands in the next few decades (WRM, 1998). To understand the potential impact of the growing demand on water, the Glowa-Volta Project was initiated. The Navrongo savannah landscape of Upper-East Ghana was selected as a case study to assess the spatio-temporal variability of ET_a and the associated controlling factors.

5.2 Biophysical and hydrological characteristics of the Navrongo savannah area

5.2.1 Land-use and land-cover mapping

In order to extract the ET_a of different land-use and land-cover ($LULC$) types, satellite images and field data were used to generate $LULC$ maps. A classification scheme based on a modified FAO-UNESCO method was used to derive the *LULC* types. A hybrid algorithm combining unsupervised and supervised classifiers was applied. A total of 10 major *LULC* types were identified in the savannah landscape, with a further class represented by the irrigated rice fields around the Tono and Vea dams. The natural savannah classes consisted of open savannah, woodlands and gallery forests; the agricultural classes are represented by farmlands, park savannah, irrigated fields and bare-land; two further *LULC* types are built-up and open water.

The results of the classification show that the natural savannah classes such as shrub land, open savannah, woodlands and gallery forests represented about 56% of the study area. The agricultural lands, including rice fields, park savannahs associated to farmland covers were about 35% of the study area. Water bodies and built-up areas were the smallest units in the study area with 0.68% and 0.19%, respectively. Relating the savannah vegetation classes to their hydrological role, the large-scale *LULC* classes may play a major role compared to the other classes.

5.2.2 Spatial distribution of fire traces in savannah vegetation

As fire traces have different impacts on the sensible heat flux compared to their surroundings, it was necessary to define their extent and spatial distribution. For this purpose, an ASTER image was acquired for the early dry season. Field data the albedo and temperatures of the fire traces, and GPS point data of potential burnt areas of fallow vegetation were also recorded during the dry season field campaign to complement the remote sensing approach. These data were valuable for differentiating land surface parameters of similar albedo.

The Principal Component Analysis (PCA) method was applied to enhance a false color composite image, which was interpreted into burned and unburned classes. The results show that old and recently burned traces were the most common types of burns with about 64% and 11% of the study area, respectively. Only 25% of the area remained non-burnt, which corresponds to either densely or sparsely vegetated areas. Thus, most of the savannah area was burnt, which has a strong influence on the climate system and the vegetation cover in general and significant implications for the hydrological function of the vegetation layer in particular.

5.2.3 Spatio-temporal patterns of hydrological units in the savannah landscape

To determine the spatial distribution of hydrological units and their relation to ET_a, the Vegetation Index Temperature Trapezoid ($VITT$) approach was applied using spectral biophysical parameters such as Normalized Difference Vegetation Index ($NDVI$), surface albedo and temperature. These data were combined into one layer to represent the distribution of moisture in the study area. Two Landsat7 ETM+ images were used to represent extreme climatic and moisture conditions at the beginning and end of the dry season, respectively.

At the beginning of the dry season, October 2002, 11 hydrological clusters were derived from the study area and were found to be dominated by wetness conditions. This situation may be explained by the recent rains and the presence of a luxuriant vegetative layer still transpiring actively. The wettest units were located in the gallery forest and the water bodies, while the driest units were found on bare-land, outcrop rocks and bare farmland. The remaining part of the landscape is represented by senescent vegetation. Globally, the difference between the hydrological classes was not significant at the beginning of the dry season.

In the second period, in March 2003, the landscape was characterized by drier hydrological conditions than in October 2002. The analysis of the $VITT$ diagram shows that the area was dominated by drier pixels. The wettest hydrological units are represented by open water bodies, rice fields and gallery forests, generally located in lower parts of the landscape where moisture is more concentrated. This relative wetness of these classes is due to the water management system and topographic location, which direct water and moisture towards valleys and depressions. The rest of the landscape was dominated by widespread drier patches, which can be interpreted as a wide extension of drought-prone areas with low ET_a rates.

5.2.4 Tree density mapping using high spatial resolution remote sensing data

Estimates of tree density were based on soil adjusted vegetation index ($SAVI$) data and ground-based assessments with verification using a localized high spatial resolution Quick-Bird image. During fieldwork, 147 sample points were collected and used to derive 7 thematic spectral classes. The changes in specific tree density (TD) class from high to low vegetative index corresponded to real quantitative changes observed from reference data. The different trends in TD classes were interpreted as consistent with the validation process. Considerable variability exists along the savannah landscape in general, and in the TD classes. The tree density class TD 71-160 occurred mostly in the gallery forests/reserves of the area. These are developed in densely vegetated stands of big canopy trees along the riverbeds of the Tono and the Volta Rivers and around depressions areas. These areas typically contained well-adapted hygrophilous trees that develop a big canopy. The variation of the number of trees in this class can reach 32%.

The TD +160 is the main densely vegetated class type. It is located mainly in woodlands, which typically form variable areas of relatively small trees. The tree variation in this class is about 32% as found in the TD71-160 class. Lowest variations of 40.2% and 32.5% were found in TD41-70 and TD21-40, respectively. These TD classes are mainly found in the more natural savannah vegetation, where mean tree height reaches 10 m. In contrast, the highest variations were found in TD4-20 and TD0-3, areas characterized by sparse vegetation and generally located in cultivated and fallow savannahs. These classes form the nearly agro-forested savannahs as they are dominated by useful tree species such as *V. paradoxa*, *A. albida*, *P. biglobosa*, *A. digitata* or *T. indica*.

The TD in savannahs suggests higher evapotranspiration rates with higher TD classes in the lowland, and lower evapotranspiration associated with a lower TD in agro-forested areas on bare-land.

5.3 ET_a assessments

Assessments of the ET_a based on the $SEBAL$ model were performed to provide a database for defining the temporal evapotranspiration rates according to the biophysical and hydrological units of the savannah. Two satellite images acquired at the beginning and end of the dry season were used in the $SEBAL$ model to estimate the spatial and temporal variation of the ET_a. This variation of the ET_a was related to the biophysical and moisture data to estimate the hydrological role of the savannah landscape. The ET_a was also related to the $LULC$ types, to the TD classes and to the hydrological units at the beginning and end of the dry season. Furthermore, to assess the real input of savannah vegetation water vapor into the atmosphere, the sap flow technique (Granier, 1985; 1987) was applied to measure individual tree water use. An up-scaling method based on tree density was used to estimate selected fallow vegetation transpiration during drought stress. The study area consisted essentially of 11 $LULC$ types, 7 tree density classes and 11 hydrological units spectrally derived from remote sensing and field data.

5.3.1 Relationships between ET_a distribution and biophysical and hydrological characteristics

To study the relationship between ET_a distribution and the derived spectral TD classes and hydrological units, a GIS-based analysis was applied. The two derived spectral layers were regressed with the ET_a data using about 5000 randomly distributed points. The ET_a was spatially extracted for each TD class, and then for each hydrological class. To ensure a temporal analysis of the ET_a, the regression was run for two time periods, from 30 October, 2002 and 7 March, 2003, files.

Temporal integration of the SEBAL ET_a by LULC types during the dry season

To monitor ET_a flux over savannah vegetation for time periods without satellite images during the dry season, a temporal integration method based on the adjusted crop coefficient K_c was used to derive the crop evapotranspiration ET_c. The ET_c data were computed for each land cover unit at the beginning and end of the dry season (October, 2002 and March, 2003), respectively. The ET_c of 7 days enclosing the satellite overpass was used to accurately derive ET_s (7-day ET_c). The results show that the ET_c for the mean 7-day observation values was not significantly different from the $SEBAL$ ET_a. This implies stable weather conditions during the experiment. During 30 October, 2002, the highest K_c of 1.36 and 1.15 were found for water bodies and rice fields, while the lowest K_c of 0.33 and 0.38 were registered in bare-land and outcrop rocks, respectively.

On the other hand, during the overpass of 7 March, 2003, the highest K_c values of 1.23, 0.86 and 0.83 were located in the wettest parts, i.e, water bodies, rice fields and gallery forest, respectively, but these K_c were lower compared to values found in October. The lowest K_c values were found in park savannah, shrub-land and farmland classes. The mean variation in K_c between classes was very high and was estimated at

109%, and the difference in K_c between *LULC* classes was not significant at the 10% level, but the coefficient of variation reached a level of up to 45%. The difference in K_c may be explained by factors such as soil moisture, vegetative cover or tree density.

In October, the ET_c of 7 days amounted 34.53 mm, 31.04 mm and 28.56 mm for water bodies, rice fields, gallery forest and reserves, respectively. The land unit types that contribute the lowest ET_s are the bare-land, shrub-land and farmland with 9.03 mm, 15.47 mm and 14.28 mm, respectively. In March ET_s the highest rates were observed over water bodies, rice fields and gallery forest/reserves with 32.10 mm, 22.35 mm and 21.59 mm, respectively. The lowest ET_s values were recorded on bare-land, farmland and shrub-land with 0.98 mm, 1.47 mm and 0.35 mm, respectively.

The estimated ET_c over the wettest areas (rice fields, water body, gallery forest/ reserves) was on average 19% higher than the ET_o, whereas ET_c was reducing over the drier parts (shrub-land, bare-land, farmland) of the landscape by about 52%. The conclusion is that *SEBAL* and the Penman-Monteith closely predict ET_c for the wettest part of the landscape where relative moisture conditions prevail over the savannah landscape. This suggests there is a potential to improve the *SEBAL* model outcome by a careful field data collection in general and the selection of representative hot and dry pixels in general and the dry pixel in particular.

Relationship between ET_c and tree density

During October 2002 (beginning of the dry season), high ET_c values of about 3.45 mm day^{-1} were observed for the TD classes TD71-160, TD+160 and TD41-70. Most of the area of the TD71-160 class, with a high ET_c of about 3.84 mm day^{-1}, was located along a small number of tributaries, which correspond to the *LULC* type forest gallery/reserves. High ET_c values of 3.31 and 3.21 mm day^{-1} were also observed in the TD classes TD+160 and TD41-70, respectively. These classes are generally associated with woodlands and open savannah, which are the densely vegetated parts of the natural savannah. However, some patches of high ET_c appear over the water bodies (5.26 mm day^{-1}) and the irrigated areas of the Tono and the Vea Dams (4.29 mm day^{-1}). These densely vegetated classes are associated with high moisture conditions that suggest high evaporation rates.

On the other hand, low ET_c values of about 1.80 mm day^{-1} were associated with the sparsely vegetated classes TD0-3, TD4-20 and TD21-40. The TD classes TD0-3 and TD4-20 were generally located in cultivated areas and bare land with a mean ET_c of 1.46 mm day^{-1}. A traditional land management system based on forest clearing explains to a great extent the net reduction of tree numbers, low infiltration and low ET_c values over farmland (2.04 mm day^{-1}). The TD21-40 class, i.e., fallow and secondary riverbed vegetation, exhibited low ET_c values (2.36 mm day^{-1}). However, the ET_c were high in all zones, as might be expected in October, which is the end of the growing season.

During March 2003 (end of the dry season), very low ET_c values were recorded over the savannah vegetation. The relatively high ET_c of 1.14 mm day^{-1}, was found in the class TD71-160, which is associated with gallery forest/reserves and closed woodland. The classes TD41-70 and TD+160 registered only 0.51 and 0.73 mm day^{-1}, respectively. These dry conditions occur after almost 4 months after the last rains. Most of the woody deciduous tree species were between the leaf shedding and green-up phases that are related to the transpiration reduction mechanism. In the case of the TD71-160 class, generally associated with gallery forest, it may be assumed that most of the ET_c was due to soil evaporation, as the groundwater table is high and water could evaporate by capillarity. Over the other part of the landscape, only very low ET_c values close to 0 mm day^{-1} were recorded, except over water bodies (4.86 mm day^{-1}). Compared to the ET_c values recorded in October, ET_c values in March were 4 to 5 times lower, which may be directly related to the drastic climatic conditions that arise during the dry season in tropical semi-arid areas characterized by high solar radiation and drought stress.

The spatial distribution of the ET_c in the study area suggests that higher TD are associated with higher ET_c rates, and lower TD classes with lower ET_c rates. However, the high ET_c rate of high TD classes is also linked to the presence of large trees generally located where the water table is high. The ET_c variability between classes may be explained by specific land management types resulting in similar ET_c values of cultivated land, shrub-land or bare-land. However, high TD classes are usually linked to the lower parts of the landscape where higher soil moisture favors the transpiration of vegetation, but also higher soil evaporation at the end of the dry season.

Relationship between ET_c and hydrological units in the savannah landscape

The extent of the savannah hydrological units in the savannah landscape over the Navrongo area was studied using high spatial resolution remote sensing data and applying the *VITT* approach. Eleven (11) units were identified in the savannah at the beginning and the end of the dry season 2002-2003.

At the beginning of the dry season, the majority of the hydrological units were relatively wet throughout the area, with only some dry units located in farmland, bare-land and on outcrop rocks. The wet hydrological units were units 1, 2, 3, and 4, which showed a mean ET_c of 3.47 mm day^{-1}. These hydrological units were mostly located in lower areas where moisture is high. On the other hand, the number of medium wetness classes was large, including units 5, 6, 7, 8 and 9, which are generally associated with park savannah, shrub-land and open savannah. The ET_c rate for these classes was found to be relatively low with a mean ET_c value of 2.60 mm day^{-1}. The driest units were units 10 and 11 with a mean ET_c of 1.32 mm day^{-1}. Globally, it should be noted that the weather conditions at the beginning of the dry season were still relatively moist, which could be seen from a luxuriant vegetation cover. Indeed, some rains occurred in the week of the satellite overpass, explaining the abundance of open waters, and the uppermost soil moisture, which contributed to a relatively high evaporation level. Although, tree transpiration may be high, it was assumed to be merely a small fraction of the global ET_c of the study area.

During the dry season, most of the hydrological units throughout the savannah landscape experienced a steep decrease in ET_c independent of vegetation cover type and topographical position. The extreme tropical semi-arid climate conditions, i.e., high air temperature, low relative humidity, high solar radiation, and Harmattan wind, are important drought factors. Indeed, the phenological events in savannahs such as leaf fall, flushing, flowering and fruiting occur principally in the dry season for most of the deciduous tree species that characterize the West African savannahs. Thus, the hydrological role of the vegetation layer decreases greatly in the dry season as it adapts to the drought. Mean ET_c for all units, except unit 1, fell to a mean value of 0.10 mm day^{-1} in March 2003 in contrast to 2.51 mm day^{-1} in October 2002, which represents a decrease of about 96.0% compared to the situation at the beginning of the dry season. The ET_c value of 4.48 mm day^{-1} unit 1, which is located over open water bodies and rice fields, remained relatively constant throughout the dry season. This exceptional situation is due to controlled water resources use.

This general trend from wet to dry hydrological units has been interpreted as being consistent with and supporting the preliminary interpretation of the *VITT* diagram (section 3.2.3; Figure 3.4). Indeed, from the beginning to the end of the dry season, the full vegetation cover of the savannah vegetation reduces due to leaf shedding caused by drought and then greens up at the beginning of the new wet season.

5.3.2 Savannah vegetation transpiration in the dry season

Transpiration was related to species and biometric characteristics of the trees in the study area. *A. albida* with an inverse phenological development during the dry season transpired more than all other tree species.

The ratio of *A. albida* mean sap velocity to other species was as high with 1.5, 2.2 and 1.1, for *V. paradoxa*, *M. indica* and *D. mespiliformis,* respectively. These unequal ratios in sap velocities suggest different water use. Tree transpiration and weather conditions were directly related, and air temperature, solar radiation, relative humidity, wind speed and vapor pressure deficit were the most important parameters determining water use. This dependence of water use on climatic parameters was linearly modeled to predict transpiration in savannah vegetation. Mean water use by *V. paradoxa* amounted to 86 l day^{-1} and 32.4 l day^{-1} for the cool and hot dry season, i.e., a transpiration rate of 0.14 mm day^{-1} and 0.05 mm day^{-1}, respectively. Compared to the ET_o, the direct input of savannah transpiration E_c to the atmosphere amounted about 3.15% and 1.08% in February and March, respectively.

Compared to both time periods of the experiment, there was a decrease in savannah transpiration between October and March of about 34%. This low level of transpiration may be explained by the drought stress that initiates phenological seasonal changes. In early February 2003, *V. paradoxa* turned yellowish and shed leaves as a symptom of drought stress, whereas at the end of March 2003, flowering was abundant and the trees were almost leafless. These phenological events are timed with weather conditions as well as with the hydrological situation (section 3.3.2) passing from relatively wet (October 2002) to dry conditions (March 2003). Therefore, it is difficult to compare the findings of the present study with results under other climatic conditions or for other tree species.

5.4 Conclusions and recommendations

There is a high rate of ET_a change during the dry season throughout the savannah landscape of the Navrongo area. Important climatic factors combined with characteristic biophysical and hydrological conditions drive this high variability. The seasonal phenological change of savannah vegetation is directly related to weather and hydrological conditions of the tropical climate due to the monsoon activity. This illustrates the importance of the role of $LULC$ types and their respective surface characteristics such as albedo, temperature, roughness length, and $NDVI$ in the energy partitioning over the land surface. There is a need for monitoring the $LULC$ changes in order to ensure reliable water management purposes. The changes in land cover, driven by human activities and erratic climatic factors, need to be qualitatively as well as quantitatively assessed to arrive at a scientifically sound management of natural resources including the hydrological component in the area. This should also help understanding the role of savannahs in the phenomenon of climate change in West Africa in general and in the Volta Basin in particular.

There is a growing regional need for water management, which is being studied in a multidisciplinary approach in the Glowa-Volta Project. As has been demonstrated in the present study, $LULC$ types and seasonal wild fires, hydrological units and tree density classes are the most important biophysical and hydrological characteristics that influence the spatial and temporal variation of the ET_a in the Volta Basin. In order to arrive at a sustainable water management, and based on the results of the study, the following recommendations are made for future research.

1. There is a need to conduct a land-use and land-cover change study to follow the recent changes in the savannahs in the Volta Basin, differentiating between natural and human-induced changes. This can be done by the implementation of remote sensing methods complemented by ground measurements. The results could give some orientation regarding the trends of land degradation and the selection of areas for protection.
2. The present method based on the *VITT* method may be used for large areas to study spatial and temporal changes in soil moisture in the savannah landscape. This is of great importance to account for the role of ecosystem moisture in the evapotranspiration process, but also for the development of biophysical components related to specific ecotypes. The use of remote sensing is suitable for local, watershed and regional studies. To account for data availability and validation purpose, low spatial resolution satellite data and field surveys can be used.
3. The proposed approach to tree density mapping needs to be experimented in another area. The present results may be improved with an intense survey on the ground to acquiring a larger dataset of tree densities. The results shown here encourage the use of this approach, as it seems more efficient than direct measurements or visual interpretation of satellite images. Furthermore, it could be implemented in similar savannah landscapes to allow quantitative management of agro-forestry resources. This is of importance for semi-arid regions in general, and especially the Sahel zone, which are characterized by erratic climatic conditions.
4. The sap flow technique in the present study gives an idea of the quantity of water transpiration in the savannah vegetation of the Volta Basin. There is a need for further long-term measurements for a variety of tree species. This may help to better understand the spatial and temporal role of tree species in water recycling in general, and their influence on the groundwater in particular.
5. There is a need for research on the water use of savannah vegetation in order to identify drought-resistant tree species for extensive afforestation purposes. Such research should take in account the ecological and hydrological functions, but also the social and economic role, of tree species.

6. To improve the ET_c spatial and temporal integration using ratios of ET_o and *SEBAL* ET_a there is a need to obtain long-term time-series-images for determining well adjusted K_c coefficients. Because these ratios are determined for the moment of satellite overpass and are applied over daily and longer time steps, it would be more accurate to use relatively high time-series images and representative ground weather stations for the reference ET_o. To improve the ET_c spatial distribution, there is a need to adopt the proposed method, which could replace the current weather-station-based estimation or other generalized adjusted crop coefficients. Incorporating remote sensing and GIS tools to map *LULC* types may help improve the spatial management of water resources. The use of the *SEBAL* model promises to be an efficient, accurate, and inexpensive procedure to predict the actual evaporation fluxes from irrigated and savannah landscapes.

6 REFERENCES

Adu S.V. 1969. Soils of the Navrongo-Bawku area, Upper Region, Ghana. Memoir No. 5, Soil Research Institute, Kumasi, Ghana.

Allen R.G., Morse A., Tasumi M., Trezza R., Bastiaanssen W.G.M., Wright J.L. and Kramber W. 2002. Evapotranspiration from a satellite-based surface energy balance for the Snake Plain Aquifer in Idaho. Proceedings of the National USCID Conference, San LUIS Obispo, California, July 8-10, 2002.

Allen R.G., Pereira L.S., Raes D. and Smith M. 1998. Crop Evapotranspiration. Guidelines for computing crop water requirements. FAO Irrigation and Drainage Paper 56. Food and Agricultural Organization of the United Nations, Rome, Italy.

Allen S.J. and Grime V.L. 1995. Measurements of transpiration from savannah shrubs using sap flow gauges. Agr. Forest Meteorol. 75: 23-41.

Andrade J.A., Meinzer F.C.G., Goldstein N.M., Holbrook J., Cavelier P., Jackson and Silvera K. 1998. Regulation of water flux through trunks, branches, and leaves in trees of a lowland tropical forest. Oecologia 115: 463-471.

Anhuf D. and Frankenberg P. 1991. Die naturnahen Vegetationszonen Westafrikas. Die Erde 122 (4): 243-265.

Avissar R. and Pielke R. 1989. A parameterization of heterogeneous land surfaces for atmospheric numerical models and its impact on regional meteorology. Mon. Weather Rev. 117: 2113-2136.

Bannert D., Hoffman R., Jöns H.P., Kruck W. 1980. Etude de reconnaissance des ressources en Afrique à l´aide d´images satellite. Etudes de recherches multidisciplinaire à l´aide d´images satellite en République de Haute-Volta : Géologie, hydrologie, pédologie et utilisation de l´espace. Rapport final, Coopération Technique- N° du projet 75.2210.5, Mai 1980.

Barnsley M.J., Barr S.L. and Tsang T. 1997. Producing large-area land cover maps from satellite images: scaling issues and generalization techniques. In: Gardingen P., Foody G., and Curran P.J., (eds.) Scaling-up: from cell to landscape. Cambridge University Press, Cambridge, pp. 173-200.

Bastiaanssen W.G.M. 1995. Regionalisation of surface flux densities and moisture indicators in composite terrain. PhD thesis, Wageningen Agricultural University, Wageningen, the Nederlands.

Bastiaanssen W.G.M., Menenti M., Feddes R.A. and Holtslag A.A.M. 1998a. A remote sensing surface energy balance algorithm for land (*SEBAL*): 1. Formulation. J. Hydrol. 212/213: 198-212.

Bastiaanssen W.G.M. 2000. *SEBAL*-based sensible and latent heat fluxes in the irrigated Gediz Basin, Turkey. J. Hydrol. 229 (1-2): 87-100.

Bastiaanssen W.G.M., Ahmad M.D. and Chemin Y. 2002. Satellite surveillance of evaporative depletion across the Indus Basin. Water Resour. Res., 38 (12): 1273-1282.

Bauerle W.L., Whitlow T.H., Pollock C.R. and Frongillo E.A. 2002. A laser-diode-based system for measuring sap flow by the heat-pulse method. Agr. Forest Meteorol. 110: 275-284.

Boulet R. 1976. Cartes des ressources en sols de la Haute-Volta. Notice explicative. ORSTOM, Paris.

Bausch W.C. 1993. Soil background effects on reflectance-based crop coefficients for corn (1991). Remote Sens. Environ. 46: 213-222.

Belward A.S. (Ed.) 1996. The IGBP-DIS Global 1 Km Land Cover Data Set "DISCover" –Proposal and Implementation Plans. Report of the Land Cover Working Group of IGBP-DIS. IGBP Data and Information System Office, Toulouse.

Belward A.S. 1999. The IGBP-DIS Global 1-km Land-Cover Data Set DISCover: A Project Overview. Photogramm. Eng. Rem. S. 9: 1013-1020.

Benneh G., Agyepong G.T. and Allotey J.A. 1990. Land degradation in Ghana. Food Production and Rural Development Division. Commonwealth Secretariat, London.

Blyth E.M. and Harding R.J. 1995. Application of aggregation models to surface heat flux from the Sahelian tiger bush. Agr. Forest Meteorol. 72: 213-235.

Booth F.M. and Wickens G.E. 1988. Non-timber uses of selected arid zone trees and shrubs in Africa. FAO Conservation Guide 19. FAO, Rome.

Boulet R. 1978. Toposéquences de sols tropicaux en Haute-Volta. Equilibre et deséquilibre pédoclimatiques. Mémoires ORSTOM N° 85. ORSTOM Paris.

Boyd M.R. and Whalley D.B. 1993. Isolation and analysis of optimization errors. Proceedings ACM SIGPLAN93 Conf. on Programming Languages Design and Implementation, pp. 26-35.

Braimoh A. 2004. Modeling land-use change in the Volta Basin of Ghana. Ph.D. Thesis, Cuvillier, Göttingen.

Braun P. and Schmid J. 1999. Sap flow measurements in grapevines (*Vitis vinifera* L.).2. Granier measurements. Plant Soil 215: 47-55.

Brooks K.N., Folliott P.F., Gregersen H.M. and Debano L.F. 1997. Hydrology and the management of watersheds, 2nd ed., Iowa State University Press, Ames. Iowa.

Brutsaert W., Hsu A.Y. and Schmugge T.J. 1993. Parametrization of surface heat fluxes above forest with satellite thermal and boundary layer soundings. J. Appl. Meteorol. 32: 909-917

Brutsaert W. 1982. Evaporation into the atmosphere: theory, history and applications, Reidel, Dordrecht.

Campbell J.B. 1987. Introduction to remote sensing. Guilford Press, New York.

Campbell J.B. 1996. Introduction to Remote Sensing, 2nd ed., Taylor & Francis, London.

Campbell G.S. and Norman J.M. 1998. An introduction to environmental biophysics. 2nd ed. Springer-Verlag, New York.

Charney J.G. 1975. The dynamics of deserts and droughts, Q. J. Roy. Meteorol. Soc. 101: 193-202.

Chehbouni A.D., Lo Seen, Njoku E.G., Lhomme J.P., Monteny B. and Kerr Y.H. 1997. Estimation of sensible heat flux over sparsely vegetated surfaces. J. Hydrol. 188-189: 855-868

Chen X.W., Tateishi R. and Ahn C.H. 1997. A method on land cover classification by combining unsupervised algorithm and training data. Proceedings of International Symposium on Remote Sensing, Pusan, Korea, 5-7 November 1997. Korean Associate of Remote Sensing, Seoul.

Choudhury B.J. 1989. Estimating evaporation and carbon assimilation using infrared temperature data: Vistas in modeling, In: Asrar G. (ed.) Theory and applications in optical remote sensing, John Wiley, New York, pp. 628-690.

Chuvieco E. 1996. Fundamentos de Teledeteción espacial. Madrid, Rialp.

Cissé L. and Vachaud G. 1988. Influence d´apports de matière organique sur la culture de mil et d´arachide sur un sol sableux du Nord-Sénégal. I. Bilans de consommation, production et développement racinaire. Agronomie 8: 315-326.

Cochrane M.A. 2003. Fire science for rainforests. Nature Publishing Group, Nature, vol. 421. Available at http://www.nature.com/nature.

Cole M.M. 1982. The influence of soils, geomorphology and geology on the distribution of land communities in savanna ecosystems. In: Huntley B.J. and Walker B.H. (eds.) Ecology of Tropical Savannas. Springer, Berlin, pp 145-175.

Cole M.M. 1992. Influence of physical factors on the nature and dynamics of forest-savanna boundaries. In: Furley P.A., Proctor J. and Ratter J.A. (eds.) Nature and Dynamics of forest-Savanna Boundaries. Chapman and Hall, New York, pp. 37-62.

Commeraat L.H. and Imeson A.C. 1999. The evolution and significance of soil-vegetation patterns following land abandonment and fire in Spain. Catena 37 (1-2): 107-127.

Congalton R.G. 1991. A review of assessing the accurracy of classifications of remotely sensed data. Remote Sens. Environ. 37: 35-46.

Cowling R.M., Richardson D.M. and Pierce S.M. 1997. Vegetation of Southern Africa. Cambridge University Press, Cambridge, UK.

Curran B.C., Holle R.L. and Lopez R.E. 1997. Lightining fatalities, injuries, and damage reports in the United States from 1959-1994. NOAA National Weather Service Southern Region Technical Memorandum, Fort Worth, Texas.

Dickinson R. and Henderson-Sellers A. 1988. Modeling deforestation: a study of global climate model land-surface parameterization. Q. J. Roy. Meteorol. Soc. 114: 439-462.

Dickson K.B. and Benneh G. 1988. A new geography of Ghana. Longman, London.

Do F. and Rocheteau A. 2002. Influence of natural temperature gradients on measurements of xylem sap flow with thermal dissipation probes. 1. Field observations and possible remedies. Tree Physiol. 22: 641-648.

Dolman A.J., Hall M., Kavvas M.L., Oki T. and Pomeroy J.W. (eds) 2001. Soil-vegetation-atmosphere transfer schemes and large-scale hydrological models. Proceedings of an International Symposium (Symposium S5) held during the sixth IAHS Scientific Assembly at Maastricht, The Netherlands, IAHS Publication 270.

Doorenbos J. and Pruitt W.O. 1977. Crop water requirements, FAO Irrigation and drainage paper n° 24, 2nd ed., Food and Agricultural Organization of UN, Rome, Italy, 1977.

Dregne H.E. and Chou N.T. 1992. Global desertification dimensions and costs. In: Desertification of arid lands. Lubbock: Texas Tech. University.

Duadze S.E.K. 2004. Land use and land cover study of the savannah ecosystem in the Upper West Region (Ghana) using remote sensing. Ph.D. Thesis. Cuvillier, Göttingen.

Ducros-Gambart D. and Gastellu-Etchegorry J.P. 1984. Automatic analysis of bi-temporal Landsat data: an application to the study of the evolution of vegetation-covered areas in a tropical region. In: Guyenne T.D. and Hunt J.J. (eds.) Proceeding IGARSS Symposium. European Space Agency, Paris, pp. 187-192.

Eastman J.R. and Fulk M. 1993. Long sequence time series evaluation using standardized principal components, Photogramm. Eng. Rem. S. 59 (8): 1307-1312.

Edmonds E.A. 1956. The geology of Bawku-Gambaga area. Accra, Gold Coast Geological Survey, Bulletin N° 19.

Elvidge C.D., Baugh K.E., Dietz J.B., Bland T., Sutton P.C. and Kroehl H.W. 1999. Radiance calibration of DMSP-OLS low-light imaging data of human settlements. Remote Sens. Environ. 68: 77-88.

Enthekhabi D., Asrar G.R., Betts A.K., Beven K.J., Bras R.L., Duffy C.J., Dunne T., Koster R.D., Lettenmaier D.P., McLaughlin D.B., Shuttleworth W.J., van Genuchten M.Th., Wei M.Y. and Wood E.F. 1999. An agenda for land surface hydrology research and a call for the second international hydrological decade. B. Am. Meteorol. Soc. 80 (10): 2043-2058.

Entekhabi D., Rodriguez-Iturbe and Bras R.L. 1992. Variability in large-scale water balance with a land surface-atmosphere interaction, J. Climatol. 5: 798-813.

ERDAS 1999. ERDAS field guide. 2nd ed, version 8.6 (ERDAS), Atlanta, USA.

Estes J.E., Hajic E.J. and Tinney L. 1983. Fundamentals of image analysis: analysis of visible and thermal infrared data. In: Colwell R.N (ed.) Manual of Remote Sensing. American Society for Photogrammetry and Remote Sensing, Falls Church, Virginia, pp. 987-1124.

Farah H.O. 2001. Estimation of regional evaporation under different weather conditions from satellite and meteorological data: A case study of the Navaisha Basin. Ph.D. Thesis. ITC, Wageningen University.

FAO (Food and Agriculture Organization of the United Nations) 2001. Management of Natural Forests of Dry Tropical Zones. FAO conservation guide 32. Publishing and Multimedia Service, Information Division, FAO, Vialle delle Terme di Caracalla, Rome, Italy.

FAO 1997. State of the World's Forests 1997, Rome, Italy.

FAO 1997. Technical document on the AFRICOVER Land cover classification scheme: a dichotomous, modular-hierarchical approach. SD dimensions

FAO 1995. Evaluation des ressources forestières, 1990, Pays tropicaux. Etude Forêts 112.

FAO 1994. Africover proposal – Working group on land cover classification and legends. Report and Recommendations – Addis Ababa, Ethiopia, 7pp.

Fontan J. 1994. Changements globaux et développement. Nature-Sciences-Sociétés, 2: 143-152.

Fontès J. 1983. Essais cartographiques de la végétation par Télédétection. Quelques exemples pris en Haute-Volta. Thèse 3e cycle, UPS Toulouse, 180pp.

Fontès J. and Guinko S. 1995. Carte de la végétation et de l'occupation du sol du Burkina Faso. Notice explicative. Institut de la Carte International de la Végétation, Université Toulouse, France; Institut du Développement Rural, Université Ouagadougou, Burkina Faso.

Forman R. and Godron M. 1986. Landscape ecology. John Wiley, New York.

Franks S.W. and Beven K.J. 1997. Estimation of evapotranspiration at the landscape scale: a fuzzy disaggregation approach. Water Resour. Res. 33: 2929-2938.

Glowa-Volta Project Proposal 1999. Sustainable water use under changing land use, rainfall reliability and water demands in the Volta Basin. Zentrum für Entwicklungsforschung, Bonn.

Goff J.A. and Gratch S. 1946. Low-pressure properties of water from -160 to 212 F. In: Transactions of the American Society of Heating and Ventilating Engineers, presented at the 52nd annual meeting of the American society of heating and ventilating engineers, New York, pp. 95–122.

Gornitz V. 1985. A survey of anthropogenic vegetation changes in West Africa during the last century- Climate implication. Climatic Change 7: 285-235.

Goudie A. 2000. The human Impact in the Natural Environment. MIT Press. Cambridge, MA.

Granier A. 1985. Une nouvelle méthode pour la mesure des flux de sève dans le tronc des arbres. Ann. Sci. Forest. 42: 81-88.

Granier A. 1987. Evaluation of transpiration in a Douglas-Fir stand by means of sap flow measurements. Tree Physiol. 3: 309-319.

Green S.R. and Clothier B.E. 1988. Water use of kiwifruit vines and apple trees by the heat-pulse technique. J. Exp. Bot. 39 (198): 115-123.

Griend A.A. Vd and Gurney R.J. 1987. Satellite remote sensing and energy balance modelling for water balance assessment in semi-arid regions: 89-116, in: I Simmers (ed.) Estimation of natural of groundwater. NATO Advanced Research Workshop, vol 222, Amsterdam.

Guinko S. 1984. Végétation de la Haute Volta. Thèse de Doct. Es Sc. Nat., Bordeaux III.

Gutman G.G. 1991. Vegetation indices from AVHRR: an update and future prospects. Remote Sens. Environ. 35: 121-136.

Hatton T., Moore S., Reece P. 1995. Estimating transpiration in a Eucaliptus populnea woodland with the heat pulse method : measurements errors and sampling strategies. Tree Physiol. 15: 219-227.

Hall F.G., Huemmrich K.F., Goetz S.J., Sellers P.J. and Nicheson J.E. 1992. Satellite remote sensing of the surface energy balance: success, failures and unresolved issues in FIFE. J. Geophys. Res., 97 (D17): 19061-19089.

Henderson-Sellers A. and Pitman A.J. 1992. Interactive vegetation schemes for climate models: a glimpse opf future problems, J. Geophys. Res. 97: 2687-2696.

Hiernaux P.H. and Justice C.O. 1986. Suivi du développement végétal au cours de l'été 1984 dans le sahel Malien. Int. J. Remote Sens. 7: 1515-1531.

Hobbs T.J. 1995. The use of NOAA-AVHRR NDVI data to assess herbage production in the arid rangelands of Central Australia. Int. J. Remote Sens. 16: 1289-1302.

Hottin G. and Ouédraogo O.F. 1975. Carte géologique a 1/ 1 000 000 de la République de Haute-Volta. Direction de la Géologie et des Mines.

Huete A.R. and Liu H. 1994. An error and sensitivity analysis of the atmospheric- and soil-correcting variants of the NDVI for the MODIS-EOS. IEEE Transactions on Geoscience and Remote sensing, 32(4): 897-905

Huete A.R. 1988. A soil-adjusted vegetation index (SAVI). Remote Sens. Environ. 25: 295-309.

Huntley B.J. and Walker B.H. 1982. Ecology of Tropical Savannas. Springer, Berlin, pp. 145-175.

Iqbal M. 1983. An introduction to solar radiation. Academic Press, Toronto.

Jackson R.D., Hatfield J.L., Reginato R.J., Idso S.B. and Pinter Jr P.J. 1983. Estimation of daily evapotranspiration from one time day measurements. Agr. Water Manage. 7: 351-362

Jenik J. 1994. The Dahomey Gap: An Important Issue in African Phytogeography. Mém. Soc. Biogéogr. IV: 125-133.

Jensen J.R. 1996. Introductory Digital Image Processing- A Remote Sensing Perspective. 2nd ed. Prentice Hall, New Jersey,

Jensen J.R. 2000. Remote sensing of the environment: an earth resource perspective. Prentice Hall, New Jersey.

Jhorar R.K., Bastiaanssen W.G.M., Feddes R.A. and van Dam J.C. 2002. Inversely estimating soil hydraulic functions using evapotranspiration fluxes. J. Hydrol. 258: 198-213.

Jøker D. 2000. *Vitellaria paradoxa*, Seed Leaflet, n°50.

Justice C.O., Townshend J.R.G., Holben B.N. and Tucker C.J. 1985. Analysis of the phenology of global vegetation using meteorological satellite data. Int. J. Remote Sens. 6: 1271-1318.

Köstner B., Granier A. and Cermàk J. 1998. Sap flow measurements in forests stands: methods and uncertainties. Ann. Sci. Forest 55: 13-27.

Knapp R. 1973. Die Vegetation von Afrika. G. Fischer Verlag, Stuttgart.

Koné N. 1992. Contribution à l´étude du fonctionnement des écosystèmes naturels en zone, soudano sahélienne (Cas du Burkina Faso). Approche de la dynamique de la sécheresse par télédétection. Thèse Doct, Univ Toulouse, ICIV.

Kouda M. 1982. Analyse synchronique et diachronique de l´ évolution de la végétation en zone semi-aride (Haute Volta). Ph.D. Thesis. Université Paul-Sabatier, Toulouse, 143p.

Koutsias N., Karteris M., Fernandez-Palacios A., Navarro C., Jurado J., Navarro R. and Lobo A. 1999. Burned land mapping at local scale. In: Chuvieco E. (ed.) Remote sensing of large wildfires in the European Mediterranean Basin. Springer-Verlag, Berlin, pp. 157-187

Kramer P.J. 1983. Water relations of plants. Academic Press, New York.

Kustas W.P. and Norman J.M. 1996. Use of remote sensing for evapotranspiration monitoring over land surfaces. Hydrolog. Sci. J. 41 (4): 495-515

Lambin E.F. and Ehrlich D. 1996. The surface temperature-vegetation index space for land cover and land-cover change analysis. Int. J. Remote Sens. 17 (3): 463-487.

Lambin E.F. and Strahler A. 1994. Multitemporal change-vector analysis: A tool to detect and categorise land-cover change processes using high temporal resolution satellite data. Remote Sens. Environ. 48: 231-244.

Landgrebe D. and Biehl L. 1995. An introduction to MultiSpec. Purdue Research Foundation, Indiana, USA.

Lark R.M. 1995. A reappraisal of unsupervised classification 1: correspondence between spectral and conceptual classes. Int. J. Remote Sens. 16 (8): 1425-1443.

Lascano R.J. 2000. A general system to measure and calculate daily crop water use. Agron. J. 92: 821-832.

Lean J. and Warilow D. 1989. Simulation of the regional climatic impact of Amazon deforestation. Nature 342: 411-413.

Leroux M. 2001. The meteorology and climate of tropical Africa. Springer, London.

Les Atlas Jeune Afrique 1993. Atlas du Burkina Faso. 2nd ed. Les éditions J.A., Paris.

Letouzey R. 1969. Manuel de botanique forestière. Afrique tropicale. Centre technique forestier tropical, Nogent Sur Marne, France.

Lillesand T.M. and Kieferm R. 2000. Remote sensing and image interpretation. 4th ed. John Wiley, New York.

Liverman D., Moran E.F., Rindfuss and Stern P.C. (eds.) 1998. People and Pixels: Linking Remote Sensing and Social Science. National Academy Press, Washington, DC.

Loveland T.R., Reed B.C., Brown J.F., Ohlen D.O., Zhu Z., Yang L. and Merchant J.W. 2000. Development of a global land cover characteristics database and IGBP DISCover from 1 km AVHRR data. Int. J. Remote Sens. 21: 1303-1330.

Lubczynski M.W. 2000. Groundwater evapotranspiration- Underestimated component of the groundwater balance in a semi-arid environment-Serowe case, Botswana. In: Sililo et al. (eds.) Groundwater: Past achievements and future challenges. Rótterdam. Balkema, pp. 199-205.

Lu J., Sun G., McNulty S.G. and Amatya D.M. 2003. Modeling actual evapotranspiration from forested watersheds across the Southeastern United States. J. Am. Water Resources Ass. 39(4): 886-896.

Lucas R.M., Honzak M., Foody G.M., Curran P.J. and Corves C. 1993. Characterizing tropical secondary forests using multi-temporal Landsat sensor imagery. Int. J. Remote Sens. 14 (16): 3061-3067.

Marengo M., Canil G., Silvestro G., Origlia L., Busso M. and Persi P. 1997. Mid-infrared imaging of AGB star envelopes: II Modeling of observed sources. Astron. Astrophys. 322: 924-932.

Mas J.-F. 1999. Monitoring land-cover changes: a comparison of change detection techniques. Int. J. Remote Sens. 20 (1): 139-152.

Massman M.J. 1992. A surface energy balance method for partitioning evapotranspiration data into plant and soil components for a surface with partial canopy cover. Water Resour. Res. 28: 1723-1732.

Mausel P.W., Kalaluka G.Y., Lee J.K., Mudderman D.E. and Davis M.R. 1990. Multispectral video analysis of micro-relief dominated poorly drained soils in western Indiana. J. Imaging Technol. 16: 113-119.

McCracken K.E., Witham J.W. and Hunter M.L., Jr 1999. Relationships between seed fall of three tree species and Peromyscus leucopus and Clethrionomys gapperi during 10 years in an oak-pine forest. J. Mammal. 80: 1288-1296.

McGarigal K. and Marks B.J. 1995. FRAGSTATS: spatial pattern analysis program for quantifying landscape structure. USDA For. Serv Tech Rep, PNW-351.

McVicar T.R., Jupp D.L.B., Yang X. and Tian G. 1992. Linking regional water balance models with remote sensing. Proceedings of the 13th Asian Conference on Remote Sensing, Ulaanbaatar, Mongolia, 7-11 October, B.6.1-B.6.6.

Menninger E.A. 1977. Edible Nuts of the World. Horticultural Books Inc., Stuart, Florida.

Mennis J. 2001. Exploring relationships between ENSO and vegetation vigor in the south-east USA using AVHRR data. Int. J. Remote Sens. 22 (16): 3077-3092.

Middleton N.J. and D.S.G. Thomas 1997. World atlas desertification. Edward Arnold, London, UK.

Middleton N. 1999. The Global Casino: An Introduction to Environmental Issues. Oxford Univ. Press, New York.

Mohamed Y.A., Bastiaanssen W.G.M., Savenije H.H.G. 2004. Spatial variability of evaporation and moisture storage in the swamps of the upper Nile studied by remote sensing techniques. J. Hydrol. 289: 145-164.

Mohr B., Malony A., Hoppe H.-C., Schlimbach F., Haab G., Hoeflinger J., Shah S. 2002. A performance monitoring interface for Open MP (EWOMP´02), Rome, Italy.

Monteith J.L. 1981. Evaporation and surface temperature. Q. J. Roy. Meteorol. Soc. 107: 1-27.

Moran S.M. and Jackson R.D. 1991. Assessing the spatial distribution of evapotranspiration using remotely sensed inputs. J. Environ. Qual. 20: 725-737

Myers N. 1988. Tropical forests: much more than stocks of wood. J. Trop. Ecol. 4: 209-221.

Mueller-Dombois and Ellenberg H. 1974. Aims and methods of vegetation ecology. John Wiley, New York.

Muller E. 1985. Etude de la végétation de la région de Kongoussi (Burkina Faso) à partir données MSS-Landsat du 12 Nov. 1972 et du 6 Nov. 1975. Rapport DESS, CETEL-GDTA.

Murray R.J. 1960. The Geology of “Zuarungu” ½ Field sheet. Accra, Geological Survey Bulletin N° 25.

Nelson R. and Holben B. 1986. Identifying deforestation in Brazil using multiresolution satellite data. Int. J. Remote Sens. 3: 429-448.

Nemani R.R. and Running S.W. 1989. Estimating of regional surface resistance to evapotranspiration from NDVI and thermal-IR AVHRR data. J. Appl. Meteorol. 28: 276-284

Nichols W.D. 1992. Energy budgets and resistances to energy transport in sparsely vegetated rangeland. Agr. Meteorol. 60: 221-247.

Nicholson S.E., Some B. and Kone B. 2000. An analysis of recent rainfall conditions in West Africa, including the rainy seasons of the 1997 El Niňo and the 1998 La Niňa years. J. Climate 13: 2628-2640.

Nicholson S.E., Tucker C.J. and Ba M.B. 1998. Desertification, drought, and surface vegetation: An example from the West African Sahel. B. Am. Meteorol. Soc. 79: 815-829.

Nicholson S.E., Ba M.B. and Kim J.Y. 1996. Rainfall in the Sahel during 1994. J. Climate 9 (7): 1673-1676.

Norman J.M., Kustas W.P. and Humes K.S. 1995. Two source approach for estimating soil and vegetation energy fluxes in observations of directional radiometric surface temperature. Agr. Forest Meteorol. 77: 263-293.

Obeng and CSIR Ghana 2000. Soil- Crop suitability map of Upper East region of Ghana, Obeng and CSIR, Accra.

Oguntunde P.G. 2004. Evapotranspiration and complimentarity relations in the water balance of the Volta Basin: Field measurements and GIS-based regional estimates. Ph.D. Thesis. Cuvillier, Göttingen.

Olbrich B.W. 1991. The verification of the heat-pulse velocity technique for estimating sap flow in Eucalyptus grandis. Can. J. Forest Res. 21: 836-841.

Oppenheimer H.R. 1960. Adaptation to drought: xerophitism. In: Plant-water relationships in arid and semi-arid conditions: reviews of research. UNESCO, Paris, pp. 105-138.

Oren R., Philips N., Katul G., Evers B.E. and Pataki D.E. 1998. Scaling xylem sap flux and soil water balance and calculating variance: a method for partitioning water flux in forest. Ann. Sci. Forest 55: 191-216.

Pallier G. 1981. Géographie générale de la Haute-Volta. 2nd ed., Univ. De Limoges, UER Lettres et Sci Hum, Limoges.

Pataki D.E., Oren R. and Smith W.K. 2000. Sap flux of co-occurring species in a western subalpine forest during seasonal soil drought. Ecology 81 (9): 2557-2566.

Payne W.A., Wendt C.W. and Lascano R.J. 1990a. Root zone water balances of three low-input millet fields in Niger, West Africa. Agron. J. 82: 813-819.

Payne W.A. and Brück H. 1996. Comparison of evapotranspiration and other water balance terms estimated from neutron and capacitance probe measurements. pp. 455-462. In: Camp C.R. et al. (ed.) International evapotranspiration and irrigation scheduling. Proceedings Int. Conf., San Antonio, TX. 3-6 Nov. 1996. ASAE, St. Joseph.

Pelgrum H. and Bastiaanssen W.G.M. 1996. An intercomparison of techniques to determine the area-averaged latent heat flux from individual in situ observations: A remote sensing approach using the European Field Experiment in a desertification-threatened area data. Water Resour. Bull. 32: 2775-2786.

Penman H.L. 1948. Natural evaporation from open water, bare soil, and grass. Proceedings of the Royal Society of London, Series A 193: 120-146.

Petit C., Scudder T. and Lambin E.F. 2001. Quantifying processes of land-cover change by remote sensing: resettlement and rapid land-cover changes in southeastern Zambia. Int. J. Remote Sens. 22 (17): 3435-3456.

Philips N., Oren R. and Zimmermann R. 1996. Radial patterns of xylem sap flow in non-diffuse ring porous tree species. Plant Cell Environ. 19: 983-990.

Prince S.D. 1991. Satellite remote sensing of primary production: comparison of results for Sahelian grasslands 1981± 1988. Int J Remote Sens, 12: 1301± 1311.

Rasmussen M.S. 1996. The assessment of crop yield and net primary production in the Sahel using remote sensing and GIS techniques. Ph.D. Dissertation, Institute of Geography. Copenhagen, University of Copenhagen.

Richards J.A. 1993. Remote sensing digital image analysis: An introduction. 2nd ed. Springer-Verlag, Berlin.

Robinson R. 1991. Les Archives de Robinson Rojas-. Rrojas Databank: analysis of information. Available at http://www.rrojasdatabank.org/stats18.htm.

Roerink G.J. 1997. Relating crop water consumption to irrigation water supply by remote sensing. Water Resour. Manage. 11: 445-465.

Rojkov V.A., Wagner V.B., Kogut B.M., Konyushkov D.E., Nilsson S., Sheremet V.B. and Shvidenko A.Z. 1996. Soil carbon estimates and soil carbon map for Russia. WP-60-60: International Institute for Applied Systems Analysis, Laxemburg, Austria.

Rosema A. 1990. Comparison of meteosat-based rainfall and evapotranspiration mapping of Sahel region. Remote Sens. Environ. 1990. 46: 27-44.

Roy R.S., Ranganath B.K., Diwakar P.G., Vohra T.P.S., Bhan S.K., Singh J.J. and Pandian V.C. 1991. Tropical forest mapping and monitoring using remote sensing . Int. J. Remote Sens. 11: 2205-2225.

Sader S.A., Powell G.V.N. and Rappole J.H. 1991. Migratory bird habitat monitoring through remote sensing. Int. J. Remote Sens. 3: 363-372.

Savenije H.H.G. 1997. Determination of evaporation from a catchment water balance at a monthly time scale. Hydrol. Earth Syst. Sc. 1: 93-100.

Savenije H.H.G. 1996b. Does moisture feedbacks affect rainfall significantly? Phys. Chem. Earth 20 (5/6): 507-513.

Scholes R.J. and Hall D.O. 1996. The carbon budget of tropical savannas, woodlands and grasslands. In: Melillo J.M.and Breymeyer A. (eds.) Global change: Carbon Cycle in Coniferous Forests and Grasslands. John Wiley and Sons, New York.

Scholes R.J. and Walker B.H. 1993. An African savanna: synthesis of the Nylsvley study. Cambridge, UK.

Schuurmans J.M., Troch P.A., Veldhuizen A.A., Bastiaanssen W.G.M., Bierkens M.F.P. 2003. Assimilation of remotely sensed latent heat flux in a distributed hydrological model. Adv. Water Resour. 26 (2): 151-159.

Sellers P.J., Randall D.A., Collatz G.J., Berry J.A., Field C.B., Dazlich D.A., Zhang C., Collelo G.D. and Bounoua I. 1996. A revised land surface parameterization (SIB2) for atmospheric GCMs. Part 1. Model formulation. J. Climate 9 (4): 676-705.

Serra P., Pons X. and Sauri D. 2003. Post-classification change detection with data from differents sensors: some accuracy considerations. Int J. Remote Sens. 24 (16): 3311-3340.

Skole D. and Tucker C.J. 1994. Tropical deforestation and habitat fragmentation in the Amazon: satellite data from 1987 to 1988. Science 260: 1905-1910.

Sicot M. 1989. Contraintes et risques hydriques encourus par l´activité agro-pastorale au Sahel. Exemple de la mare d´Oursi au Burkina Faso. Le risque en agriculture. ORSTOM, pp. 131-141.

Sivakumar M.V.K. 1991. Drought Spells and Drought Frequencies in West Africa. ICRISAT Research Bulletin 13. Patancheru, Andhra Pradesh.

Smith D.M. and Allen S.J. 1996. Measurement of sap flow in plant stems. J. Exp. Bot. 47 (305): 1833-1844.

Statistics, Research and Information Directorate (SRID) 2001. Agriculture in Ghana. Facts and figures. Ministry of Food and Agriculture, Accra, Ghana.

Stephenne N. and Lambin E.F. 2001. A dynamic simulation model of land-use changes in the African Sahel (SALU). Agr. Ecosyst. Environ. 85: 145-162.

Swanson R.H. and Whitfield W.A. 1981. A numerical analysis of heat-pulse velocity theory and practice. J. Exp. Bot. 32 (126): 221-239.

Tasumi M. 2003. Progress in operational estimation of regional evapotranspiration using satellite imagery. University of Idaho: Moscow, Idaho.

Tasumi M. and Allen R.G. 2000. Application of the SEBAL methodology for estimating consumptive use of water and streamflow depletion in the Bear River Basin of Idaho through Remote Sensing. Appendix A: The theoretical basis of SEBAL. Final report. The Raytheon Systems Company. EOSDIS Project.

Tasumi M. and Allen R.G. 2000. Application of the SEBAL methodology for estimating consumptive use of water and streamflow depletion in the Bear River Basin of Idaho through Remote Sensing. Appendix C: A step by step guide to running SEBAL. Final report. The Raytheon Systems Company. EOSDIS Project.

Taylor C.J. 1952. The vegetation zones of the Goal Costa. Accra. Forestry Department Bulletin N°4.

Terrible M. 1982. Occupation du sol en Haute-Volta : son évolution entre 1952-56 et 1975. Rapport CRTO.

Timmermans W.J., Meijerink A.M.J. and Lubczynski M.W. 2001. Satellite derived actual evapotranspiration and groundwater modeling, Botswana. Remote Sensing and Hydrology 2000. Proceedings of a symposium held at Santa Fe, New Mexico, USA, April 2000. IAHS Publ no. 267: 252-258.

Timmermans W.J. and Meijerink A.M.J. 1999. Remotely sensed actual evapotranspiration: implications for groundwater management in Botswana. Int. J. Appl. Earth Obs. 1(3/4): 222-233.

Townshend J.R.G., Justice C.O., Gurney C. and McManus J. 1992. The impact of misregistration on change detection, IEEE Transactions on Geoscience and Remote Sensing, 30(5): 1054-1060.

Townshend J.R.G. and Justice C.O. 1986. Analysis of the dynamics of African vegetation using the normalized difference vegetation index.

Tucker C.J. 1979. Red and photographic infrared linear combination for monitoring vegetation, Remote Sens. Environ. 8: 127-150

Turner B.L., Meyer W.B. and Skole D.L. 1994. Global land-use / land-cover change: towards an integrated study. Ambio 23: 91-95.

Turner M.G. 1989. Landscape Ecology: The effect of pattern on process. Annu. Rev. Ecol. Syst. 20: 171-197.

Turner M.G. 1987. Spatial simulation of landscape changes in Georgia: A comparison of 3 transition models. Landscape Ecol. 1: 29-36.

United Nations Educational, Scientific and Cultural Organization (UNESCO), 1973. International classification and mapping of vegetation. Paris, France.

UP Umweltanalytische Produkte GmbH (2001) UP Sap Flow-System- User manual version 2.3. Available at www.upgmbh.com, www.sapflow.com

Van den Hurk B.J.J.M., Bastiaanssen W.G.M., Pelgrum H. and van Meijgaard E. 1997. A new methodology for assimilation of initial soil moisture fields in weather prediction models using meteosat and NOAA data. J. Appl. Meteorol. 36: 127-1283.

Vertessy R.A., Hatton T.J., Reece P., O´Sullivan S.K., Benyon R.G. 1977. Estimating stand water use of large mountain ash trees and validation of the sap flow measurement technique. Tree Physiol. 17: 747-756.

Vlek P.L.G. 1993. Strategies for sustaining agriculture in sub-Saharan Africa: the fertilizer technology issue. In: Technologies for sustainable agriculture in the tropics. ASA Special Publication N°. 56. Madison. Wisconsin, USA.

Vörösmarty C.J., Federer C.A. and Schloss A.L. 1998. Potential evaporation functions compared on US watersheds: possible implications for global-scale water balance and terrestrial ecosystem modeling. J. Hydrol. 207: 147-169.

Walker J.P., Willgoose G.R., Kalma J.D. 2001. One-dimensional soil moisture profile retrieval by assimilation of near-surface observations: a comparison of retrieval algorithms. Adv. Water Resour. 24: 631-650.

Wallace J.S., Lloyd C.R. and Sivakumar M.V.K. 1993. Measurements of soil, plant and total evaporation from millet in Niger. Agr. Forest Meteorol. 63: 149-169.

WRI (World Resource Institute) 1994. World Resources 1994-1995. Oxford University Press, New York.

7 APPENDICES

Appendix 1: Savannah fallow vegetation at the beginning of the dry season

The savannah fallow vegetation shows full canopy cover and dry grasses recovering the land surface. Large patches of dead leaves can also be seen that, combined with the dry grass, are a potential biomass that easily burns throughout the fallow areas.

Savannah fallow vegetation trees presenting full canopy cover, while the ground surface is occupied by a high quantity of grass. Beginning December, the grass layer dries and is the main sources of wild fires in the savannahs.

Appendix 2: Impacts of bush fires on the savannah fallow vegetation: effects of fire events on *Vitellaria paradoxa* trees

Wide spatial extent of bush fires at the beginning of the dry season. All the dry grass has been burnt, and the fire affects mostly tree crowns. Black ash covering the ground can be seen.

Bush fire impact on the savannah fallow vegetation. Most of the trees have a canopy of about 10 m, which is burnt by the fire at the beginning of the dry season. This potentially affects the photo-synthetic and physiological functions of the trees.

Appendix 3: Savannah fallow vegetation at the end of the dry season

The savannah landscape is dominated by the drought. Most trees and shrubs are leafless, and the ground is covered by dead leaves. The picture shows leafless *Vitellaria paradoxa* trees at the sap flow experimental site.

Leafless *Vitellaria paradoxa* trees and dead grass covering the ground; *Combretum glutinosum* shrubs are the only understory with green leaves.

ACKNOWLEDGEMENTS

To The Lord of The Lord, all the gratitude for the successful completion of the present work.

I am thankful to Prof. Dr. Paul Vlek, my first supervisor, for the supervision, understanding, encouragement, and his fatherly approach at all stages of my research study. I thank PD Dr. Jürgen Burkhardt, my second supervisor, for his prompt interest, support, and suggestions on the work. I sincerely appreciate the constructive support, openness and encouragements from both Prof. Dr. Nick van de Giesen (TU Delft-Nederland) and Jan Hendrickx (New Mexico Tech-USA) for orienting my research in land surface-atmosphere interrelations. I would like to thank Dr. Jörg Szarzynski for the interest shown in the study. My profound gratitude goes to the Glowa-Volta Project and the German Federal Ministry of Education, Science and Technology (BMBF), who provided stipend and research grant for this study. My thanks to Drs. Charles Rodgers, Marc Andreini, Mathias Fosu, and Konrad Vielhauer, the project co-coordinators, for their support at ZEF and during the field campaign. Special thanks go to Dr. Günther Manske, Ms Rose-Marie Zabel and Ms Hanna Peters, Ms Hagedorn-Mensah, Ms Sabine Aengenendt-Baer and Ms Andreas Berg for their help with many administrative matters. I also thank Ms Margaret Jend for editing my thesis.

Many thanks to the management of Centre National de la Recherche Scientifique et Technologique (CNRST), and Institut de l´Environnement et de Recherches Agricoles (INERA) for granting the study leave. I acknowledge the contribution of Profs. Hamidou Boly and Sita Guinko, Drs. Michel Sedogo, Lamourdia Thiombiano, Seydou N. Traoré, Fidel Hien, Valère Somé, Léopold Somé and Mme Martine Adoubé for their moral support.

I cordially thank Drs. Mandfred Denich at ZEF, Nicolas Koné at INERA-Burkina, and Dr. John A. Yidana at UDS-Ghana for their constructive advice. I am grateful to Drs. M. Lubczynski and W.J. Timmermans for their contributions during my visit at ITC-Nederlands. Thanks to my friends and colleagues Mrs Souleymane Paré, Issa Lamizana, Jean-Pierre Tiendrebeogo and Adama Bandaogo, Didier and Delphine Tégré for their inspirations.

Thanks to my field assistants at Tanyellé-Kompienga and Telania-Navrongo and the local population who were involved in my field investigations in Ghana and Burkina Faso.

Thanks are extended to my friend Kelebogili Mfundisi and all the ZEF colleagues. I appreciate the friendship and collaboration with Desmond Manful and Delys Sefakor, Philip Oguntunde, Nicola Martin, Andreas Schlömann, Jan Friesen, and Wolfram and Kubra Laube, Charlotte van der Schaaf, Fafré Bagayoko and Jean-Pierre Sandwidi, Dr. Daniel Tsegai, Franklin Simtowe and Dr. Tamene Lulseged, Dr. Eva Youkhana and Oliver Korth.

Finally, my sincere gratitude goes to all who contributed to the success. Special thanks to my brothers Mahamoudou, Abdoulaye, Karim, Saïdou and Souleymane, my sisters Salamata, Bibata, Rasmata, Bernandine, Zalissa, Fati, and Aïssata for their faithful prayers to The Gracious of The Gracious.